(86)

The Effects of Thermal Radiation on Dry Convection

by

Vincent Edwin Larson

B.A., Yale University (1992)

Submitted to the Department of Earth, Atmospheric and Planetary Sciences
in partial fulfillment of the requirements for the degree of

Doctor of Philosophy

at the

MASSACHUSETTS INSTITUTE OF TECHNOLOGY

February 1999

Author .....
Department of Earth, Atmospheric and Planetary Sciences
February, 1999

Certified by .....
Kerry A. Emanuel
Professor
Thesis Supervisor

Accepted by .....
Ronald G. Prinn
Chairman, Department Committee on Graduate Students

The Effects of Thermal Radiation on Dry Convection

by

Vincent Edwin Larson

Submitted to the Department of Earth, Atmospheric and Planetary Sciences
on February, 1999, in partial fulfillment of the
requirements for the degree of
Doctor of Philosophy

Abstract

This work seeks to improve understanding of atmospheres in radiative-convective equilibrium. We use two types of idealized, dry radiative-convective models. The first type of model resembles Rayleigh-Bénard convection, except that thermal radiative transfer is included. This type of system can be investigated in the laboratory. The second type of model is a more faithful representation of the earth's atmosphere. In this model, the temperature at the upper boundary is left unspecified, unlike the case of Rayleigh-Bénard convection. For these two types of radiative-convective models, we perform various theoretical and numerical analyses of the stability properties, and various analyses of the weakly nonlinear convecting state.

We prove that in these models, convection arises as monotonically growing cells, not as an oscillatory instability. That is, we prove exchange of stabilities.

We investigate the linear stability modes. We find that in most cases, the linear stability threshold can be described approximately or exactly in terms of a radiative Rayleigh number. The radiative Rayleigh numbers used are like the classical Rayleigh number but with modified temperature and thermal diffusivity scales. Inspection of the radiative Rayleigh numbers reveals how various external parameters, such as the net incoming solar radiation or infrared opacity, affect the stability properties.

We use the energy method to find a threshold value of a stability parameter below which all disturbances to the radiative equilibrium state, regardless of magnitude, decay. For those radiative equilibrium states which have a linear temperature profile, the energy stability threshold coincides with the linear stability threshold, thereby ruling out the possibility of subcritical instabilities. When the temperature profile is nonlinear, the energy stability profile lies below the linear stability threshold.

We study weakly nonlinear convection in the atmospheric radiative-convective model via the mean field approximation. In contrast to the stability threshold, the vertical convective heat flux in the weakly nonlinear convecting state turns out to be little affected by the values of viscosity, thermal diffusivity, or radiative damping. However, the convective heat flux is strongly affected by the net incoming solar radiation and the optical depth. We formulate scaling laws for vertical convective heat flux, vertical velocity, and temperature perturbations. These scales extend the Prandtl scales to higher altitudes.

Thesis Supervisor: Kerry A. Emanuel
Title: Professor

Acknowledgments

A number of people have left their mark on my thinking and on this thesis. I am greatly indebted to them. Below, I list some of the most substantial contributions to the content of this thesis, so far as my poor memory serves me.

My advisor, Professor Kerry A. Emanuel, allowed me to pursue my own research interests, a freedom which seems to be rare these days. He is to be commended for his great generosity in this regard. Furthermore, he taught me much about atmospheric convection, and in particular he pointed out the importance of constant heat flux boundaries to the behavior of radiative-convective atmospheres.

Professor Glenn R. Flierl gave me a great deal of help with the numerics in this thesis. He also suggested estimating the magnitude of the neglected nonlinear terms in the mean field equations.

Professor W. V. R. Malkus introduced me to the mean field approximation and the energy method. In addition, he was the first to suggest that I examine a radiative-convective model with zero thermal diffusivity.

Professor R. Alan Plumb raised some good questions about the importance (or lack thereof) of radiative damping and questions about the meaning of energy stability.

Professor Emeritus Richard M. Goody offered insightful comments on the merits and drawbacks of grey radiative transfer models, the Newtonian approximation, and convective adjustment.

I have enjoyed many conversations with Pablo Zurita. He had particularly insightful thoughts on the nature of subcritical instability and the reason that molecular effects are relatively unimportant in the radiative-convective model in Chapter 4.

Gerard Roe carefully proofread and gave comments on this thesis.

Brian Arbic gave advice on several talks based on this thesis.

I greatly appreciate the help that these people and others not mentioned here have given me.

I would also like to acknowledge the fact that this research received financial support from the Department of Energy, which in turn receives support from American taxpayers.

Contents

List of Figures

List of Tables

Chapter 1

Introduction and Background

This work seeks to better understand radiative-convective equilibrium states through the use of idealized models. The goal is to develop physical intuition about how convection responds to changes in radiative forcing. The physical questions that we discuss are posed in the introductory sections of Chapters 2, 3, and 4. This thesis focuses on the effects of thermal radiation on dry convection and omits moist processes such as latent heating and cloud albedo. This omission enables us to obtain simple results, some of which may reasonably be supposed to hold in the earth's atmosphere. To investigate the behaviors of our radiative-convective models, we employ both theory and numerical computation, both stability analyses and analyses of weak convection.

The thesis is organized as follows. Chapter 2 discusses the linear and nonlinear stability properties of a dry radiative-convective system which resembles Rayleigh-Bénard convection, except that thermal radiation is included. Such a system can be studied via laboratory experiments. Chapter 3 discusses the linear and nonlinear stability properties of a dry radiative-convective model which more nearly represents atmospheric convection. Chapter 4 uses essentially the same radiative-convective model as Chapter 3 to find scaling laws for a weakly nonlinear convecting system. Chapter 5 provides a brief summary and discussion.

One topic of great current interest, which is not covered in this thesis, is the topic of convective feedbacks in moist atmospheres. These feedbacks are important to understanding how a climate responds to a perturbation in radiative forcing (e.g. a doubling of carbon dioxide). Since this thesis is restricted to dry convection, it can only make tangential remarks about moist feedbacks. However, we do discuss how dry convection responds to perturbations in radiative forcing, a question which is intimately related to the question of feedbacks. Therefore, to help motivate the analysis in this thesis, we mention two examples of feedbacks here. First, most general circulation models (GCMs) predict that if the atmosphere warmed, the relative humidity of the atmosphere would remain approximately constant, leading to an increase in specific humidity and a consequent amplification of the warming. This is called the water vapor feedback. It is the strongest feedback mechanism in most GCMs. However, Lindzen (1994) has noted that meteorologists have a poor understanding of the processes by which convection transports water to the upper troposphere. For this reason, he challenges the reliability of GCMs' predictions of warming. Second, most GCMs predict that a warming is associated with a decrease in cloud cover (Del Genio et al. 1996; Cess et al. 1990). Since clouds have a net cooling effect, the decrease in cloud cover is a positive feedback. This is the so-called cloud-cover feedback. Del Genio et al. (1996) has commented that there is no theoretical understanding of the sign of this feedback.

The remainder of this chapter provides some background on the theoretical methods used in this thesis and prior applications of these methods to Rayleigh-Bénard convection. (In Rayleigh-Bénard convection, fluid is contained between upper and lower plates held at constant temperatures. No radiation is present.) Many of these methods have never, to the author's knowledge, been applied to radiative-convective models.

Pellew and Southwell (1940) proved that convection in the Rayleigh-Bénard system arises as overturning cells which grow monotonically in amplitude, not as an oscillatory instability. That is,

they proved 'exchange of stabilities.' Therefore the linear modes in Rayleigh-Bénard convection do not resemble the overstable waves which can arise in an unstable system with a restoring force; nor do the modes propagate, like precipitating linear modes (Emanuel 1994, p. 344). Thus exchange of stabilities tells us something about the physical nature of incipient convection. Proving exchange of stabilities also facilitates numerical computation of linear modes, because it enables us to assume that the growth rate for marginal modes has no imaginary part.

The Rayleigh-Bénard linear stability problem for free-slip boundaries was solved by Rayleigh (1916). He found that the critical threshold for linear stability is determined by the so-called Rayleigh number Ra. Above the critical Rayleigh number, at least one mode grows, even if initially it is only infinitesimal in amplitude. It is easy to forget how remarkable it is that the critical threshold is determined by a single parameter (although dimensional analysis alone indicates that the threshold can depend on at most two parameters, the Rayleigh and Prandtl numbers). The Rayleigh number contains within it the separate influences of viscosity, layer depth, and the other relevant dimensional parameters.

A stability method that complements linear stability analysis is the energy method. The energy method determines a threshold below which all perturbations decay to zero, regardless of their initial magnitude. Below the energy stability critical threshold, all disturbances decay; above the linear stability critical threshold, all disturbances which project onto the unstable mode grow; between the two thresholds, finite-amplitude perturbations may or may not grow. In the case of Rayleigh-Bénard convection, Joseph (1965) showed that the energy and linear stability thresholds coincide. Therefore subcritical instabilities are prohibited.

In addition to the extensive stability analyses of Rayleigh-Bénard convection, several other stability problems with relevance to atmospheric convection have been performed. For instance, Emanuel (1994, Chapter 12) has studied the stability of an atmosphere to slantwise convection. He shows that a parcel may be unstable to sloping displacements even though the parcel is stable to both vertical and horizontal displacements. To cite another example, Ingersoll (1964) and others have studied the effects of vertical shear on convective instability. However, the stability problem for a radiative-convective atmosphere has not been previously posed. This is perhaps because atmospheric convection, when it does occur, is extremely turbulent, and hence might be expected to bear little relation to marginal modes. This thesis argues that the linear stability problem does shed some light on weakly nonlinear convection and perhaps on strongly nonlinear convection as well.

Useful theoretical techniques have been developed to study supercritical Rayleigh-Bénard convection. Herring (1963) introduced an approximation to the Boussinesq equations called the 'mean field approximation.' To derive the mean field equations, certain nonlinear terms are dropped and others are retained, so that the resulting approximation is valid for weakly nonlinear, high-Prandtl-number convection. The mean field approximation has been used to study penetrative convection (Musman 1968) and time-dependent convective flows (Elder 1969), but recently the approximation seems to have fallen into disuse. Presumably this is because present-day computers are capable of computing weakly nonlinear flows directly, thereby obviating approximate solutions. However, we are interested in deriving scaling laws, which requires performing many computations with the external parameters varied. The mean field equations are useful for us because they reduce to a system which is one-dimensional and hence fast to compute.

Another theoretical technique that has been applied with success to Rayleigh-Bénard convection is mixing length theory. Mixing length theory has addressed the question, How does the nondimensionalized heat flux, or Nusselt number Nu, scale with the Rayleigh number? Kraichnan (1962) hypothesized, on the basis of mixing length theory, that for very high Rayleigh number, one finds $Nu \sim Ra^{1/2}$, with a logarithmic correction. This is the scaling law which renders the dimensional heat flux independent of molecular viscosity or diffusivity, for fixed Prandtl number. Experimental observations of this scaling have been claimed by Chavanne et al. (1997). Other authors, studying systems at lower, but still large, Rayleigh numbers, have obtained the scaling $Nu \sim Ra^{2/7}$ (see Siggia 1994).

Mixing length theory and dimensional analysis have also been used to some extent in meteorological convection problems. An example is Monin-Obukhov theory, which describes the relative contributions of shear and convection to the generation of turbulence in the atmospheric boundary

layer. Another example is the 'Prandtl layer.' Prandtl (1932) proposed velocity and buoyancy scales for a dry, semi-infinite layer which is cooled at a constant rate while the lower boundary is fixed at a constant temperature (see also Emanuel, 1994, pp. 89–91). Priestley (1959) and Deardorff (1970) have suggested similar scales for the dry atmospheric boundary layer. The velocity scale proposed by Prandtl, Priestley, and Deardorff increases monotonically with altitude. This scaling must fail near the top of the convecting layer. This thesis uses mixing length theory to construct a velocity scale which increases with height in the lower part of the convecting layer, reaches a maximum, and then decreases with increasing altitude.

The theoretical and numerical methods that we have just introduced are the ones that will be employed in this thesis to investigate several dry radiative-convective models.

Chapter 2

The Effects of Thermal Radiation on a Laboratory Model

2.1 Introduction

Rayleigh-Bénard convection has attracted much attention among fluid dynamicists because it serves as a simple paradigm of fluid mechanical stability and turbulence. Meteorologists, however, have not devoted much attention to Rayleigh-Bénard convection, primarily because it suffers from several shortcomings as a model of atmospheric convection. The limitation which this chapter addresses is that Rayleigh-Bénard convection does not include thermal radiative transfer, whereas in a radiative-convective atmosphere, radiation largely determines the radiative equilibrium basic state and also damps temperature perturbations. Many simple linear and nonlinear stability results for Rayleigh-Bénard convection have been established (see e.g. Drazin and Reid 1981; Joseph 1965). This chapter derives some equally simple linear and nonlinear stability properties for two idealized fluid mechanical systems in which thermal radiation is added to Rayleigh-Bénard convection. Our goal is to improve physical intuition about the effects of thermal radiative transfer on convection.

In a seminal paper, Goody (1956a) studied the linear stability of a fluid layer which, like Rayleigh-Bénard convection, is confined between parallel plates at specified temperatures, but which is subject to thermal radiative transfer. The atmosphere has no analog to an upper plate at which temperature is fixed, but Goody's model has some advantages over a more faithful model of the atmosphere. First, theoretical predictions for the model can be tested by laboratory experiments, as demonstrated by Gille and Goody (1964). Second, results from Goody's model can be compared directly with those from Rayleigh-Bénard convection, thereby isolating the effects of thermal radiative transfer on convective stability. Goody noted that radiation introduces primarily two new effects on the onset of Rayleigh-Bénard convection. First, radiative damping tends to diminish temperature perturbations. Second, radiation causes the basic state temperature profile in the interior of the domain to have a more stable lapse rate. Both are stabilizing influences. (In the earth's atmosphere, on the contrary, thermal radiation tends to set up a radiative equilibrium basic state which is convectively unstable.)

Goody (1956a) used a variational technique and a grey, two-stream radiative model to find the critical conditions for linear stability in the limits of optically thin and thick gases, for free-slip, optically black boundaries. Following papers treated more realistic systems and made further calculations. Spiegel (1960) considered the full range of optical depths, proved exchange of stabilities for a linear basic state temperature profile $\bar{T}$, and introduced an approximate stability criterion in the form of a radiative Rayleigh number. Christophorides and Davis (1970) studied the separate contributions of the basic state temperature profile and radiative damping to convective stability, and made calculations of the vertical heat flux when convection ensues. Arpaci and Gőzűm (1973) considered the effects of nongrey fluids and boundary emissivities. Bdéoui and Soufiani (1997) provide a sophisticated treatment of nongrey fluids and also a short review of prior work. Vincenti and Traugott (1971) review the early work.

Since our goal is to gain physical intuition, we eschew the trend toward more elaborate models. Instead, we study idealized models which have grey, transparent, Boussinesq fluids and black, free-slip boundaries. In the first model, we simplify Goody's model by setting the thermal diffusivity κ to zero, in order to permit a complete analytic stability analysis. In the second model, we allow $\kappa \neq 0$, which is Goody's model. It turns out that when $\kappa \to 0$, we recover several of the $\kappa = 0$ results, thereby indicating that the simple $\kappa = 0$ results have relevance to the more realistic case when thermal diffusivity is present.

This chapter contributes to prior work in two main areas. First, we show that when $\kappa = 0$, the linear stability threshold is exactly determined by a single parameter, a radiative Rayleigh number, which resembles the Rayleigh number used to characterize the onset of Rayleigh-Bénard convection. The radiative Rayleigh number also turns out to be a useful concept when thermal diffusivity is small but nonzero. Second, we find a threshold below which the system is stable to any perturbations, regardless of magnitude; below this threshold, the basic state is monotonically stable. When $\kappa = 0$, we prove that no subcritical instabilities can exist, as in Rayleigh-Bénard convection (Joseph 1965).

2.2 Governing Equations

Both models that we study consist of a horizontally infinite slab of fluid bounded by upper and lower solid, free-slip boundaries. Although our models are more appropriate to a laboratory flow than a meteorological flow, meteorological applications motivate the choice of parameter values in some of our calculations. A non-zero adiabatic lapse rate $\Gamma_* = g_*/c_{p*}$ is included in the equations because the lapse rate is significant in the atmosphere. (In this thesis, subscript asterisks shall denote dimensional quantities.) Thermal radiation is absorbed but not scattered by the fluid. Solar radiation is neglected. We assume the fluid is radiatively grey — that is, its optical properties are taken to be independent of the wavelength of radiation — even though atmospheric gases are nongrey. This assumption is somewhat unrealistic because it restricts the fluid to one radiative length scale, the photon mean free path. However, the assumption of a grey gas greatly simplifies the radiative transfer equation. We consider only transparent fluid layers, that is, fluid layers with small optical depth. This is the limit which interests us in part because the formula we finally employ for perturbation radiative heating rates (2.12) is mathematically similar to a common meteorological approximation for nongrey atmospheric gases which can emit to space.

Following Spiegel and Veronis (1960), we adopt the Boussinesq approximation for an ideal gas, valid when the depth of the system h_* is much less than the scale heights of pressure, density and temperature, and when the motion-induced fluctuations in pressure and density are less than or equal to the corresponding variations in the basic state. In the Boussinesq approximation, the momentum equation is

$$\frac{\partial \mathbf{v}_*}{\partial t_*} + \mathbf{v}_* \cdot \nabla \mathbf{v}_* = -\frac{1}{\rho_*} \nabla_* p'_* + g_* \alpha_{T*} T'_* \mathbf{k} + \nu_* \nabla_*^2 \mathbf{v}_*, \tag{2.1}$$

where $\mathbf{v}_*$ is the velocity, T'_* the temperature perturbation from the basic state temperature $\bar{T}_*$, p'_* the pressure perturbation, t_* the time, ρ_* a constant reference density, α_{T*} the constant volume coefficient of expansion, $\mathbf{k}$ the unit vertical vector, ν_* the kinematic viscosity, and g_* the gravitational constant. The momentum equation remains entirely unaltered by radiation. The heat equation becomes

$$\frac{\partial T_*}{\partial t_*} + \mathbf{v}_* \cdot \nabla_* T_* + w_* \Gamma_* = -\frac{1}{\rho_* c_{p*}} \nabla_* \cdot \mathbf{F}_* + \kappa_* \nabla_*^2 T_*. \tag{2.2}$$

Here $T_* = \bar{T}_* + T'_*$ is the total temperature, w_* the vertical component of $\mathbf{v}_*$, $\mathbf{F}_*$ the flux of radiative energy, c_{p*} the specific heat at constant pressure, $\Gamma_* = g_*/c_{p*}$ the adiabatic lapse rate, and κ_* the thermal diffusivity. In the Boussinesq approximation, the continuity equation becomes

$$\nabla_* \cdot \mathbf{v}_* = 0. \tag{2.3}$$

An equation governing the radiative flux $\mathbf{F}_*$ can be derived via the Eddington approximation, as in Goody and Yung (1989) or Goody (1956a). The result is

$$\nabla_* \frac{1}{\alpha_*} \nabla_* \cdot \mathbf{F}_* - 3\alpha_* \mathbf{F}_* = 4\nabla_* \sigma_* T_*^4, \tag{2.4}$$

where α_* is the coefficient of absorption of radiation per unit volume, and σ_* is the Stefan-Boltzmann constant.

We nondimensionalize these equations with the following scales:

$$\mathbf{v}_* = \frac{h_*}{t_{T_{m*}}} \mathbf{v} \qquad T_* = \mathcal{T}_* T \qquad \mathbf{F}_* = \frac{16}{3} \sigma_* T_{m*}^3 \mathcal{T}_* \mathbf{F}$$

$$p'_* = g_* \alpha_{T*} \mathcal{T}_* \rho_* h_* p' \qquad \mathbf{x}_* = h_* \mathbf{x} \qquad \frac{1}{t_*} = \frac{1}{t_{T_{m*}}} \frac{1}{t},$$

where

$$t_{T_{m*}} \equiv \frac{3}{16} \frac{\rho_* c_{p*} h_*}{\sigma_* T_{m*}^3},$$

and T_{m*} is the basic state temperature $\bar{T}$ evaluated at the midpoint of the layer. The length scale h_* is the depth of the fluid layer, the time scale $t_{T_{m*}}$ is a radiative cooling time scale, and the velocity scale is the velocity of a parcel which travels a distance h_* in a time $t_{T_{m*}}$. All temperatures are nondimensionalized with the temperature scale $\mathcal{T}_*$, which can be freely specified as convenient. Unless otherwise noted, this chapter shall set $\mathcal{T}_* = T_{L*} - T_{U*}$, where T_{L*} is the temperature of the lower plate and T_{U*} is the temperature of the upper plate. The nondimensionalized momentum, heat, continuity, and radiative transfer equations are, respectively,

$$\chi \frac{\partial \mathbf{v}}{\partial t} + \chi \mathbf{v} \cdot \nabla \mathbf{v} = -\gamma \nabla p' + \gamma \, T' \mathbf{k} + \nabla^2 \mathbf{v}, \tag{2.5}$$

$$\frac{\partial T}{\partial t} + \mathbf{v} \cdot \nabla T + w\Gamma = -\nabla \cdot \mathbf{F} + \kappa \nabla^2 T, \tag{2.6}$$

$$\nabla \cdot \mathbf{v} = 0, \tag{2.7}$$

and

$$\nabla \frac{1}{\alpha} \nabla \cdot \mathbf{F} - 3\alpha \mathbf{F} = 3\nabla T, \tag{2.8}$$

where we have linearized the thermal source function on the right-hand side of the radiation equation (2.8). The specified dimensionless constants and functions which govern the behavior of the system are defined as follows:

$$\gamma = \frac{g_* \alpha_{T*} \mathcal{T}_* h_*^3}{\nu_* \left(h_*^2 / t_{T_{m*}}\right)} \qquad \kappa = \frac{\kappa_*}{h_*^2 / t_{T_{m*}}} \qquad \Gamma = \frac{\Gamma_*}{\mathcal{T}_* / h_*} = \frac{g_* / c_{p*}}{\mathcal{T}_* / h_*}$$

$$\alpha = \alpha_* h_* \qquad \chi = \frac{16 \sigma_* T_{m*}^3 h_*}{3 \rho_* c_{p*} \nu_*} = \frac{h_*^2 / t_{T_{m*}}}{\nu_*}.$$

Here γ is a coefficient, akin to a Rayleigh number, which multiplies the buoyancy term in the momentum equation. κ is a nondimensional thermal diffusivity which measures the strength of thermal diffusivity relative to a 'radiative diffusivity' h_*^2 / t_{Tm*}. For a typical dry atmospheric boundary layer of depth $h_* = 1$ km and $T_{m*} = 285$ K, $\kappa \sim 3 \times 10^{-6}$; a typical laboratory value is $\kappa \sim 0.1$. Therefore this chapter selects values of κ which range from very low values to moderate values. Γ is a dimensionless adiabatic lapse rate. α represents the number of photon mean free paths per layer depth, at the local value of α_*. When $\alpha = \alpha_c$ is constant, then α_c is simply the optical depth of the layer.

The quantity χ is an inverse radiative Prandtl number which turns out not to enter our analysis, since it only multiplies time-dependent and nonlinear terms.

We choose solid, free-slip, constant-temperature boundaries located at $z = \pm 1/2$. This leads to the boundary conditions (Drazin and Reid 1981):

$$w|_{z=\pm 1/2} = \left.\frac{\partial^2 w}{\partial z^2}\right|_{z=\pm 1/2} = 0.$$

When $\kappa \neq 0$,

$$T'|_{z=\pm 1/2} = 0.$$

2.3 Linear Stability Equations

We postulate a basic state in which $\mathbf{v} = 0$, and in which the temperature $\bar{T} = \bar{T}(z)$, radiative flux $\overline{\mathbf{F}} = \bar{F}_z(z)\mathbf{k}$, and radiative absorption coefficient $\alpha = \alpha(z)$ are functions of z alone. Substituting these forms into the heat equation (2.6) and the radiative transfer equation (2.8) leads to, respectively,

$$0 = -\frac{d\bar{F}_z}{dz} + \kappa \frac{d^2\bar{T}}{dz^2} \tag{2.9}$$

and

$$\frac{d}{dz}\frac{1}{\alpha}\frac{d\bar{F}_z}{dz} - 3\alpha\bar{F}_z = 3\frac{d\bar{T}}{dz}. \tag{2.10}$$

Subtracting the basic state radiative equation (2.10) from the full radiative equation (2.8), we obtain an equation for the perturbation radiative flux $\mathbf{F}'$

$$\nabla\frac{1}{\alpha}\nabla\cdot\mathbf{F}' - 3\alpha\mathbf{F}' = 3\nabla T'. \tag{2.11}$$

For transparent fluid layers — more specifically, those with $\alpha^2 \ll a^2$, where a is the wavenumber of the unstable mode under consideration — we may neglect the $3\alpha\mathbf{F}'$ term. Consequently

$$\nabla\cdot\mathbf{F}' \cong 3\alpha T'. \tag{2.12}$$

The integration constant has been set to zero because a zero temperature perturbation requires that there be no perturbative contribution to the radiative cooling. Equation (2.12) is the Newtonian approximation (Goody 1995). This limit is of interest to meteorologists because, although our derivation is for a transparent grey gas, the Newtonian approximation is also a common meteorological approximation for nongrey, noncloudy atmospheres. In these cases the perturbation radiative heating is dominated by the cooling-to-space contribution, and the divergence of the perturbation radiative flux is again proportional to T', as shown by Goody (1995).

We obtain a perturbation temperature equation upon subtracting the basic state heat equation (2.9) from the full heat equation (2.6), using the Newtonian approximation (2.12), and linearizing:

$$\frac{\partial T'}{\partial t} + w\left(\frac{d\bar{T}}{dz} + \Gamma\right) = -3\alpha T' + \kappa\nabla^2 T'. \tag{2.13}$$

Applying the operator $\mathbf{k}\cdot\nabla\times\nabla\times$ to the momentum equation (2.5) and linearizing yields

$$\chi\frac{\partial}{\partial t}\nabla^2 w = \gamma\nabla_h^2 T' + \nabla^2\nabla^2 w, \tag{2.14}$$

where $\nabla_h^2 \equiv (\partial^2/\partial x^2 + \partial^2/\partial y^2)$ is the horizontal Laplacian. We have used the continuity equation (2.7) here. Eliminating T' from (2.14) and the linearized heat equation (2.13) leaves an equation for w alone:

$$\left(\frac{\partial}{\partial t} + 3\alpha - \kappa\nabla^2\right)\left(\chi\frac{\partial}{\partial t} - \nabla^2\right)\nabla^2 w = -\left(\frac{d\bar{T}}{dz} + \Gamma\right)\gamma\nabla_h^2 w \tag{2.15}$$

We seek normal mode solutions of the form

$$w = Re\left\{W(z)f(x,y)e^{st}\right\} \qquad T' = Re\left\{\Theta'(z)f(x,y)e^{st}\right\} \tag{2.16}$$

where

$$\nabla_h^2 f(x,y) = -a^2 f(x,y),$$

and a is a real, nondimensionalized horizontal wavenumber. Linear stability analysis leaves the planform of convection, which is described by $f(x,y)$, undetermined. In general, s can be complex: $s = \sigma + i\omega$, where the growth rate σ is a real constant and so is ω. Substituting the modal forms (2.16) into the linear equations for w (2.14) and T' (2.13) yields, respectively,

$$\chi s(D^2 - a^2)W = -\gamma\, a^2\Theta' + (D^2 - a^2)^2 W \tag{2.17}$$

and

$$s\Theta' = -W\left(\frac{d\bar{T}}{dz} + \Gamma\right) - 3\alpha\Theta' + \kappa(D^2 - a^2)\Theta', \tag{2.18}$$

where the operator $D \equiv d/dz$. Likewise, substituting the modal form (2.16) for w into the linear stability equation (2.15) yields

$$\left(s + 3\alpha - \kappa(D^2 - a^2)\right)\left(\chi s - (D^2 - a^2)\right)\left(D^2 - a^2\right)W(z) = \left(\frac{d\bar{T}}{dz} + \Gamma\right)\gamma\, a^2\, W(z). \tag{2.19}$$

Mathematically, radiation enters the equation through the radiative damping term 3α and the basic state temperature gradient $d\bar{T}/dz$.

Exchange of stabilities holds if it is true that whenever the growth rate $\sigma = 0$, also $\omega = 0$. In this case convection arises as overturning cells whose amplitude increases monotonically in time. Alternatively, if $\omega \neq 0$ as σ approaches zero, then oscillatory instability or overstability sets in (Drazin and Reid, 1981). If exchange of stabilities holds for our system, we may set $\sigma = 0$ in our linear stability analysis, thereby speeding up numerical calculations.

We are interested in the case in which $\alpha \equiv \alpha_c$ is constant, and free-slip constant-temperature boundary conditions are imposed. Murgai and Khosla (1962) study exchange of stabilities for a system which is like ours, but in addition includes a vertical magnetic field. Exchange of stabilities for our problem follows if the magnetic field in their analysis is set to zero. One difficulty in proving exchange of stabilities is the fact that when radiation is introduced into the convection problem, the basic state temperature profile $\bar{T}(z)$ is no longer linear. A key to Murgai and Khosla's proof is to eliminate the Θ' variable and restrict the appearance of $d\bar{T}/dz$ to a term which can be seen by inspection to have no imaginary part. Spiegel (1962) and Veronis (1963) also illustrate this technique. In a similar manner, one can prove exchange of stabilities when $\kappa = 0$, for free-slip and no-slip boundaries. When $\kappa = 0$, the boundary conditions on temperature are dropped.

2.4 Linear Stability with no Thermal Diffusivity

In this section, we explore a minimal radiative-convective model. We let $\alpha \equiv \alpha_c$ be a constant and neglect the thermal diffusivity of heat entirely by setting $\kappa = 0$. All damping of temperature perturbations is then due to radiation. These approximations simplify the system sufficiently to permit a complete analytic solution for the linear stability problem. A similar analysis for a highly idealized atmospheric radiative-convective model is given in Chapter 3. A later section in the present chapter shows that when κ is small but non-vanishing, the critical condition for linear stability

approaches that for the $\kappa = 0$ case. The $\kappa = 0$ results constitute an important limiting case, because in the atmosphere, thermal diffusive damping is much smaller than radiative damping.

First we find the basic state for the linear stability analysis. The basic state heat equation (2.9) implies that

$$\bar{F}_z = F_T,$$

where F_T is a constant which must be determined by the boundary conditions on $\bar{F}_z$. Inserting this relation into the basic state radiation equation (2.10) yields the basic state temperature gradient

$$\frac{d\bar{T}}{dz} = -\alpha_c F_T \equiv -(T_l - T_u), \tag{2.20}$$

where T_l and T_u denote the (nondimensionalized) temperatures of the fluid adjacent to the lower and upper boundaries, respectively. The temperature decreases linearly with altitude. Such a simple profile would not have resulted if we had not linearized the radiative equation (2.8).

We formulate radiative boundary conditions following the procedure in Goody (1995, pp. 114–115). Assuming that the temperature difference across the layer is small and that the Eddington approximation holds, we obtain, for the upper and lower boundaries respectively,

$$T_U - T_u = -\frac{2}{3}\bar{F}_z\Big|_{z=1/2} = -\frac{2}{3}F_T \tag{2.21}$$

and

$$T_L - T_l = \frac{2}{3}\bar{F}_z\Big|_{z=-1/2} = \frac{2}{3}F_T. \tag{2.22}$$

We have specified the (nondimensionalized) temperatures of the upper and lower boundaries to be T_U and T_L respectively. There are discontinuities in temperature at the boundaries.

We may now solve for F_T and $d\bar{T}/dz$ using equations (2.20), (2.21), and (2.22). F_T is given by

$$F_T = \frac{\frac{3}{4}}{1 + \frac{3}{4}\alpha_c}. \tag{2.23}$$

Substituting F_T into expression (2.20) for $d\bar{T}/dz$, we find

$$\frac{d\bar{T}}{dz} = -\frac{\frac{3}{4}\alpha_c}{1 + \frac{3}{4}\alpha_c}. \tag{2.24}$$

Recall that $T_L - T_U \equiv 1$. The smaller the optical depth, the smaller the magnitude of $d\bar{T}/dz$. Hence smaller optical depths imply more stable basic states.

We now find the marginally stable modes when $\alpha = \alpha_c$ is constant and the thermal diffusivity is neglected. Since exchange of stabilities holds, $s = 0$ at the onset of instability. Also recall that we are assuming that $\kappa = 0$. Hence the stability equation (2.19) for W becomes

$$3\alpha_c \left(D^2 - a^2\right)^2 W(z) = -\left(\frac{d\bar{T}}{dz} + \Gamma\right) \gamma\, a^2\, W(z). \tag{2.25}$$

As in Rayleigh-Bénard convection, the eigenfunctions are sinusoidal:

$$W(z) = \cos \pi z, \tag{2.26}$$

$$\Theta'(z) = \frac{(\pi^2 + a^2)^2}{\gamma\, a^2} \cos \pi z. \tag{2.27}$$

Substituting this form for $W(z)$ into the stability equation (2.25) yields a critical condition on $\gamma = \gamma_m$ for marginal stability,

$$-\left(\frac{d\bar{T}}{dz}+\Gamma\right)\frac{\gamma_m}{3\alpha_c}=\frac{\left(\pi^2+a^2\right)^2}{a^2}.$$

Whereas the classical Rayleigh-Bénard system first goes unstable at $a=\pi/\sqrt{2}$ (Drazin and Reid 1981), our system does so at a shorter wavelength corresponding to $a=\pi$. Therefore, the critical value of $\gamma=\gamma_C$ is

$$-\left(\frac{d\bar{T}}{dz}+\Gamma\right)\frac{\gamma_C}{3\alpha_c}=4\pi^2. \tag{2.28}$$

In the critical condition, all the individual governing parameters — γ_C, α_c, and $-(\frac{d\bar{T}}{dz}+\Gamma)$ — are conveniently lumped together into one factor on the left-hand side. This factor can be interpreted as a radiative Rayleigh number

$$Ra_R=-\left(\frac{d\bar{T}}{dz}+\Gamma\right)\frac{\gamma}{3\alpha_c}$$

with critical value $Ra_{RC}=4\pi^2$. If we define a radiative diffusivity

$$\kappa_{R*}\equiv\frac{16\sigma_* T_{m*}^3\alpha_{c*}h_*^2}{\rho_* c_{p*}}=\nu_* 3\alpha_c\chi$$

and a lapse rate difference from adiabatic

$$\beta_*=\frac{\frac{3}{4}\alpha_{c*}h_*}{1+\frac{3}{4}\alpha_{c*}h_*}\frac{(T_{L*}-T_{U*})}{h_*}-\frac{g_*}{c_{p*}},$$

then the radiative Rayleigh number becomes

$$Ra_R=\frac{g_*\alpha_{T*}\beta_* h_*^4}{\nu_*\kappa_{R*}}=\frac{g_*\alpha_{T*}\left(\frac{\frac{3}{4}\alpha_{c*}h_*}{1+\frac{3}{4}\alpha_{c*}h_*}\frac{(T_{L*}-T_{U*})}{h_*}-\frac{g_*}{c_{p*}}\right)h_*^4}{\nu_*\frac{16\sigma_* T_{m*}^3\alpha_{c*}h_*^2}{\rho_* c_{p*}}}. \tag{2.29}$$

Despite the complexity introduced by radiation, the critical condition depends on only one parameter, as in Rayleigh-Bénard convection. This parameter, Ra_R, is like the standard Rayleigh number, except that β_* is the *interior* temperature gradient (which does not include the temperature jumps at the boundaries) and κ_{R*} is a radiative diffusivity, not the thermal diffusivity. Spiegel (1960) used an approximate variational technique and physical arguments to derive and interpret a similar radiative Rayleigh number. Goody (1964, pp. 358–360) also discusses a similar radiative Rayleigh number.

One can assess the effect of any dimensional parameter on the linear stability threshold by inspecting Ra_R. For instance, an increase in T_{m*} leads to a stabilizing increase in the radiative diffusivity κ_{R*} but has no effect on the lapse rate parameter β_*, because we have specified the temperature on the boundaries. Also, increasing α_{c*} leads to a stabilizing linear increase in κ_{R*} but also leads to a more unstable β_*. The net effect depends on the lapse rate g_*/c_{p*}.

2.5 Linear Stability with Thermal Diffusivity

When $\kappa=0$, a temperature profile may be stable even though there are temperature discontinuities in the unstable sense at the boundaries. The temperature discontinuities do not lead to instability because there exists no thermal diffusivity to communicate heat from the boundaries to the adjacent fluid. When a small amount of thermal diffusivity is added, however, one might suppose that the solutions change fundamentally. After all, $\kappa=0$ multiplies the highest derivative in the heat equation (2.6). Therefore, $\kappa\to 0$ is a singular limit. It turns out, however, that in many cases the addition of a small but nonzero thermal diffusivity term does not qualitatively alter either the threshold for marginal stability γ_m or the vertical velocity linear modes. But the addition of a small

amount of thermal diffusivity does not leave the entire solution qualitatively unchanged. Rather, the temperature perturbation linear modes Θ' develop thin boundary layers. To show this, we now permit non-zero values of κ. We also set $\alpha = \alpha_c =$ constant. This is the problem first studied in the seminal paper by Goody (1956a).

Goody (1956a) derived boundary conditions on radiation using the assumption that thermal diffusivity causes temperatures infinitesimally close to the boundaries to equal the temperatures of the boundaries themselves. The conditions are:

$$\left.\frac{d\bar{F}_z}{dz}\right|_{z=1/2} = -2\alpha_c \left.\bar{F}_z\right|_{z=1/2} \qquad \left.\frac{d\bar{F}_z}{dz}\right|_{z=-1/2} = 2\alpha_c \left.\bar{F}_z\right|_{z=-1/2}. \tag{2.30}$$

With these conditions, Goody (1956a) derived the following basic state temperature profile:

$$\frac{d\bar{T}}{dz} = -L\cosh\lambda z - M \tag{2.31}$$

$$\bar{F}_z = \kappa\left(-L\cosh\lambda z + \frac{1}{\kappa\alpha_c}M\right)$$

where

$$L \equiv \frac{1}{\kappa\alpha_c}\left[\frac{2}{\kappa\alpha_c\lambda}\sinh\frac{1}{2}\lambda + \frac{1}{2}\frac{\lambda}{\alpha_c}\sinh\frac{1}{2}\lambda + \cosh\frac{1}{2}\lambda\right]^{-1},$$

$$M \equiv L\kappa\alpha_c\left(\frac{1}{2}\frac{\lambda}{\alpha_c}\sinh\frac{1}{2}\lambda + \cosh\frac{1}{2}\lambda\right) = 1 - \frac{2L}{\lambda}\sinh\frac{1}{2}\lambda,$$

and

$$\lambda^2 \equiv 3\alpha_c^2\left(1 + \frac{1}{\kappa\alpha_c}\right).$$

Figure 2-1 shows sample basic state temperature profiles for $\kappa \neq 0$, along with one profile for $\kappa = 0$ (thick dashed line). When $\kappa \to 0$, the shape of $\bar{T}$ approaches that for the $\kappa = 0$ case, in which the boundary layers have zero thickness, i.e. are discontinuities. More specifically, when thermal diffusion of features of scale h_* is much weaker than radiative damping (i.e. $\kappa/3\alpha_c \ll 1$), and the layer is transparent (i.e. $\alpha_c \leq 1$), the fraction of the layer occupied by the boundary layers goes as $\sqrt{\kappa/3\alpha_c}$. Furthermore, when $\kappa \to 0$, the value of $d\bar{T}/dz$ in the middle of the convecting region tends toward the interior value of $d\bar{T}/dz$ when $\kappa = 0$. As α_c decreases, radiation tends to stabilize the profile in the interior more strongly, leaving strongly superadiabatic gradients near the boundaries. In the opposite limit, when thermal diffusivity dominates radiative damping, $\bar{T}$ reduces to the linear profile of Rayleigh-Bénard convection.

We now compute the linear eigenmodes and the marginal Rayleigh number $Ra_m = \gamma_m/\kappa$. Because of exchange of stabilities, we may set $s = 0$ in the linear stability equation for W (2.19):

$$\left((D^2 - a^2) - 3\alpha_c/\kappa\right)\left(D^2 - a^2\right)^2 W(z) = Ra\left(\frac{d\bar{T}}{dz} + \Gamma\right)a^2\, W(z). \tag{2.32}$$

Given values of α_c, κ, and a^2, we compute all eigenmodes $W(z)$ and eigenvalues Ra_m numerically and select the least eigenvalue. Details of the numerical method can be found in the appendix to Chapter 2. Similar numerical calculations have also been performed by Getling (1980), but he did not examine the Θ' profiles. Numerical computations yield the shape of the eigenmodes explicitly. This is an advantage over the variational method used in most past studies, in which the eigenvalues are computed using a guess or series expansion for the eigenmodes.

The eigenvalues Ra_m are plotted versus a^2 in Figure 2-2. In all our numerical work, we have set $\Gamma = 0$. When κ is small, then the minimum of $Ra_m(a^2)$ usually occurs near the wavenumber $a^2 = \pi^2$, as for the $\kappa = 0$ case. When κ is larger, the curve $Ra_m(a^2)$ reduces to that for Rayleigh-Bénard

convection, with a minimum Ra_C at $a^2 = \pi^2/2$.

Some curves contain a kink at higher wavenumbers. This kink is associated with a change in the vertical structure of the eigenmodes. Goody (1956a) hypothesized that the eigenmodes in w might take one of two shapes: a sinusoidal shape which penetrates the full layer depth, as suggested by the eigenmodes of Rayleigh-Bénard convection; or a shape which is concentrated near the boundaries, where the temperature gradients are strongly superadiabatic. Getling (1980) showed that both types of modes are realized, depending on the values of the external parameters and the wavenumber. Our calculations agree. In Figure 2-2, all points with small wavenumbers ($a^2 \lesssim \pi^2$) correspond to eigenfunctions with approximately sinusoidal w. (If Γ were nonzero, a stably stratified region might result in the interior, preventing the mode from penetrating the full layer; however, we have set $\Gamma = 0$ in these calculations.) At some wavenumber $a^2 \gtrsim \pi^2$, often near a kink in the marginal stability curve, a transition region of about an order of magnitude or two in a^2 exists. By the time $a^2 = 10^5$ has been reached, w exhibits boundary layers for all cases. As an illustration of this, Figure 2-3 displays numerically-calculated eigenmodes for three wavenumbers along the marginal stability curve corresponding to $\alpha_c = 0.1$ and $\kappa = 10^{-6}$ in Figure 2-2b. The first eigenmode has a wavenumber at the global minimum of Ra_m, the second has a wavenumber near the kink in the curve, and the third has a wavenumber at the local minimum in Ra_m at high wavenumbers. The solid curves represent a sinusoidal approximation (2.26) for W and a corresponding approximation (2.33) for Θ' discussed below.

Long wavelength modes prefer to traverse the full layer from bottom to top. On the contrary, the short-wavelength modes prefer to form two separate overturning layers near the boundaries, rather than form tall, skinny cells which penetrate the full layer. When the modes confine themselves near the boundaries, they can enjoy the superadiabatic temperature gradient there. For certain parameter values, e.g. $\alpha_c = 0.002$ and $\kappa = 5 \times 10^{-8}$, the boundary-layer motions become unstable much sooner than the sinusoidal motions (not shown). The change in form of the most unstable mode was suggested by Goody (1956a) and explicitly calculated by Getling (1980). This result is quite reasonable. When the optical depth is small, so is the temperature gradient $d\bar{T}/dz$ in the interior. Then the modes have little incentive to penetrate the full layer and prefer to hug the boundaries instead.

When $a^2 \cong \pi^2$ and $\kappa = 0$, both $W(z)$ and $\Theta'(z)$ are sinusoidal. However, when $a^2 \cong \pi^2$ and $\kappa \to 0$, $W(z)$ still approaches a sinusoid, but $\Theta'(z)$ develops thin boundary layers (although the interior of $\Theta'(z)$ remains nearly sinusoidal). When $a^2 \cong \pi^2$, $W(z)$ can be approximated by the sinusoidal form given in (2.26), regardless of κ. We would also like to find a simple approximate formula for $\Theta'(z)$. To do so, we invert the linear stability equation (2.18) for Θ', assuming that W has the sinusoidal form (2.26), and that $s = 0$. Then we find

$$\begin{aligned}\Theta' \cong \frac{1}{\kappa}\Bigg\{ & \frac{M-\Gamma}{\pi^2+q^2}\cos\pi z \\ & + \frac{L}{(-\pi^2-q^2+\lambda^2)^2+(2\pi\lambda)^2}\Bigg(2\pi\lambda\frac{\sinh\frac{1}{2}\lambda}{\cosh\frac{1}{2}q}\cosh qz \\ & \qquad -2\pi\lambda\sin\pi z\sinh\lambda z-(-\pi^2-q^2+\lambda^2)\cos\pi z\cosh\lambda z\Bigg)\Bigg\}, \end{aligned} \tag{2.33}$$

where $q^2 \equiv a^2 + 3\alpha_c/\kappa$. The first term on the right-hand side gives rise to the sinusoidal interior of Θ'. As $\kappa \to 0$, the first term reduces exactly to the $\kappa = 0$ eigenmode (2.27) for Θ' if, in (2.27), we set $a^2 = \pi^2$ and use formula (2.35) for γ_C below. The remaining terms in the expression (2.33) for Θ' produce the boundary layers. From this expression, we may see that the boundary layers in Θ' occupy a fraction $\sim 1/\lambda$ of the total depth of the layer; this is also true of the boundary layers in $\bar{T}$.

In Figure 2-4, we compare numerically computed eigenmodes (dots) with the approximate formulas (2.26) and (2.33) (solid lines). The approximate formulas are accurate whenever W is nearly sinusoidal, regardless of the value of κ. As κ decreases, sharp gradients in $\bar{T}$ form near the boundaries. Lifting of fluid parcels in these superadiabatic regions then gives rise to the boundary layers in Θ'. As κ increases, the Rayleigh-Bénard limit is approached, in which $\bar{T}$ is linear and the boundary

layers in Θ' disappear.

We now write down an approximate expression for Ra_m, following Goody (1956a,b). Then we demonstrate that in the limit $\kappa \to 0$, this expression can be reduced to the critical condition (2.28) for the $\kappa = 0$ case. In those cases in which we have established numerically that the most unstable mode has a nearly sinusoidal profile for $W(z)$, we can have confidence that the variational method with a sinusoidal trial function for $W(z)$ will yield accurate values of Ra_m. Therefore, we can write

$$Ra_m \cong \frac{\int_{-1/2}^{1/2} dz\, W \left\{ -\left(D^2 - a^2 - 3\alpha_c/\kappa\right)\left(D^2 - a^2\right)^2 W \right\}}{a^2 \int_{-1/2}^{1/2} dz \left(-\frac{d\bar{T}}{dz} - \Gamma \right) W^2}.$$

Substituting into this expression our trial function $W(z) = \cos \pi z$, we find

$$Ra_m = \frac{\gamma_m}{\kappa} \cong \frac{\frac{(\pi^2+a^2)^2}{a^2}\left((\pi^2 + a^2) + 3\alpha_c/\kappa\right)}{2(2\pi)^2 L \frac{\sinh \frac{1}{2}\lambda}{\lambda} \frac{1}{\lambda^2 + (2\pi)^2} + M - \Gamma}. \tag{2.34}$$

We can approximate γ_m for the case in which κ is small enough. By 'small enough,' we mean that $3\alpha_c/\kappa \gg (2\pi)^2$ and that

$$\frac{\frac{3}{4}\alpha_c}{1 + \frac{3}{4}\alpha_c} - \Gamma \gg \frac{4\pi^2\kappa}{3\alpha_c} \frac{1}{1 + \frac{3}{4}\alpha_c}.$$

With small κ, the assumption of optical transparency ($\alpha_c \leq 1$), and the assumption that the most unstable mode has wavenumber $a^2 \cong \pi^2$, the expression (2.34) becomes

$$\left(\frac{\frac{3}{4}\alpha_c}{1 + \frac{3}{4}\alpha_c} - \Gamma \right) \frac{\gamma_C}{3\alpha_c} \cong 4\pi^2. \tag{2.35}$$

Since the interior temperature gradient is given by $d\bar{T}/dz\big|_{z=0} \cong -\frac{3}{4}\alpha_c/(1 + \frac{3}{4}\alpha_c)$, this reduces to the condition $Ra_{RC} = 4\pi^2$ found for the $\kappa = 0$ case. The critical conditions approach each other despite the fact that Θ' as $\kappa \to 0$ does not approach Θ' when $\kappa = 0$ exactly. Whether $\bar{T}$ possesses thin boundary layers or discontinuities near the boundaries does not appear to be as important as the interior value of $d\bar{T}/dz$.

To illustrate the region of validity of these approximations, Figure 2-5 depicts the critical Rayleigh number $Ra_C \equiv \gamma_C/\kappa$ versus $1/\kappa$. For small enough κ, the value of Ra_C obtained numerically from (2.32) and the estimate of Ra_C obtained from the variational approximation (2.34) both approach the analytic expression (2.28) for $\kappa = 0$.

2.6 Energy Stability Theory

The energy method establishes a threshold value of Ra below which all perturbations, whether infinitesimal or finite-amplitude, decay. In contrast, linear stability analysis establishes a threshold in Ra above which at least one infinitesimal mode grows. The linear stability threshold is always greater than or equal to the energy stability threshold. Between the two thresholds lies a region in which subcritical instabilities may or may not exist. To minimize the size of this region of indeterminate stability properties, we strive to bring the energy stability threshold as close as possible to the linear stability threshold. The energy method can yield powerful results because it provides information about nonlinear perturbations.

The energy method involves the construction of an energy equation with generation and dissipation terms. The basic state is stable if the dissipation terms outweigh the generation terms. For the case in which $\kappa = 0$ and $\alpha = \alpha_c$ is constant, the basic state temperature profile is linear, and consequently we can prove that subcritical instabilities do not exist, as in Rayleigh-Bénard convection (Joseph 1965). When κ is nonzero, the energy stability threshold lies below the linear stability threshold; in this case, we cannot rule out the possibility of subcritical instabilities.

We now perform an energy stability analysis for our radiative-convective model with arbitrary κ and $\alpha = \alpha_c$ = constant, following the methodology of Straughan (1992). A similar analysis for an idealized atmospheric radiative-convective model is given in Chapter 3. For later convenience, we introduce the new temperature variable $\hat{T}' \equiv \sqrt{\gamma}\, T'$, but we do not specify the temperature scale $\mathcal{T}_*$ yet. We construct an energy equation as follows. First we form a kinetic energy equation by dotting $\mathbf{v}$ into the momentum equation (2.5) and averaging over the entire fluid domain. (We assume the perturbations are periodic in the horizontal; then the domain consists of one period cell.) The advection of kinetic energy term vanishes because it represents a redistribution of kinetic energy within the fluid domain rather than a net change. This yields

$$\chi \frac{d}{dt}\left\langle \frac{1}{2}\mathbf{v}^2 \right\rangle = \sqrt{\gamma}\left\langle w\hat{T}' \right\rangle - \left\langle |\nabla \mathbf{v}|^2 \right\rangle, \tag{2.36}$$

where brackets $\langle\rangle$ denote an average over the entire fluid volume. The first term on the right-hand side represents generation of kinetic energy by buoyancy fluctuations, and the second term represents viscous dissipation. Multiplying the heat equation (2.6) by $\hat{T}'$ and averaging over the entire fluid volume yields

$$\frac{d}{dt}\left\langle \frac{1}{2}\hat{T}'^2 \right\rangle = \sqrt{\gamma}\left\langle w\hat{T}'\left(-\frac{d\bar{T}}{dz} - \Gamma\right)\right\rangle - \kappa\left\langle \left|\nabla \hat{T}'\right|^2 \right\rangle - \left\langle 3\alpha \hat{T}'^2 \right\rangle. \tag{2.37}$$

We have neglected dissipative heating. We now define an 'energy' E:

$$E = \left\langle \frac{1}{2}\mathbf{v}^2 \right\rangle + \frac{\eta}{\chi}\left\langle \frac{1}{2}\hat{T}'^2 \right\rangle,$$

where η is a constant. The energy E is not necessarily a real energy, but instead is used as our measure of the perturbation strength. By optimizing the constant η, we may choose this measure so that the energy stability threshold is brought as close as possible to the linear stability threshold.

Combining equations (2.36) and (2.37) yields an energy equation:

$$\chi \frac{dE}{dt} = \sqrt{\gamma}\, I - \mathcal{D}, \tag{2.38}$$

where

$$I \equiv \left\langle w\hat{T}'\left(1 - \eta\frac{d\bar{T}}{dz} - \eta\Gamma\right)\right\rangle$$

represents generation of E, and

$$\mathcal{D} \equiv \left\langle |\nabla \mathbf{v}|^2 \right\rangle + \kappa\eta\left\langle \left|\nabla \hat{T}'\right|^2 \right\rangle + \eta\left\langle 3\alpha\hat{T}'^2 \right\rangle$$

represents dissipation. Each term in $\mathcal{D}$ is positive definite. We now define a threshold, γ_E, such that

$$\frac{1}{\sqrt{\gamma_E}} = \max\left(\frac{I}{\mathcal{D}}\right). \tag{2.39}$$

An upper bound on dE/dt is formed by combining (2.39) and (2.38):

$$\frac{dE}{dt} = -\mathcal{D}\sqrt{\gamma}\left(\frac{1}{\sqrt{\gamma}} - \frac{I}{\mathcal{D}}\right) \leq -\mathcal{D}\sqrt{\gamma}\left(\frac{1}{\sqrt{\gamma}} - \frac{1}{\sqrt{\gamma_E}}\right) \equiv -\mathcal{D}A.$$

Suppose now that $\sqrt{\gamma} < \sqrt{\gamma_E}$, so that $A > 0$. Poincaré's inequality (Straughan 1992) shows that

$$\frac{dE}{dt} \leq -\mathcal{D}A \leq -AcE,$$

where c is some positive constant. Integrating in time, we find

$$E(t) \leq e^{-Act} E(0).$$

Therefore, if $\sqrt{\gamma} < \sqrt{\gamma_E}$, the energy decreases monotonically with time, regardless of the size of the initial perturbation. That is, the basic state is monotonically stable.

To find $\sqrt{\gamma_E}$, we derive and solve the Euler-Lagrange equations for (2.39) following the standard procedure (Straughan, 1992, pp. 43–44). The Euler-Lagrange equation associated with $\mathbf{v}$ is

$$0 = -\nabla \Pi + \frac{1}{2}\sqrt{\gamma_E}\left(1 - \eta\frac{d\bar{T}}{dz} - \eta\Gamma\right)\hat{T}'\mathbf{k} + \nabla^2\mathbf{v}. \tag{2.40}$$

Here $\Pi(\mathbf{x})$ is a Langrange multiplier which enforces the continuity constraint. Applying $\mathbf{k}\cdot\nabla\times\nabla\times$ to the preceding equation (2.40) yields

$$0 = \frac{1}{2}\sqrt{\gamma_E}\left(1 - \eta\frac{d\bar{T}}{dz} - \eta\Gamma\right)\nabla_h^2\hat{T}' + \nabla^2\nabla^2 w. \tag{2.41}$$

The Euler-Lagrange equation for T' is

$$-\frac{1}{2}\sqrt{\gamma_E}w\left(1 - \eta\frac{d\bar{T}}{dz} - \eta\Gamma\right) = \kappa\eta\nabla^2\hat{T}' - \eta 3\alpha\hat{T}'. \tag{2.42}$$

We now need to find the smallest eigenvalue $\sqrt{\gamma_E}$ associated with equations (2.41) and (2.42). We substitute in the normal modes (2.16) with wavenumber a. We then minimize the eigenvalue with respect to a^2, holding η fixed. To enlarge the region of monotonic stability, we may, if we so desire, maximize $\sqrt{\gamma_E}$ with respect to η. Restated mathematically, we perform the optimization

$$\gamma_{EC} = \max_{\eta}\left(\min_{a^2}\sqrt{\gamma_E}\right).$$

The operations of minimization with respect to a^2 and maximization with respect to η do not commute in general. Therefore it is safest to perform the minimization with respect to a^2 first.

When $\kappa = 0$ is constant, the basic state temperature profile $\bar{T}$ is linear, and we can rule out subcritical instabilities. We shall set $\eta = 1$, since this turns out to be the optimum value. We choose the temperature scale such that $\mathcal{T}_*/h_*$ equals the basic state lapse rate minus the adiabatic lapse rate. Then $-d\bar{T}/dz - \Gamma = 1$. The energy method Euler-Lagrange equations for w (2.41) and $\hat{T}'$ (2.42) become, respectively,

$$0 = \sqrt{\gamma_E}\nabla_h^2\hat{T}' + \nabla^2\nabla^2 w \tag{2.43}$$

and

$$-\sqrt{\gamma_E}w = -3\alpha_c\hat{T}'. \tag{2.44}$$

It remains only to note that with the assumptions we have made for the energy method equations, the linear stability equations (2.14) and (2.13) at marginal stability reduce to the energy method equations (2.43) and (2.44) respectively. Since the two sets of stability equations and boundary conditions are identical, $\gamma_E = \gamma_m$. This completes the proof that no subcritical instabilities exist.

We now consider the case in which $\kappa \neq 0$. We must return to the full Euler-Lagrange equations (2.41) and (2.42). These equations are not identical with the linear stability equations (2.14) and (2.13), because the basic state temperature profile $\bar{T}$ is no longer linear. We shall find that $\gamma_E < \gamma_m$, and we cannot rule out subcritical instabilities. Equations (2.41) and (2.42) are solved by separating variables and eliminating the temperature variable:

$$\left((D^2 - a^2) - 3\alpha/\kappa\right)(D^2 - a^2)^2 W(z)$$

$$+ \left\{ \frac{\eta \frac{d^3\bar{T}}{dz^3}}{\left(1-\eta\frac{d\bar{T}}{dz}-\eta\Gamma\right)} + \frac{2\eta^2\left(\frac{d^2\bar{T}}{dz^2}\right)^2}{\left(1-\eta\frac{d\bar{T}}{dz}-\eta\Gamma\right)^2} + \frac{2\eta\frac{d^2\bar{T}}{dz^2}}{\left(1-\eta\frac{d\bar{T}}{dz}-\eta\Gamma\right)} D \right\} (D^2-a^2)^2 W(z)$$

$$= Ra_E \left(-\frac{a^2}{4\eta}\right)\left(1-\eta\frac{d\bar{T}}{dz}-\eta\Gamma\right)^2 W(z), \tag{2.45}$$

where the temperature scale is $\mathcal{T}_* = T_{L*} - T_{U*}$ and $Ra_E \equiv \gamma_E/\kappa$. We set $\alpha = \alpha_c$ and solve this eigenvalue equation for Ra_E numerically. Our computational procedure is to find all eigenvalues and then choose the smallest one. The we perform a minimization with respect to a^2 and a maximization with respect to η numerically. The numerical method is described in more detail in the appendix to Chapter 2.

Figure 2-6 shows plots of the critical Rayleigh number Ra_{EC} versus a^2 (circles) from the energy stability problem, superimposed on plots of the critical Rayleigh number Ra_C (asterisks) from the linear stability problem. On these plots, the areas of parameter space below the monotonic stability curves (circles) are stable to arbitrarily large perturbations. The areas above the linear stability curves (asterisks) are unstable to at least one infinitesimal mode. In the areas or gaps between the monotonic and linear stability curves, subcritical instability may or may not occur. In Figure 2-6, the largest gap between Ra_{EC} and Ra_C is about a factor of ten, and it occurs for small optical depth ($\alpha_c = 0.01$) and small thermal diffusivity ($\kappa = 10^{-7}$). This is probably related to the fact that small α_c and κ imply a highly nonlinear basic state temperature $\bar{T}$. For large κ, the gap between monotonic and linear stability curves is small, which is not surprising since large κ corresponds to the Rayleigh-Bénard limit, for which the monotonic and linear stability curves coincide. Also, as α_c increases, $\bar{T}$ becomes more linear, and the gap between Ra_{EC} and Ra_C narrows.

2.7 Conclusions

This chapter has examined two radiative-convective models in order to improve physical intuition about the effects of thermal radiation on convection. The properties of the radiative-convective systems have much in common with Rayleigh-Bénard convection. The main results are summarized below.

In the first model, the thermal diffusivity κ is set to zero. This is a minimal radiative-convective model, whose linear and energy stability problems can be solved analytically. The radiative-convective system is comparable in simplicity to Rayleigh-Bénard convection but includes thermal radiation, which is important in the atmosphere. Because the interior basic state temperature profiles are linear in both systems, the stability properties of the two systems are remarkably similar. First, both linear stability thresholds depend on only a single parameter: for Rayleigh-Bénard convection, this parameter is the Rayleigh number, while for the radiative-convective system, the parameter is a radiative Rayleigh number Ra_R. Ra_R is defined like the Rayleigh number, but with the interior lapse rate (neglecting temperature jumps at the boundaries) replacing the full lapse rate, and a radiative diffusivity replacing the thermal diffusivity. Second, for both systems, one can rigorously rule out the possibility of subcritical instabilities.

In the second model, nonzero κ is permitted. The behavior in this case is more complicated because the basic state temperature profile $\bar{T}$ is no longer linear. When κ is small, we recover several properties of the $\kappa = 0$ linear stability analysis. In particular, the linear stability threshold can be characterized approximately in terms of Ra_R. Therefore the analytical analysis for the $\kappa = 0$ case has relevance to the case when κ is small, as in the atmosphere. However, we do find that the temperature perturbation eigenmodes differ between the two cases. Finally, we determine a threshold below which no infinitesimal or finite-amplitude perturbation may grow. This analysis restricts the possibility of subcritical instability to a small range in Ra at the larger values of κ and optical depth considered.

A quantitative comparison of our results with laboratory experiments is precluded by several of our assumptions, such as the assumptions of free-slip boundaries and a radiatively grey gas. Some of our qualitative conclusions, however, may be amenable to laboratory tests. In particular, it may

be possible to test experimentally whether or not subcritical instabilities exist. Our calculations suggest that subcritical instability can exist only over a small range of Ra, particularly at the values of thermal diffusivity ($\kappa \sim 0.1$) appropriate to a laboratory experiment. Bdéoui and Soufiani (1997) have found fair agreement between their detailed linear stability calculations and the laboratory experiments of Gille and Goody (1964), for a similar system to the one considered here. This result already suggests that for Rayleigh numbers somewhat below the critical Rayleigh number for linear stability, subcritical instabilities do not occur, at least for initial perturbations no larger than experimental noise.

2.8 Appendix: Numerical Techniques

This appendix describes the numerical methods used to solve the linear and energy stability problems for $\kappa \neq 0$. We follow the textbook of Boyd (1989). The interested reader is directed there for further information.

First we consider the linear stability problem. Defining the function $V(z)$ by $V(z) \equiv (D^2 - a^2)W(z)$, the linear stability problem (2.32) can be cast as

$$\left((D^2 - a^2) - 3\alpha_c/\kappa\right)\left(D^2 - a^2\right)V(z) \;=\; Ra\, a^2 \left(\frac{d\bar{T}}{dz} + \Gamma\right)\,(D^2 - a^2)^{-1}V(z) \tag{2.46}$$

subject to the boundary conditions

$$V|_{z=\pm 1/2} = D^2 V\big|_{z=\pm 1/2} = 0.$$

This is a generalized eigenvalue problem (Press et al., 1992) for the eigenvectors $V(z)$ and eigenvalues Ra, so-called because operators acting on $V(z)$ appear on both sides of the equation. In our procedure, we choose values of the parameters α_c, κ, Γ, and a^2, compute all eigenvalues Ra and eigenvectors $V(z)$ for these parameter settings, and then select the least eigenvalue and its associated eigenvector.

To resolve the thin boundary layers that appear in the temperature variables $\Theta'(z)$ and $\bar{T}(z)$, fine resolution is needed near the boundaries. For this reason, we use a pseudospectral method based on Chebyshev polynomials. That is, we construct a set of basis functions $\{\phi_n\}$, evaluate them on a non-uniformly spaced grid, expand $V(z)$ in terms of the $\{\phi_n\}$ basis, solve for the coefficients of $V(z)$, and finally reconstruct $V(z)$, $W(z)$, and $\Theta'(z)$. Our set of basis functions is denoted

$$\{\phi_n(z)\} \qquad\qquad n = 4, 5, ..., N+1,$$

where $N+1$ is the highest function represented. We insist that each member of the set $\{\phi_n\}$ satisfy the boundary conditions

$$\phi(z)|_{z=\pm 1/2} = D^2\phi(z)\big|_{z=\pm 1/2} = 0.$$

To ensure this, we construct each particular basis function ϕ_n by adding to the Chebyshev polynomial T_n a certain linear combination of the first four Chebyshev polynomials T_0, T_1, T_2, and T_3. Specifically, if we define

$$f(n) \equiv \frac{(n^2-1)n^2}{3} = \left.\frac{d^2 T_n(x)}{dx^2}\right|_{x=1},$$

then for even n,

$$\phi_n(z) = T_n(2z) + \left(-1 + \frac{1}{4}f(n)\right)T_0(2z) - \frac{1}{4}f(n)T_2(2z),$$

and for odd n,

$$\phi_n(z) = T_n(2z) + \left(-1 + \frac{1}{24}f(n)\right) T_1(2z) - \frac{1}{24}f(n)T_3(2z).$$

Like the higher-order Chebyshev polynomials, each of the functions ϕ_n varies rapidly near its endpoints and relatively slowly in the interior. Therefore functions possessing boundary layers can be represented accurately with relatively few basis functions. The basis functions ϕ_n are evaluated on an 'interior' or 'Gauss-Chebyshev' grid which has been modified to span $z = [-1/2, 1/2]$:

$$z_j = \frac{1}{2}\cos\left(\frac{\pi(j-1/2)}{N}\right) \qquad\qquad j = 1, ..., N.$$

The gridpoints are spaced close together near the boundaries and far apart in the interior. Hence gridpoints are not wasted on the interior region, where the functions are smooth. The functions $V(z)$ and $W(z)$ are expanded in terms of $\phi_n(z_j) \equiv \phi_{jn}$ at the gridpoints z_j:

$$V(z_j) = \sum_{n=4}^{N+1} \phi_{jn}\tilde{V}_n \qquad\qquad W(z_j) = \sum_{n=4}^{N+1} \phi_{jn}\tilde{W}_n. \tag{2.47}$$

We want to write the eigenvalue problem in terms of the coefficients $\left\{\tilde{V}_n\right\}$. From the definition of $V(z)$, we find that

$$W(z_k) = \phi_{kl}\left(\frac{d^2\phi}{dz^2} - a^2\phi\right)^{-1}_{lm}\phi_{mn}\tilde{V}_n. \tag{2.48}$$

Substituting the expressions (2.48) for $W(z_k)$ and (2.47) for $V(z_j)$ into the linear stability equation (2.46), we obtain

$$\sum_{n=4}^{N+1}\left(-3\alpha_c/\kappa + (D^2 - a^2)\right)\left(D^2 - a^2\right)\phi_{jn}\tilde{V}_n$$
$$= Ra\sum_{n=4}^{N+1} a^2\left(\frac{d\bar{T}}{dz} + \Gamma\right)_{jk}\phi_{kl}\left(\frac{d^2\phi}{dz^2} - a^2\phi\right)^{-1}_{lm}\phi_{mn}\tilde{V}_n. \tag{2.49}$$

Here $(d\bar{T}/dz + \Gamma)_{jk}$ is a diagonal matrix with element jj given by $d\bar{T}(z_j)/dz + \Gamma$. This eigenvalue problem was solved using the *eig* command from the mathematical software package MATLAB. The *eig* command is based on EISPACK routines. With the spectral coefficients $\tilde{V}_n$ in hand, the spatial functions $V(z_j)$ and $W(z_j)$ can be reconstructed from equations (2.47) and (2.48) respectively. Θ' is obtained from the momentum equation (2.17). The energy stability eigenvalue problem (2.45) is solved in a very similar manner.

To find the critical Rayleigh number for linear or monotonic stability, we must minimize with respect to a^2. These minimizations are performed with the golden section search (Press et al. 1992). This method finds local extrema, so we must carefully bracket the desired extremum before commencing the search. The maximization with respect to η in the energy stability problem is optional. In most cases, we use the golden section search to perform the maximization. In some cases in which there is a double minimum with respect to a^2, the golden section search for maximum η fails. We then find an approximate maximum in η by trial and error.

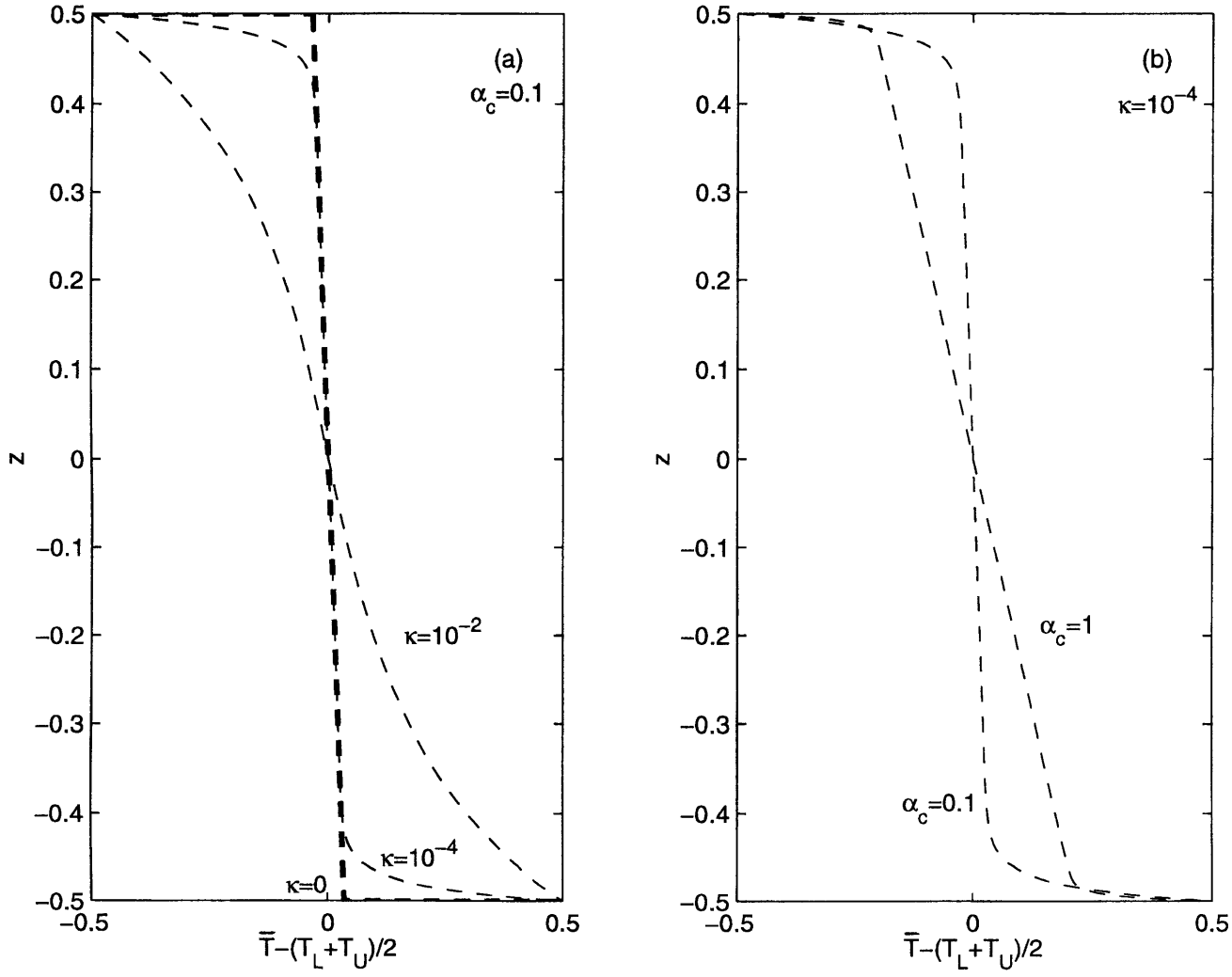

Figure 2-1: Shifted basic state temperature profiles $\bar{T} - (T_L + T_U)/2$ versus z, for $\kappa \neq 0$ (thin dashed lines) as obtained from equation (2.31), and for $\kappa = 0$ (thick dashed lines) as obtained from (2.24). In (a), we fix $\alpha_c = 0.1$ and let $\kappa = 10^{-2}, 10^{-4}, 0$. As the thermal diffusivity κ approaches zero, temperature discontinuities form at the boundaries, and a linear temperature profile forms in the interior. In (b), we fix $\kappa = 10^{-4}$ and let $\alpha_c = 0.1, 1$. As the optical depth α_c decreases, the interior temperature gradient decreases.

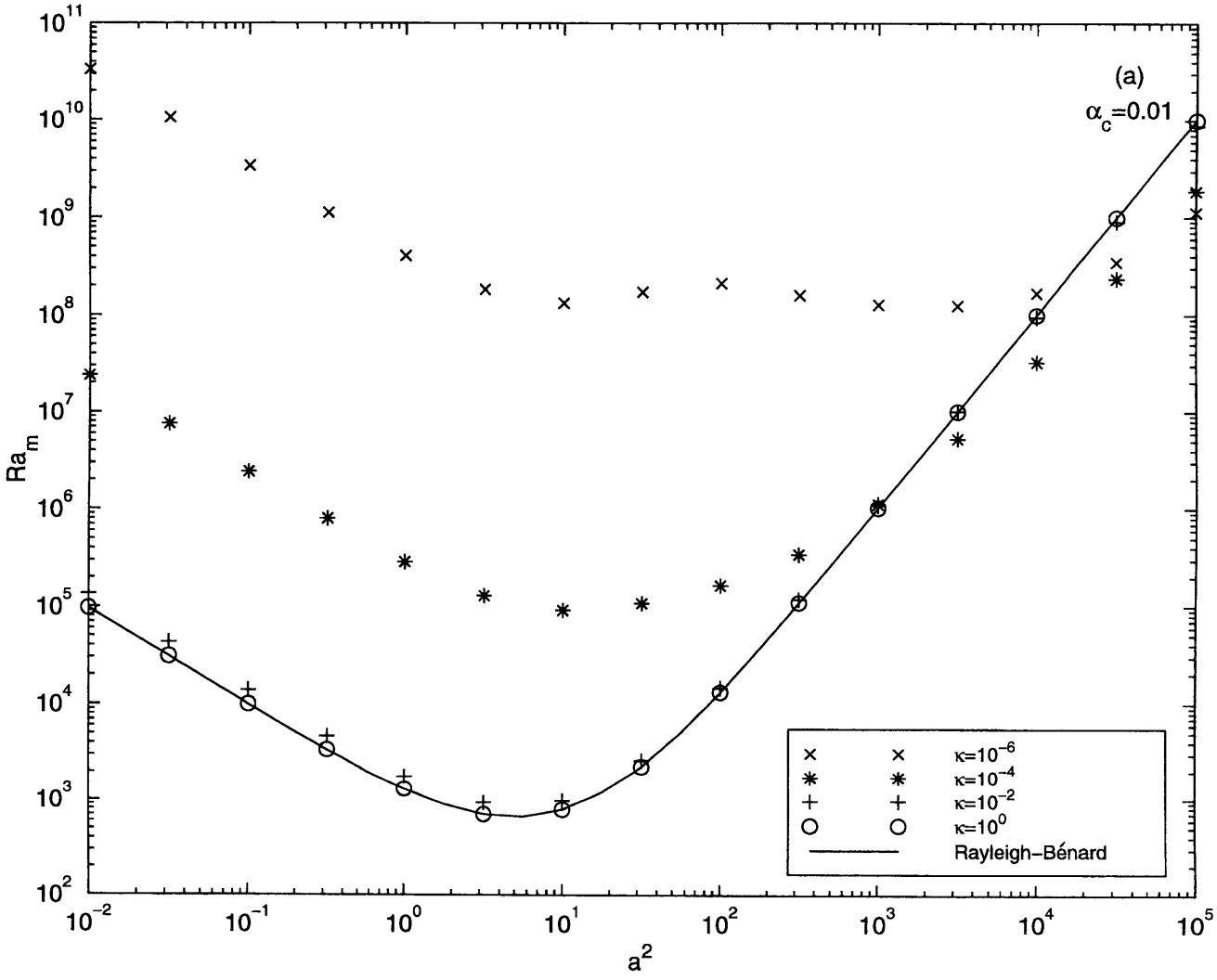

Figure 2-2: The Rayleigh number for marginal stability Ra_m versus wavenumber squared a^2 obtained from numerical solution of (2.32). The markers denote the value of κ given in the legends. In parts (a), (b), and (c), the solid line denotes the marginal stability curve for Rayleigh-Bénard convection (which has no radiation). Also in parts (a), (b), and (c) we set $\Gamma = 0$. In (a), we set $\alpha_c = 0.01$. In (b), we set $\alpha_c = 0.1$. In (c), we set $\alpha_c = 1$. When κ decreases, the basic state temperature profile is stabilized in the interior.

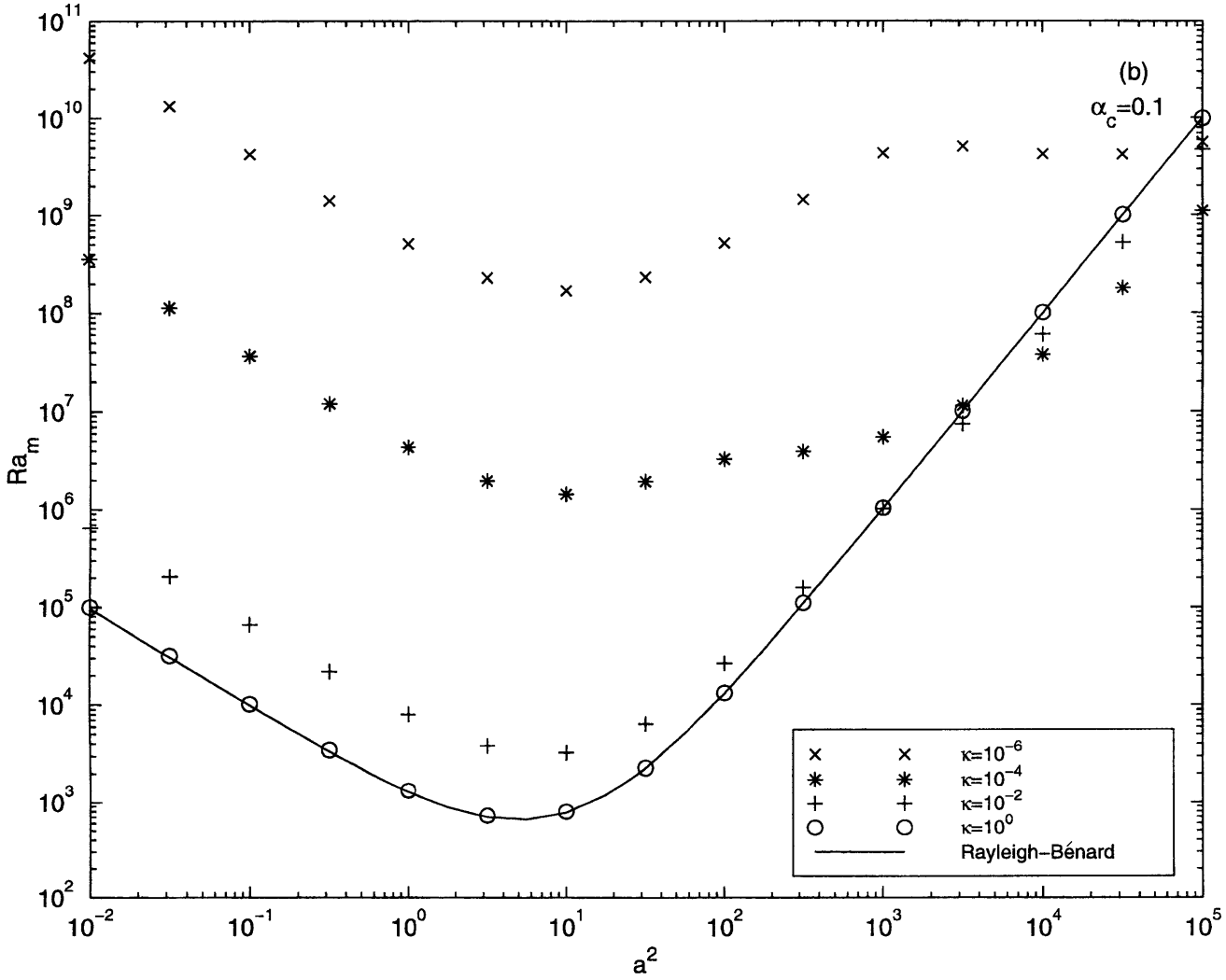
(b)
α_c=0.1
Ra_m
a^2
10^{11}
10^{10}
10^{9}
10^{8}
10^{7}
10^{6}
10^{5}
10^{4}
10^{3}
10^{2}
10^{-2}
10^{-1}
10^{0}
10^{1}
10^{2}
10^{3}
10^{4}
10^{5}
κ=10^{-6}
κ=10^{-4}
κ=10^{-2}
κ=10^{0}
Rayleigh–Bénard

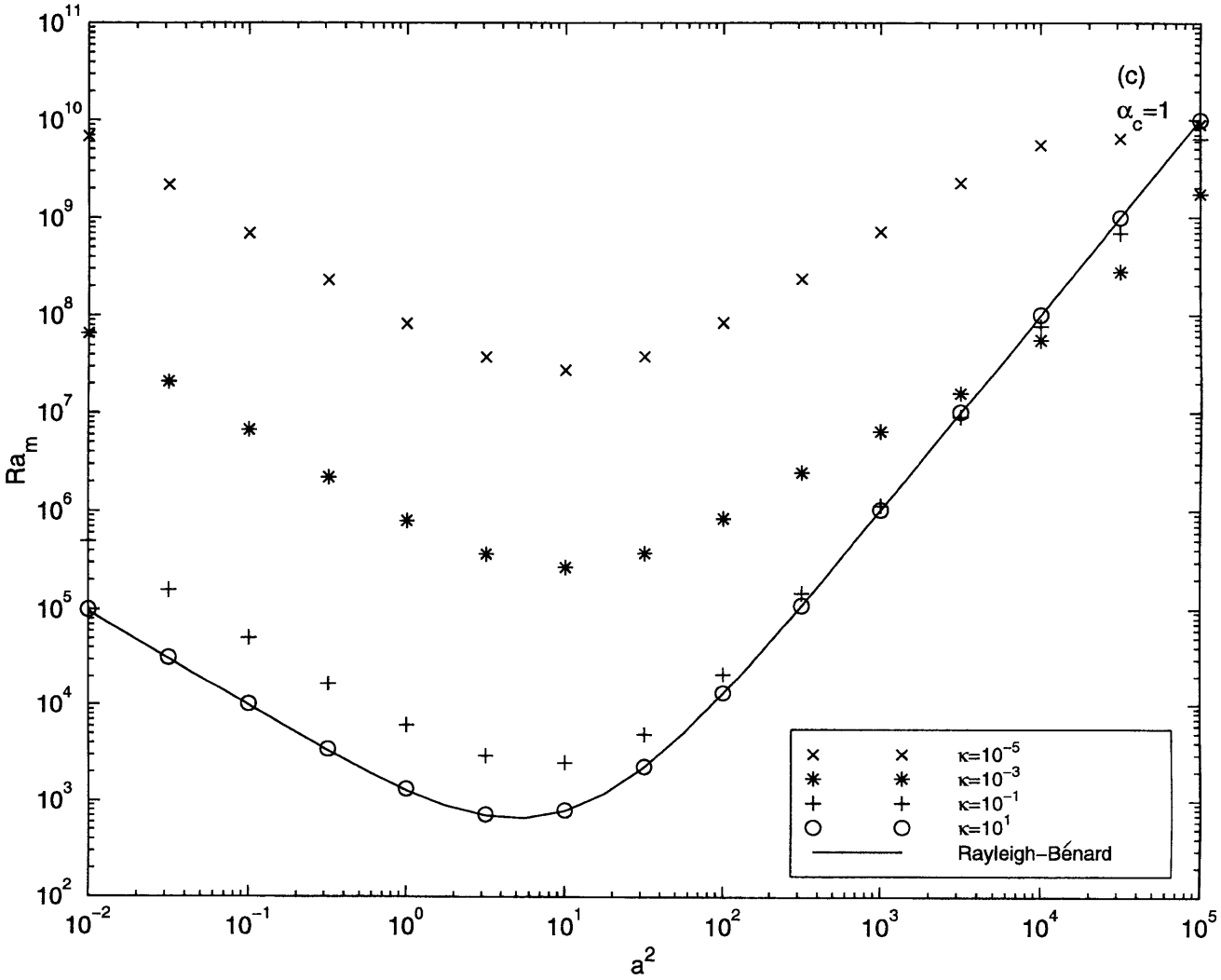
(c)
α_c=1
Ra_m
a^2
10^{11}
10^{10}
10^9
10^8
10^7
10^6
10^5
10^4
10^3
10^2
10^{-2}
10^{-1}
10^0
10^1
10^2
10^3
10^4
10^5
κ=10^{-5}
κ=10^{-3}
κ=10^{-1}
κ=10^1
Rayleigh–Bénard

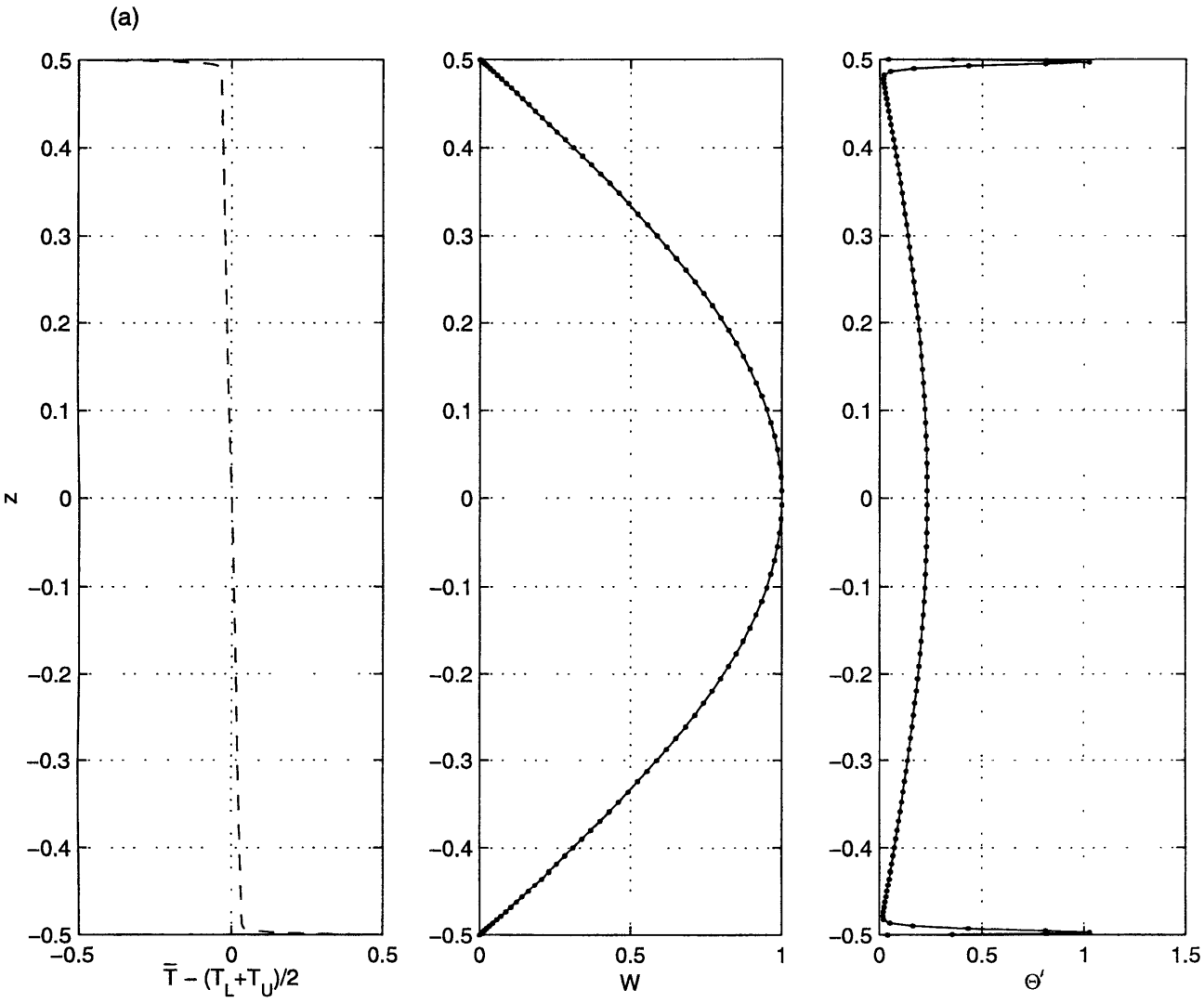

Figure 2-3: The shifted basic state temperature profile $\bar{T} - (T_L + T_U)/2$ (dashed line) and the linear eigenmodes $W(z)$ and $\Theta'(z)$ (dots) as computed numerically from (2.32). The solid lines in (a) and (b) correspond to the approximation (2.26) for W and (2.33) for Θ'. We set $\alpha_c = 0.1$, $\kappa = 10^{-6}$, and $\Gamma = 0$. In (a) $a^2 = 9.8690$, in (b) $a^2 = 10^3$, and in (c) $a^2 = 1.9127 \times 10^4$. As the wavelength decreases, the W eigenfunction becomes concentrated near the boundaries.

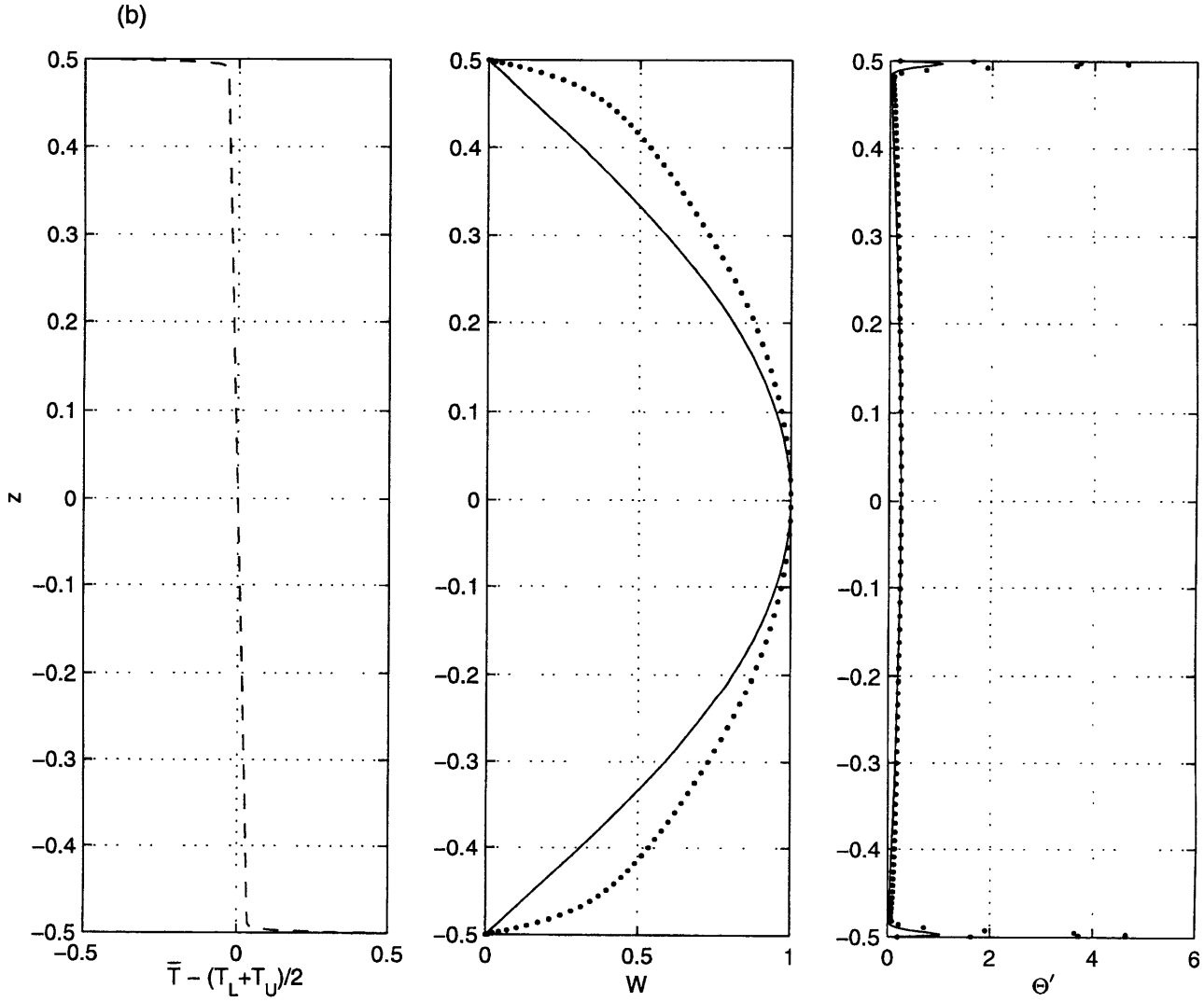
(b)
z
0.5
0.4
0.3
0.2
0.1
0
−0.1
−0.2
−0.3
−0.4
−0.5
−0.5
0
0.5
$\bar{T} - (T_L+T_U)/2$
0
0.5
1
W
0
2
4
6
Θ′

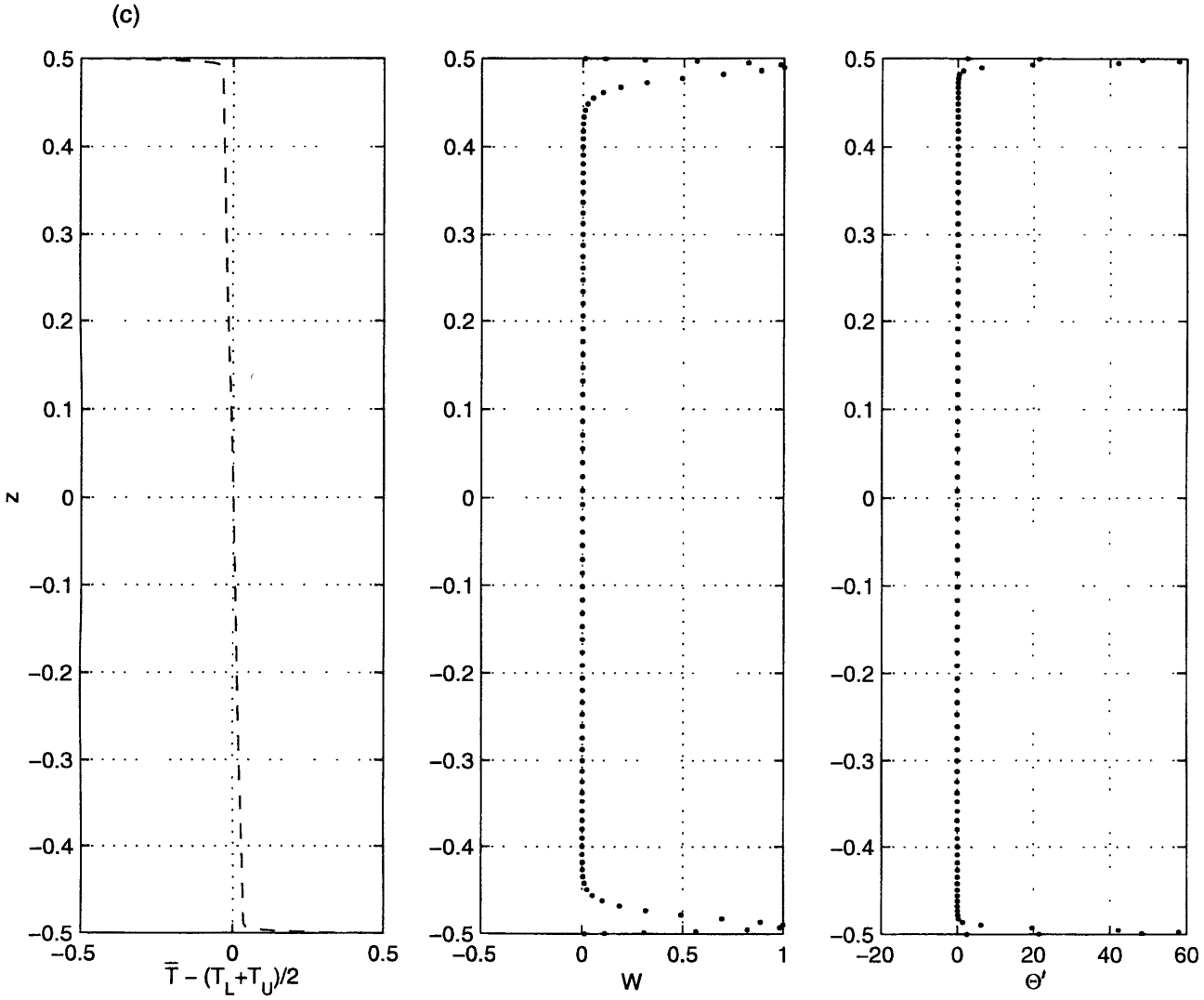
(c)
z
0.5
0.4
0.3
0.2
0.1
0
−0.1
−0.2
−0.3
−0.4
−0.5
−0.5
0
0.5
$\overline{T} - (T_L+T_U)/2$
−0.5
0
0.5
1
W
−20
0
20
40
60
Θ′

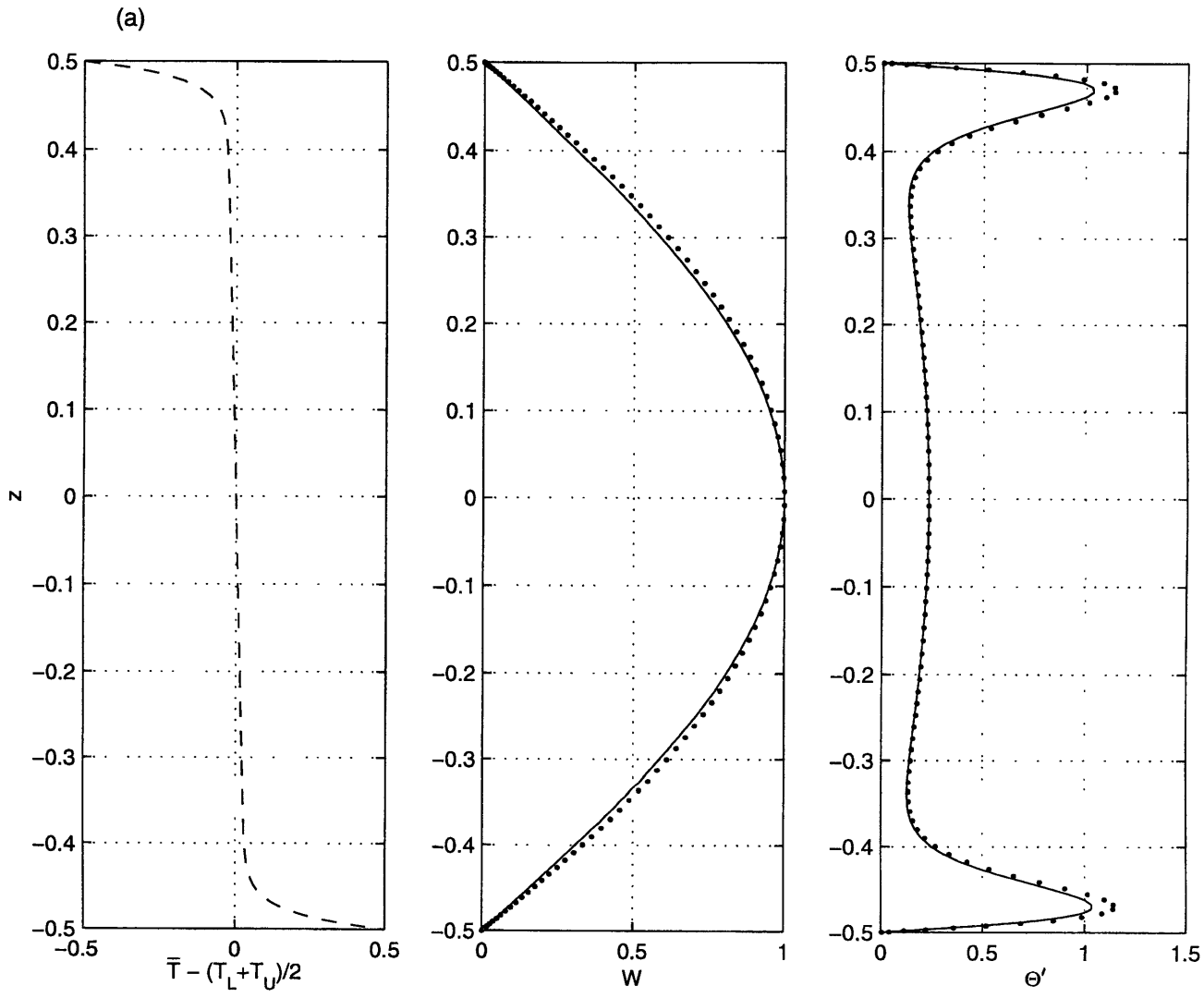

Figure 2-4: Linear eigenmodes computed numerically from (2.32) (dots), the approximations to these eigenmodes given by (2.26) and (2.33) (solid lines), and shifted basic state temperature profiles $\bar{T} - (T_L + T_U)/2$ (dashed lines). We set $\alpha_c = 0.1$ and $\Gamma = 0$, and choose the value of a^2 which minimizes γ_m. In (a), $\kappa = 10^{-4}$ and $a^2 = 10.02$; in (b), $\kappa = 10^{-2}$ and $a^2 = 7.260$; and in (c), $\kappa = 1$ and $a^2 = 4.984$. The approximate eigenmodes are adequate over a wide range of κ, if $a^2 \sim \mathcal{O}(\pi^2)$.

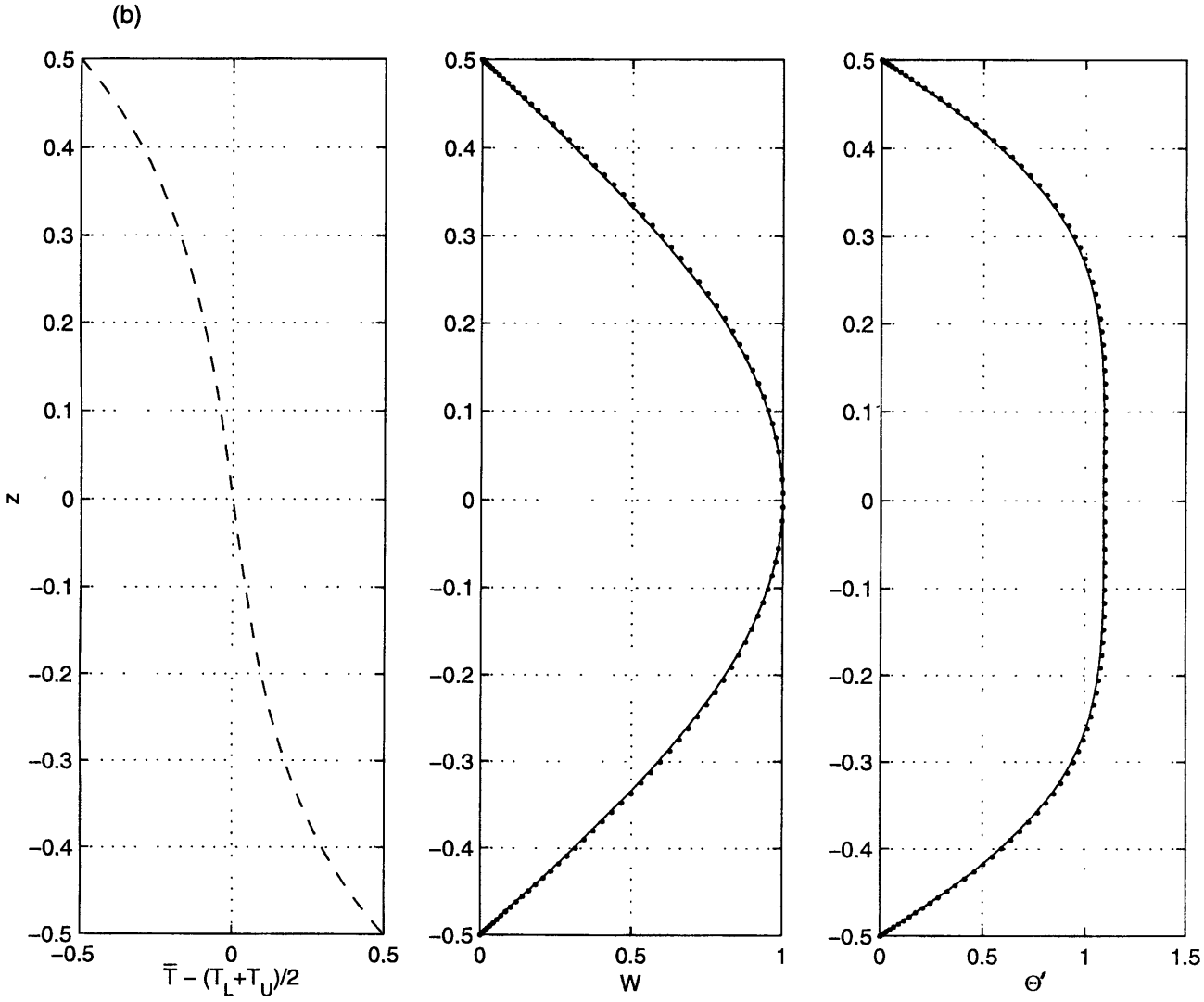
(b)
z
$\overline{T} - (T_L+T_U)/2$
W
Θ'

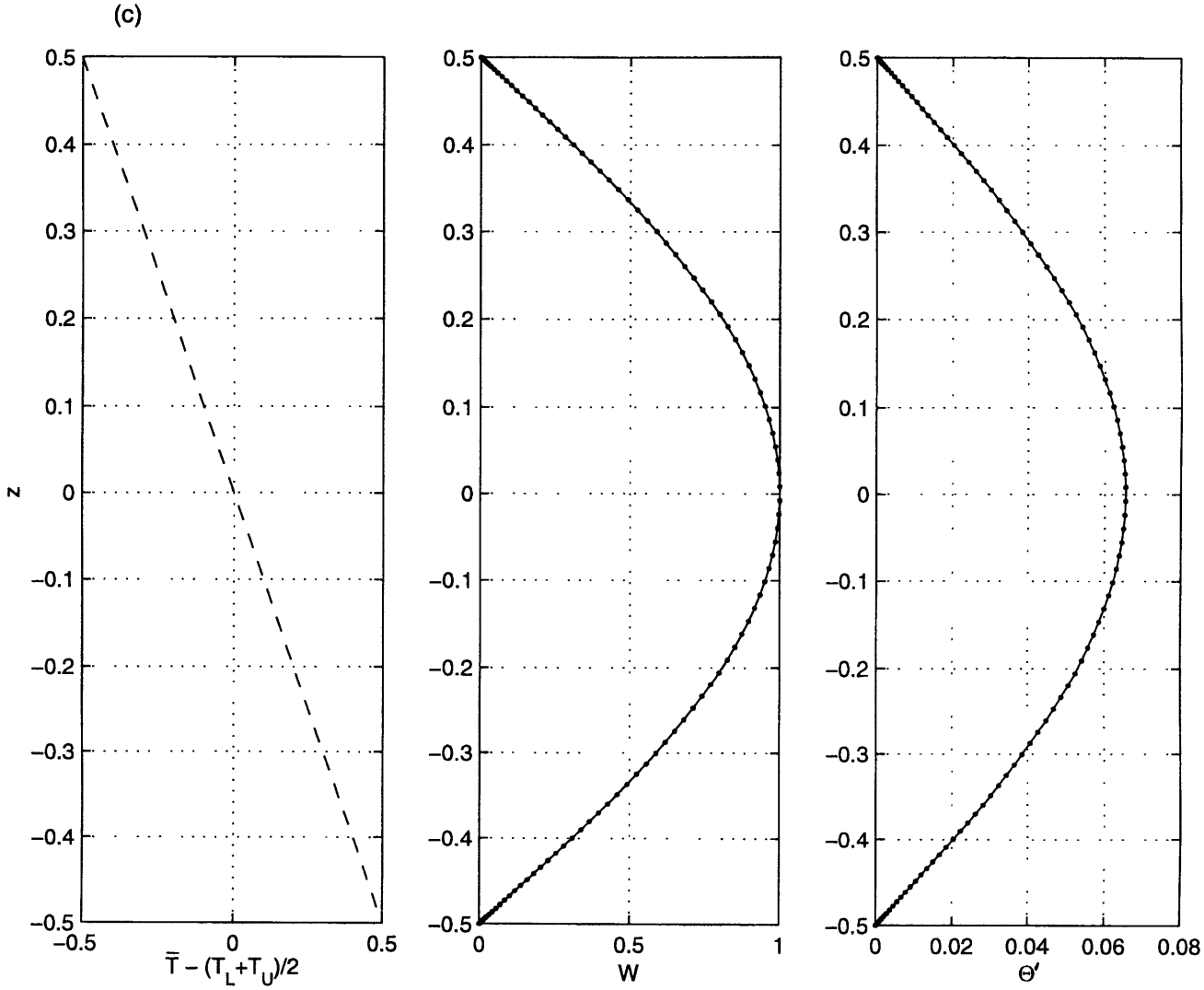
(c)
z
$\bar{T} - (T_L+T_U)/2$
W
Θ′

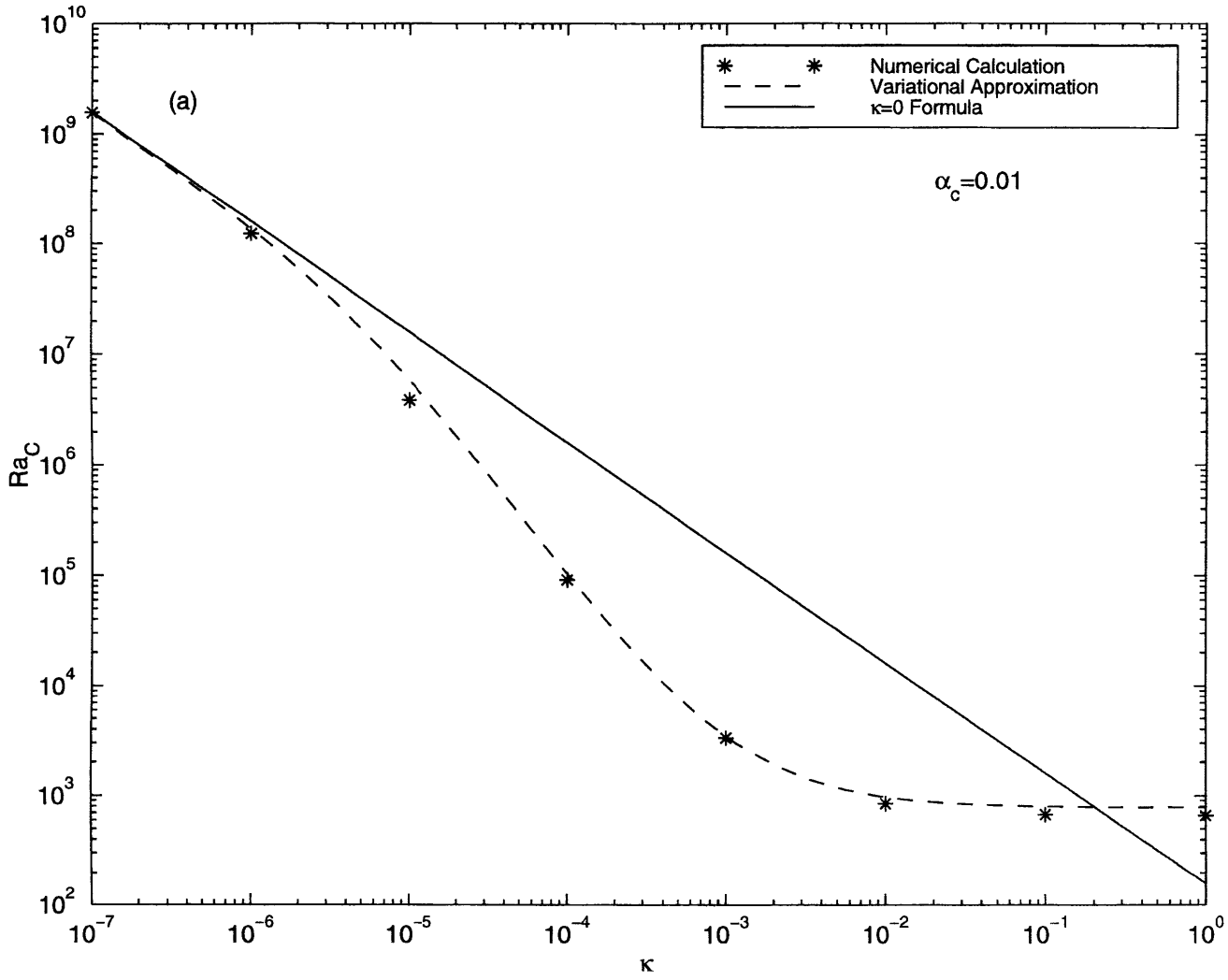

Figure 2-5: The critical Rayleigh number $Ra_C \equiv \gamma_C/\kappa$ for linear stability versus the thermal diffusivity κ. The asterisks are obtained from numerical solution of (2.32), the dashed line is obtained from (2.34) with $a^2 = \pi^2$, and the solid line is obtained from (2.28) with $d\bar{T}/dz = -\frac{3}{4}\alpha_c/(1+\frac{3}{4}\alpha_c)$. In (a) $\alpha_c = 0.01$, in (b) $\alpha_c = 0.1$, and in (c) $\alpha_c = 1$. In all cases, $\Gamma = 0$. For small enough κ, the solution for $\kappa \neq 0$ approaches the $\kappa = 0$ formula (2.28).

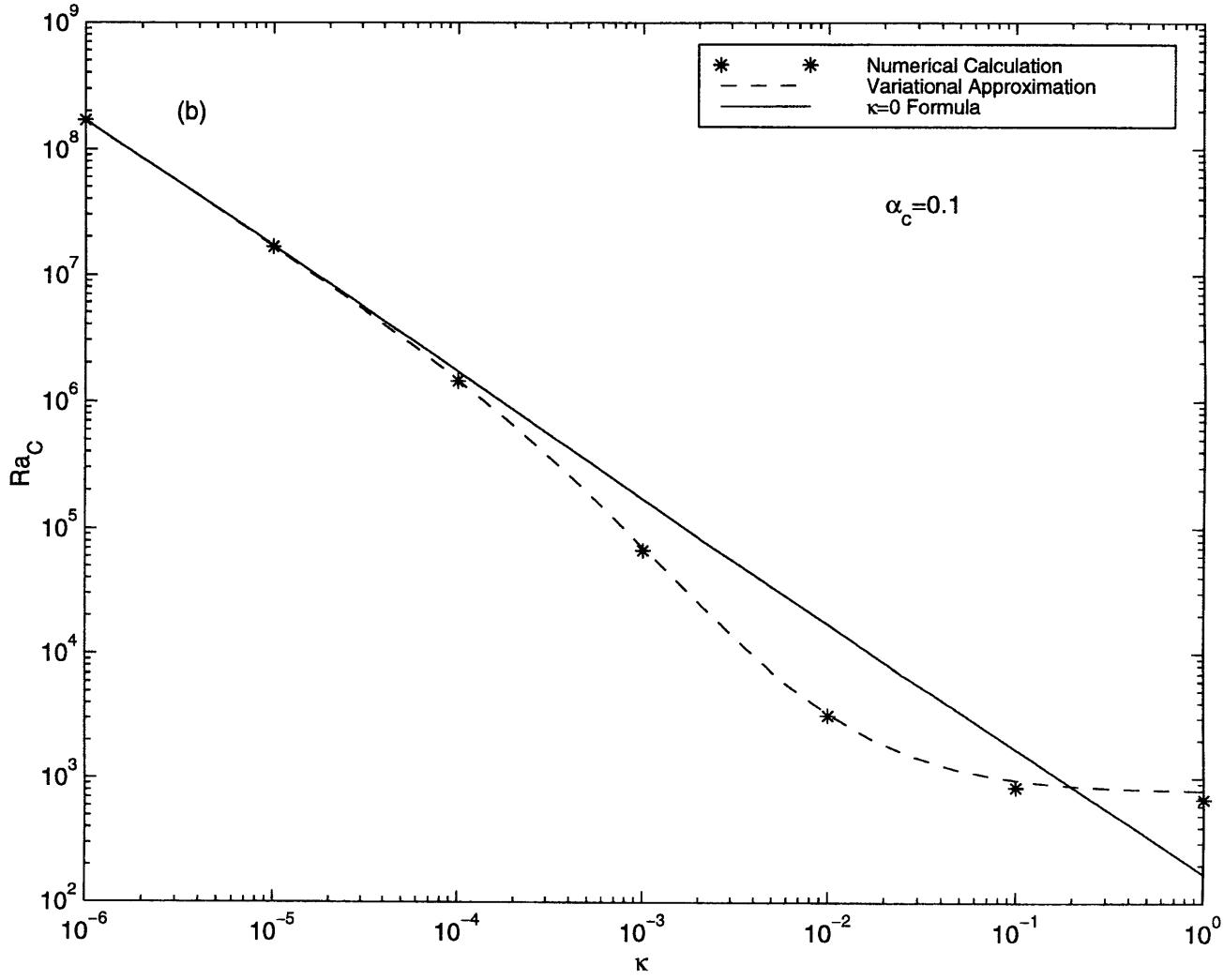
(b)
Numerical Calculation
Variational Approximation
κ=0 Formula
α_c=0.1
Ra_c
κ
10^9
10^8
10^7
10^6
10^5
10^4
10^3
10^2
10^{-6}
10^{-5}
10^{-4}
10^{-3}
10^{-2}
10^{-1}
10^0

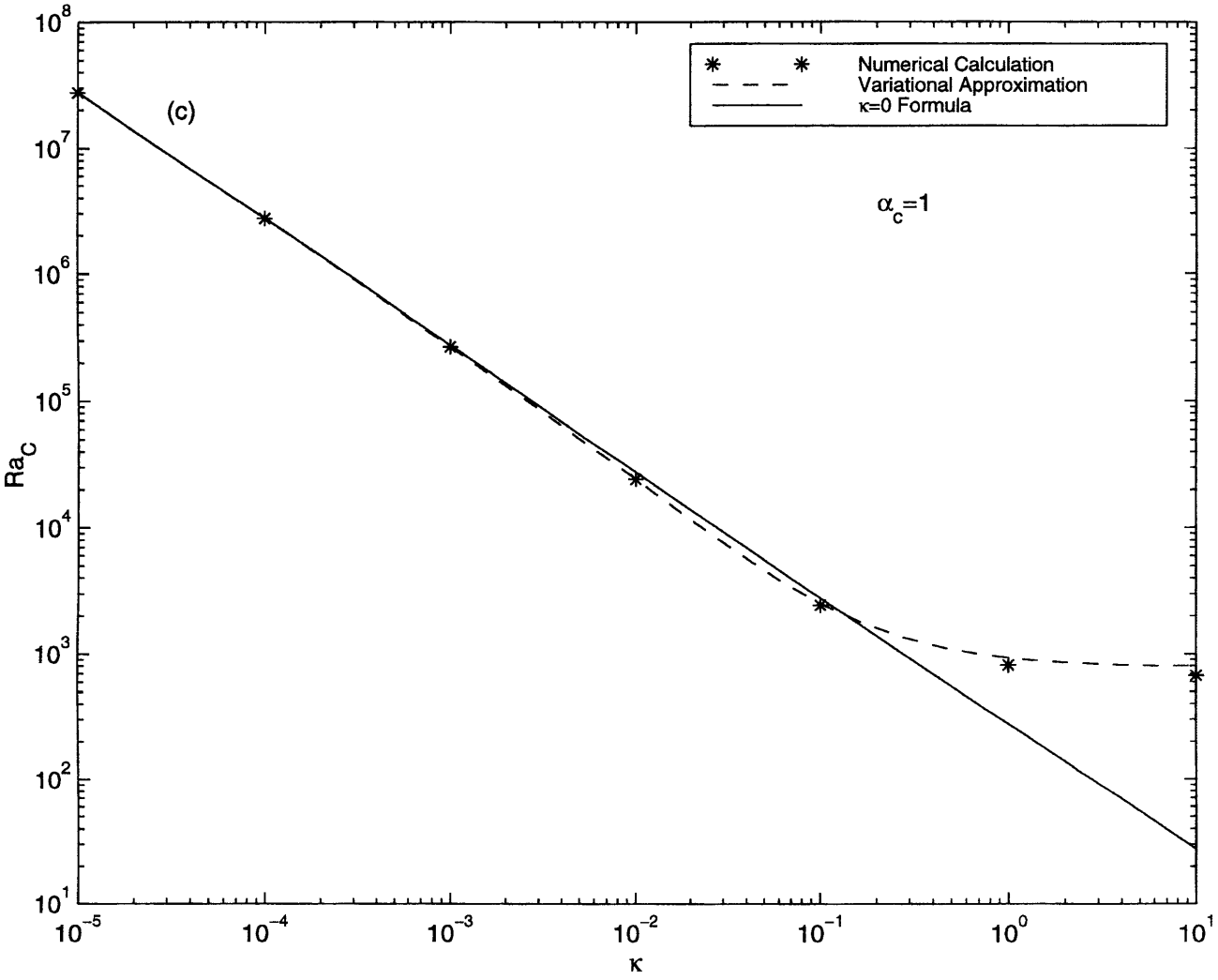
(c)
Numerical Calculation
Variational Approximation
κ=0 Formula
α_c=1
Ra_C
κ
10^8
10^7
10^6
10^5
10^4
10^3
10^2
10^1
10^{-5}
10^{-4}
10^{-3}
10^{-2}
10^{-1}
10^0
10^1

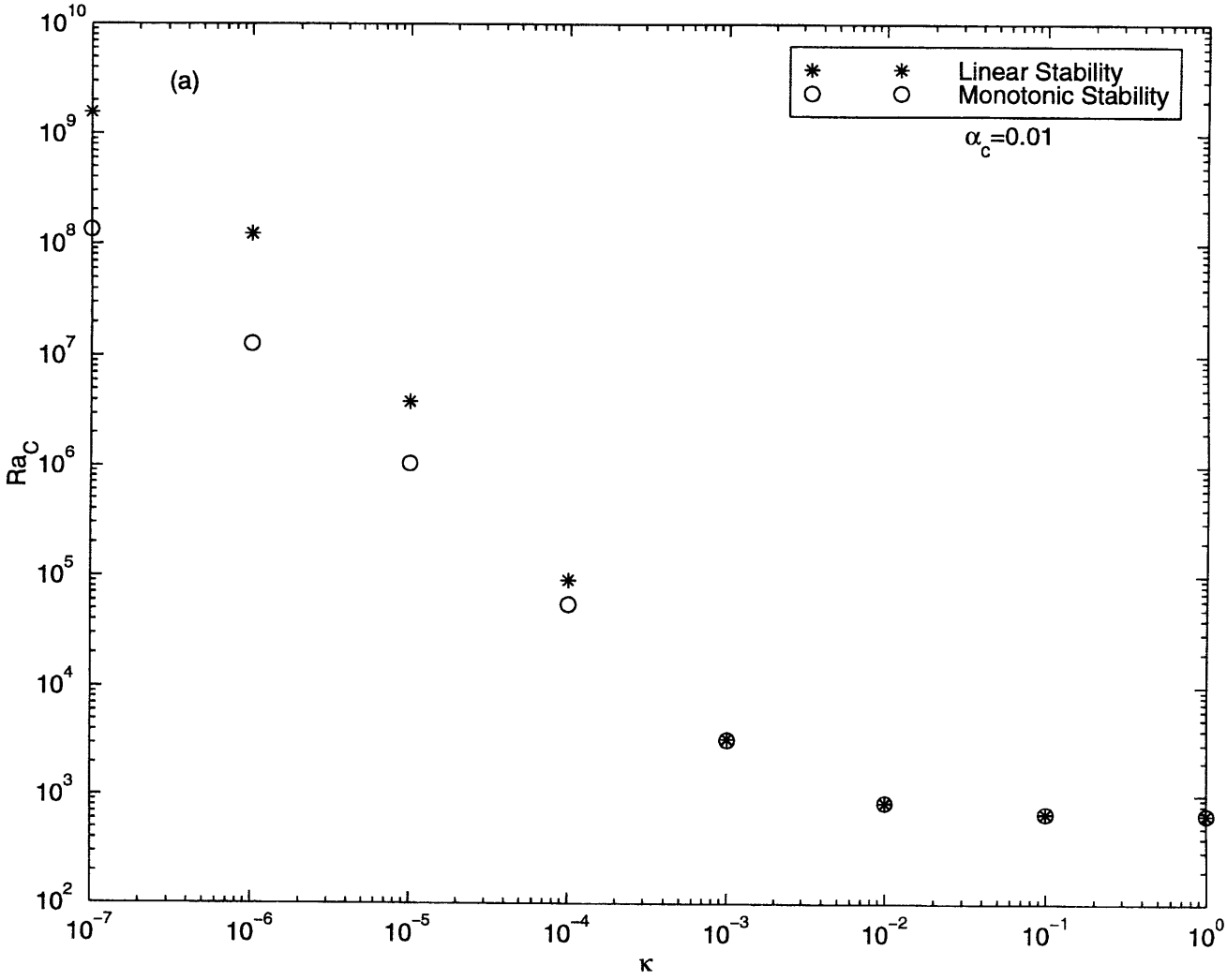

Figure 2-6: The critical Rayleigh number Ra_C for linear stability (asterisks) and the marginal Rayleigh number Ra_{EC} for monotonic stability (circles), plotted versus κ. In (a) $\alpha_c = 0.01$, in (b) $\alpha_c = 0.1$, and in (c) $\alpha_c = 1$. In all cases, $\Gamma = 0$. The region of possible subcritical instability is very small at the larger values of κ and α_c.

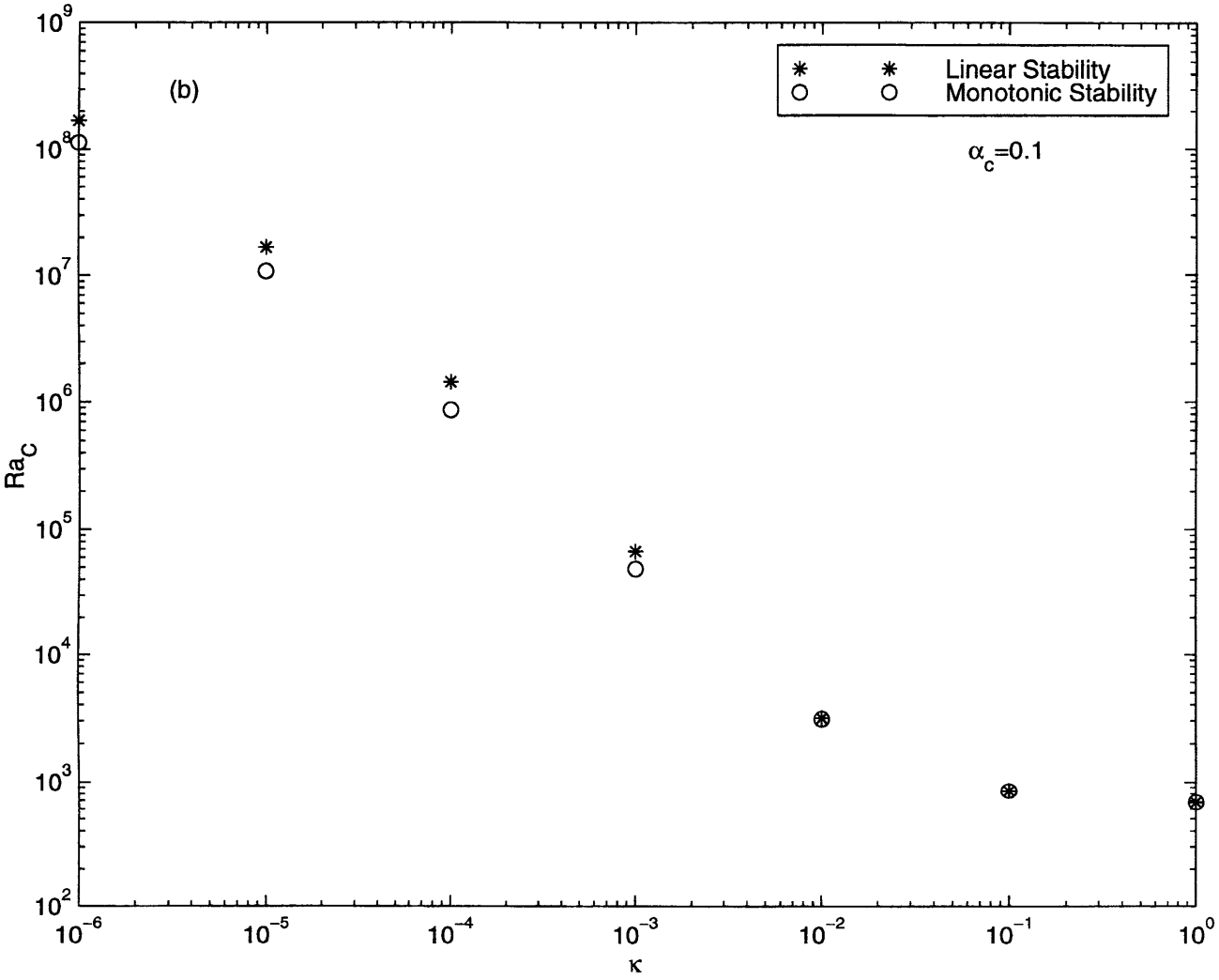
(b)
Linear Stability
Monotonic Stability
α_c=0.1
Ra_c
κ
10^9
10^8
10^7
10^6
10^5
10^4
10^3
10^2
10^{-6}
10^{-5}
10^{-4}
10^{-3}
10^{-2}
10^{-1}
10^0

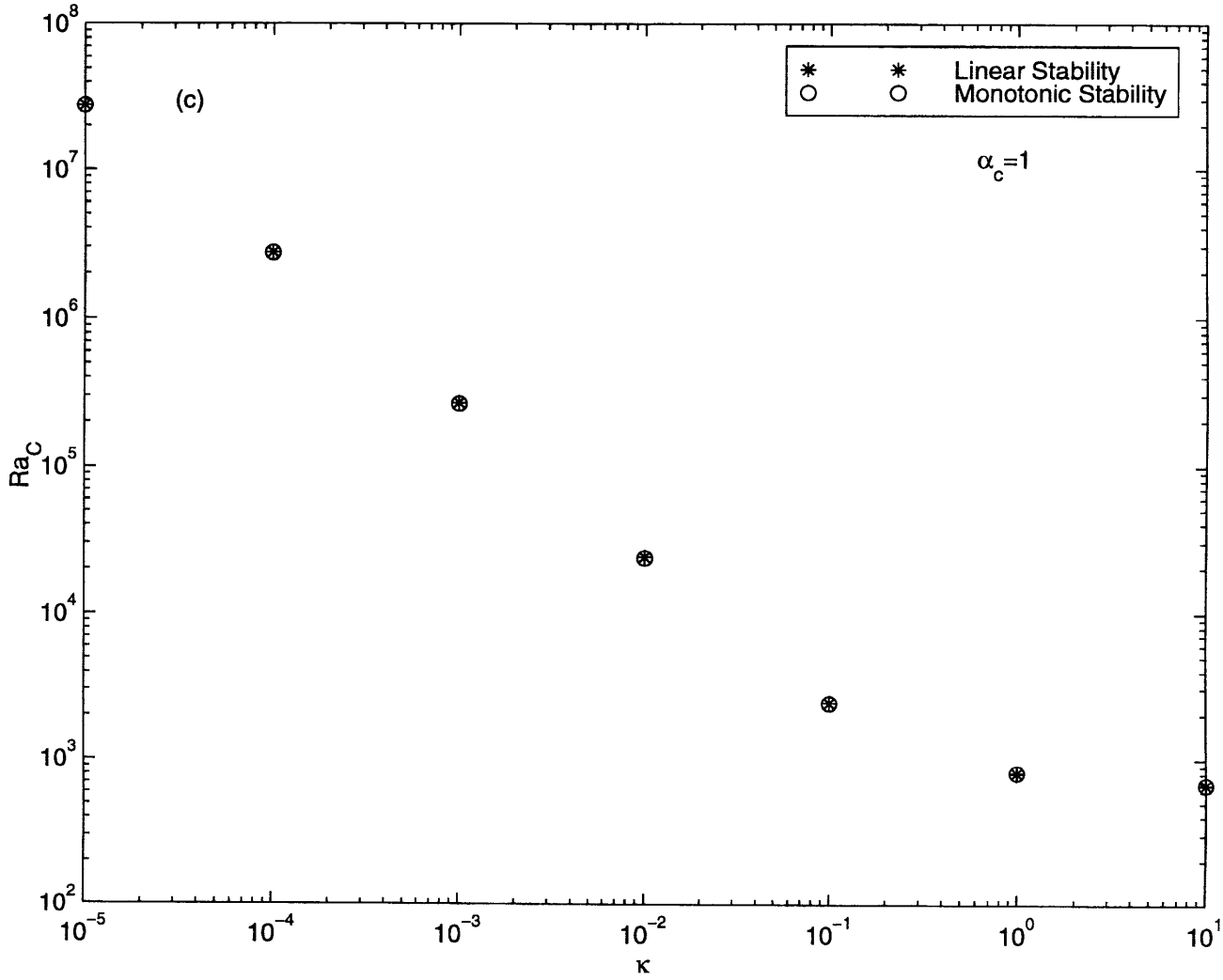
(c)
Linear Stability
Monotonic Stability
α_c=1
Ra_C
κ
10^8
10^7
10^6
10^5
10^4
10^3
10^2
10^{-5}
10^{-4}
10^{-3}
10^{-2}
10^{-1}
10^0
10^1

Chapter 3

Stability Analyses for an Idealized Atmospheric Radiative Equilibrium State

3.1 Introduction

For decades meteorologists have studied fully convecting radiative-convective atmospheres, mostly as idealized models of climate but also as contexts in which to examine convection itself (Ramanathan and Coakley 1978, and references therein; Islam et al. 1993; Held et al. 1993; Emanuel and Bister 1996). In contrast, the *stability* of radiative equilibrium states has been largely neglected. This neglect is not entirely unreasonable. The radiative equilibrium temperature profile of the earth's atmosphere is highly unstable to small perturbations and is therefore never observed. When atmospheric convection does occur, it is extremely turbulent and in many ways profoundly different from marginally stable modes. On the other hand, atmospheric convection is a response to instability (Emanuel 1994, p. 527; Emanuel, Neelin, and Bretherton 1994). We believe that a quantitative understanding of the instability which ultimately gives rise to much of atmospheric convection would aid the understanding of fully turbulent atmospheric convection.

This chapter discusses the linear and nonlinear stability properties of an idealized, dry radiative-convective model. Other branches of meteorology have benefited from the study of idealized models, such as the Eady model of baroclinic instability (Eady 1949). Such models capture the qualitative mechanism of an atmospheric instability yet produce behaviors that are straightforward to interpret. At present there exists no canonical stability problem for a radiative-convective atmosphere. Rayleigh-Bénard convection, in which a fluid layer is confined between upper and lower plates with fixed temperatures, does not suffice as a model of atmospheric convection because it does not include radiation. Goody (1956a) put forth a convective model which includes thermal radiation, but also specifies the temperature on the boundaries, as in Rayleigh-Bénard convection. Goody's model also falls short as a model of atmospheric convection because the atmosphere does not have an analogue to an upper lid at which the temperature is fixed. The tropopause temperature in a radiative-convective atmosphere is not specified, but determined by the constraints of radiation and convection. In both Rayleigh-Bénard convection and Goody's model, the basic state is influenced by the temperature difference maintained between the upper and lower boundaries, whereas in the atmosphere, the radiative equilibrium basic state is set up solely by radiation. Also, a radiative-convective atmosphere contains the further complication that radiation is what destabilizes the atmosphere, but at the same time radiation acts as a stabilizing influence through radiative damping of temperature perturbations.

This chapter advances a radiative-convective model which is a more faithful model of the atmosphere than Goody's model. At the same time, the model is simpler than radiative-convective models which include nongrey radiative transfer schemes or cloud effects. In particular, our model's

behavior can be described in terms of a small number of nondimensional parameters.

This chapter employs several types of stability analysis which have been used successfully in the study of Rayleigh-Bénard convection. First, we prove that for our system, convection arises as overturning cells and not as an oscillatory instability. That is, we prove exchange of stabilities. Second, we perform a linear stability analysis for a highly idealized radiative-convective model. The model is a more faithful representation of atmospheric convection than Rayleigh-Bénard convection, yet possesses an analytic solution of comparable simplicity. It turns out that the linear stability threshold can be written in terms of a 'radiative Rayleigh number' which is a variant of the conventional Rayleigh number. A less idealized radiative-convective model is then studied numerically. Its stability properties can be described approximately in terms of another radiative Rayleigh number. Third, we find a threshold below which all perturbations, regardless of magnitude, decay. For the highly idealized model, we can rule out the possibility of subcritical instabilities; for the less idealized model, we cannot.

Chapter 4 discusses weakly nonlinear convection in essentially the same radiative-convective model as one of the models considered here. Although there are large differences between the stability problem and the weakly convecting problem, we shall note some similarities, particularly in the vertical velocity profiles and in the response to changes in net incoming solar radiation and optical depth.

3.2 Linear Stability Equations

The set-up of our idealized radiative-convective model is summarized here. The atmosphere in our model consists of an infinite horizontal slab of fluid, bounded above and below by rigid, free-slip boundaries. In the analytic stability problem to be discussed, the upper lid is located at the tropopause. In the later problem, the lid is placed in the lower stratosphere, so that the modes may find their own vertical extent. Solar radiation illuminates the top of the atmosphere, passes through the atmosphere unimpeded, and is absorbed entirely at the ground. Its only effect is to establish the proper ground temperature in the radiative equilibrium basic state; solar radiation does not appear in the model equations. The model does not include clouds. The albedo of clouds is crudely taken into account by adjusting the solar constant appropriately. One of the effects of latent heating is crudely simulated by setting the model's 'adiabatic' lapse rate to the approximate climatological average, 6.5 K/km, instead of the dry adiabatic lapse rate. The two-stream, grey model of Goody (1995) is used to represent radiative transfer, despite the fact that real atmospheric gases are nongrey. We use the grey model, however, because it greatly simplifies the radiative transfer equation. The profile of radiative absorption coefficient, which depends on the profiles of radiatively active gases such as water vapor, is specified. Therefore the model contains no interaction between greenhouse gas amounts and other model variables. The model employs the Boussinesq approximation of Spiegel and Veronis (1960), strictly valid only when the domain height is much less than the scale heights of pressure, density, and temperature. This condition does not hold for the earth's atmosphere, but we feel that violation of the Boussinesq assumptions will only distort the solutions, not change them qualitatively.

In the Boussinesq approximation, the governing equations may be written as follows. (In this thesis, subscript asterisks shall denote dimensional quantities.) The momentum equation is

$$\frac{\partial \mathbf{v}_*}{\partial t_*} + \mathbf{v}_* \cdot \nabla_* \mathbf{v}_* = -\frac{1}{\rho_*} \nabla_* p'_* + g_* \alpha_{T*} T'_* \mathbf{k} + \nu_* \nabla_*^2 \mathbf{v}_*, \tag{3.1}$$

where $\mathbf{v}_*$ is the velocity, T'_* the temperature perturbation from the basic state temperature, p'_* the pressure perturbation, ρ_* the (constant) fluid density, g_* the acceleration due to gravity, α_{T*} the thermal expansion coefficient, $\mathbf{k}$ the vertical unit vector, and ν_* the kinematic viscosity. The heat equation is

$$\frac{\partial T_*}{\partial t_*} + \mathbf{v}_* \cdot \nabla_* T_* + w_* \Gamma_* = -\frac{1}{\rho_* c_{p*}} \nabla_* \cdot \mathbf{F}_* + \kappa_* \nabla_*^2 T_*, \tag{3.2}$$

where T_* is the full temperature, $\mathbf{F}_*$ is the (thermal) radiative flux, w_* the vertical component of velocity, Γ_* the 'adiabatic' lapse rate (6.5 K/km), c_{p*} the specific heat at constant pressure, and κ_* the thermal diffusivity. For generality, the thermal diffusivity term will be kept in our equations, although all our computations will assume $\kappa = 0$. The continuity equation is simply

$$\nabla_* \cdot \mathbf{v}_* = 0. \tag{3.3}$$

The (thermal) radiative transfer equation is based on the Eddington approximation as in Goody and Yung (1989) or Goody (1995):

$$\nabla_* \frac{1}{\alpha_*} \nabla_* \cdot \mathbf{F}_* - 3\alpha_* \mathbf{F}_* = 4\nabla_* \sigma_* T_*^4, \tag{3.4}$$

where α_* is the specified radiative absorption coefficient and σ_* is the Boltzmann constant. We have assumed the gas is grey; then the fluid possesses only one length scale, the photon mean free path.

We nondimensionalize the variables according to the following scales:

$$T_* = \mathcal{T}_* T \qquad \mathbf{F}_* = \frac{16}{3}\sigma_* \mathcal{T}_*^4 \mathbf{F} \tag{3.5}$$

$$\mathbf{v}_* = \frac{h_*}{t_{\mathcal{T}*}}\mathbf{v} \qquad p'_* = \rho_* h_* g_* \alpha_{T*} \mathcal{T}_* p'$$

$$\frac{1}{t_*} = \frac{1}{t_{\mathcal{T}*}}\frac{1}{t} \qquad \mathbf{x}_* = h_* \mathbf{x}$$

$$\alpha_* = \frac{\alpha}{h_*},$$

where

$$t_{\mathcal{T}*} \equiv \frac{3}{16}\frac{\rho_* h_* c_{p*}}{\sigma_* \mathcal{T}_*^3}.$$

Here h_* is the height of the domain. The temperature scale $\mathcal{T}_*$ has been left unspecified. The time scale $t_{\mathcal{T}*}$ in our calculations is on the order of the time scale for radiative cooling of the earth's atmosphere, roughly 10 days (Goody, 1995, pp. 116, 283). The velocity scale is the velocity of an air parcel which traverses the depth of the domain in one time scale; this is of the order of the subsidence velocity of air between clouds in a moist atmosphere. The radiative flux scale is proportional to the blackbody radiation emitted by a body at temperature $\mathcal{T}_*$.

With the above scaling, the momentum (3.1), heat (3.2), continuity (3.3) and radiative transfer (3.4) equations may be nondimensionalized to yield, respectively,

$$\chi \frac{\partial \mathbf{v}}{\partial t} + \chi \mathbf{v} \cdot \nabla \mathbf{v} = -\gamma \nabla p' + \gamma\, T' \mathbf{k} + \nabla^2 \mathbf{v}, \tag{3.6}$$

$$\frac{\partial T}{\partial t} + \mathbf{v} \cdot \nabla T + w\Gamma = -\nabla \cdot \mathbf{F} + \kappa \nabla^2 T, \tag{3.7}$$

$$\nabla \cdot \mathbf{v} = 0, \tag{3.8}$$

and

$$\nabla \frac{1}{\alpha} \nabla \cdot \mathbf{F} - 3\alpha \mathbf{F} = \frac{3}{4}\nabla T^4. \tag{3.9}$$

The following nondimensional parameters have been defined:

$$\gamma = \frac{g_* \alpha_{T*} \mathcal{T}_* h_*^3}{\nu_* (h_*^2 / t_{\mathcal{T}*})} \qquad \kappa = \frac{\kappa_*}{h_*^2 / t_{\mathcal{T}*}}$$

$$\Gamma = \frac{\Gamma_* h_*}{\mathcal{T}_*} \qquad\qquad \chi = \frac{h_*^2/\nu_*}{t_{\mathcal{T}*}}.$$

The governing nondimensional parameters are interpreted at the end of this section.

We now write down equations for the basic states whose stability properties we wish to investigate. We are interested in motionless, horizontally uniform basic states. Therefore the basic state profiles may be denoted by $\mathbf{v} = 0$, $\bar{T} = \bar{T}(z)$, and $\overline{\mathbf{F}} = \bar{F}_z(z)\mathbf{k}$. In addition, we specify $\alpha = \alpha(z)$. Substituting these forms into the heat equation (3.7) yields

$$0 = -\frac{d\bar{F}_z}{dz} + \kappa \frac{d^2\bar{T}}{dz^2}. \tag{3.10}$$

The computations we perform assume that $\kappa = 0$; in this case, the basic state is a radiative equilibrium state in which heat is transported solely by radiation. Substituting $\bar{T}$, $\overline{\mathbf{F}}$, and α into the radiative transfer equation (3.9) yields

$$\frac{d}{dz}\frac{1}{\alpha}\frac{d\bar{F}_z}{dz} - 3\alpha\bar{F}_z = 3\bar{T}^3\frac{d\bar{T}}{dz}. \tag{3.11}$$

The linear stability equations, for perturbations about the basic state equations (3.10) and (3.11), can be formulated as follows. We apply the operator $\mathbf{k}\cdot\nabla\times\nabla\times$ to the momentum equation (3.6) and neglect the nonlinear term. This yields

$$\chi\frac{\partial}{\partial t}\nabla^2 w = \gamma\nabla_h^2 T' + \nabla^2\nabla^2 w, \tag{3.12}$$

where $\nabla_h^2 \equiv (\partial^2/\partial x^2 + \partial^2/\partial y^2)$ is the horizontal Laplacian. Next we subtract the basic state heat equation (3.10) from the full heat equation (3.7), drop the nonlinear terms, and replace the divergence of the perturbation radiative flux with the Newtonian approximation,

$$\nabla\cdot\mathbf{F}' = rT' \qquad\qquad r = \frac{t_{\mathcal{T}*}}{t_{R*}}, \tag{3.13}$$

where

$$t_{R*} \equiv \frac{\rho_* h_* c_{p*}}{\sigma_* T_{e*}^3}$$

is the radiative time scale of the atmosphere and T_{e*} is the emission temperature of the atmosphere. These manipulations yield

$$\frac{\partial T'}{\partial t} + w\left(\frac{d\bar{T}}{dz} + \Gamma\right) = -rT' + \kappa\nabla^2 T'. \tag{3.14}$$

The first term on the right-hand side shows that radiation causes the 'radiative damping' of temperature perturbations, with a strength given by r. Given its simplicity, the Newtonian approximation is remarkably accurate for the earth's clear-sky atmosphere, as discussed by Goody (1995, pp. 115–117).

Goody (1995) shows that the Newtonian approximation follows from the fact that in thin to moderately transparent, nongrey atmospheres, radiative heating is dominated by the cooling-to-space contribution. At first sight, it might appear inconsistent to treat the radiative perturbations with the Newtonian approximation, which is derived assuming a nongrey atmosphere, but treat the radiative basic state with a grey model. There is no inconsistency here; rather, we have made the modeling assumption that the grey model is adequate to approximate the earth's basic state radiative profile but not adequate to represent the radiative perturbations. Figure 3-2 below shows that the earth's radiative equilibrium state can be fairly well approximated by a grey calculation, if an optical depth of 4 is chosen. But using an optical depth of 4 in the full grey radiative perturbation equation would prohibit temperature perturbations near the ground from radiating to space, as occurs in a nongrey atmosphere. Hence for temperature perturbations, the Newtonian approximation is superior

to a grey model.

To find the linear modes, we assume the following forms for the perturbations:

$$w = Re\left\{W(z)f(x,y)e^{st}\right\} \qquad T' = Re\left\{\Theta'(z)f(x,y)e^{st}\right\} \tag{3.15}$$

where $f(x,y)$, which describes the horizontal planform, satisfies

$$\nabla_h^2 f(x,y) = -a^2 f(x,y),$$

and a is a real, nondimensionalized horizontal wavenumber. In general, s can be complex: $s = \sigma + i\omega$, where the growth rate σ is a real constant and so is ω. Substituting the modal forms (3.15) into the linear equations for w (3.12) and T' (3.14) yields, respectively,

$$\chi s(D^2 - a^2)W = -\gamma\, a^2\Theta' + (D^2 - a^2)^2 W \tag{3.16}$$

and

$$s\Theta' = -W\left(\frac{d\bar{T}}{dz} + \Gamma\right) - r\Theta' + \kappa(D^2 - a^2)\Theta', \tag{3.17}$$

where the operator $D \equiv d/dz$.

An advantage of the idealized system of equations we have constructed is that it is governed by a small set of dimensionless parameters which may be explicitly written down and physically interpreted. When $\kappa = 0$, the set turns out to consist of two parameters, γ/r and F_T, plus the parameters needed to specify the radiative absorption coefficient $\alpha(z)$. The parameter γ/r is a Rayleigh number based on a 'radiative diffusivity' h_*^2/t_{R*} and the temperature scale $\mathcal{T}_*$. γ/r is the only parameter through which viscosity and radiative damping enter the dynamics. F_T is the (nondimensionalized) outgoing thermal radiation at the top of the domain; for an atmosphere in radiative-convective equilibrium, F_T also equals the net incoming solar radiation. Although our model specifies the ground temperature T_g and computes F_T, we shall regard F_T as the given parameter, since this is conceptually more straightforward. We shall consider two types of α profile: a constant profile, $\alpha = \alpha_c$; and an exponentially decreasing profile, $\alpha = b\, \exp(-Sz)$. In the former case, we must add the optical depth α_c to our list of parameters. In the latter case, we must add to the list S, the (nondimensionalized) inverse scale height of absorbers, and b, a prefactor which sets the overall magnitude of α. The parameter χ is an inverse radiative Prandtl number which turns out not to affect the stability threshold because it multiplies only time-dependent or nonlinear terms.

3.3 Exchange of Stabilities

The principle of exchange of stabilities holds for a convective system if the linear modes arise as steadily growing, overturning cells and not as an oscillatory instability. More precisely, exchange of stabilities is valid if, for any linear mode, the imaginary part of the growth rate ω is zero whenever the real part of the growth rate σ is zero (Drazin and Reid 1981, p. 12). Establishing exchange of stabilities not only illuminates the physical character of the onset of convection but also speeds up numerical calculations of the linear stability threshold. Pellew and Southwell (1940) proved that exchange of stabilities holds in Rayleigh-Bénard convection. It is not obvious, however, that exchange of stabilities also holds in a radiative-convective system. The lapse rate in Rayleigh-Bénard convection is everywhere unstably stratified. In contrast, the stratosphere in a radiative-convective system is stably stratified. It thereby provides a restoring force for vertical motions and hence raises the possibility of oscillatory instability (Spiegel 1960). Furthermore, the proof of Pellew and Southwell (1940) relies on the fact that the Rayleigh-Bénard basic state temperature profile is linear, whereas one of the radiative-convective models we consider has a curved basic state. Spiegel (1962) proves exchange of stabilities for a system with an arbitrary temperature profile but no radiation. Other authors (Spiegel 1960; Murgai and Khosla 1962; Davis 1969; Arpaci and Gőzűm 1973) prove exchange of stabilities for different variations of a radiative-convective system which specifies the

temperature on both boundaries, thereby departing from the radiative-convective systems considered here.

We set $\kappa = 0$ and position the lower and upper boundaries of the model domain at $z = 0$ and $z = 1$ respectively. Our proof is valid for either free-slip boundaries

$$W|_{z=0,1} = D^2 W|_{z=0,1} = 0 \tag{3.18}$$

or rigid boundaries

$$W|_{z=0,1} = DW|_{z=0,1} = 0.$$

Our procedure is to eliminate the Θ' variable from the linear stability equations (3.16) and (3.17), as in Spiegel (1962). We find

$$(s+r)\left(s\chi - (D^2 - a^2)\right)\left(D^2 - a^2\right) W = \gamma a^2 \left(\frac{d\bar{T}}{dz} + \Gamma\right) W. \tag{3.19}$$

To the equation (3.19) we apply the operator $\int_0^1 dz\, W^*(z)$, where W^* denotes the complex conjugate of W, and integrate by parts multiple times, resulting in

$$\begin{aligned} s^2\chi(a^2 J_0 + J_1) \;+\; & s\left(r\chi(a^2 J_0 + J_1) + J_2\right) + rJ_2 \\ = \; & -\gamma\, a^2 \int_0^1 dz\ |W(z)|^2 \left(\frac{d\bar{T}}{dz} + \Gamma\right). \end{aligned} \tag{3.20}$$

We have defined the following positive, real constants:

$$J_0 = \int_0^1 dz\, |W|^2 \qquad\qquad J_1 = \int_0^1 dz\, |DW|^2$$

and

$$J_2 = \int_0^1 dz\, \left|(D^2 - a^2)W\right|^2.$$

By eliminating Θ', we have relegated the troublesome $d\bar{T}/dz$ factor to a term which is always real and hence does not enter our evaluation of the imaginary part of the growth rate σ. The imaginary part of (3.20) is, recalling that $s = \sigma + i\omega$,

$$\omega\left(\chi(2\sigma + r)(a^2 J_0 + J_1) + J_2\right) = 0.$$

By inspection, we see that if $\sigma \geq 0$, then $\omega = 0$, thereby proving exchange of stabilities.

3.4 An Analytic Linear Stability Problem

The purpose of this section is to pose and analytically solve an idealized radiative-convective linear stability problem which retains the simplicity of the Rayleigh-Bénard problem but is a somewhat more realistic model of the atmosphere. To construct a model of this simplicity requires several rather extreme modeling assumptions. The first is to linearize the thermal source function in the basic state radiative transfer equation about T_{g*}. In this section, we choose the temperature scale $\mathcal{T}_* = T_{g*}$. Therefore, linearizing the thermal source function amounts to setting the $\bar{T}^3$ factor in (3.11) equal to unity. This approximation introduces errors of roughly 40 per cent into the radiative equilibrium state, but linearization of the thermal source function is necessary to obtain simple, analytic eigenmodes. Second, we set the radiative absorption coefficient $\alpha(z) = \alpha_c$ to be a constant with altitude. In contrast, the profile of the main radiative absorber in the earth's atmosphere, water vapor, falls off exponentially with altitude with a scale height of approximately 2 km. Third, we fix

the altitude of the rigid, upper lid at the tropopause, thereby preventing the modes from seeking their own vertical extent. Fourth, we set the thermal diffusivity κ to zero. All damping of temperature perturbations is then due to radiation. In the atmosphere, the thermal diffusive damping is much smaller than radiative damping, and hence the $\kappa = 0$ results constitute an important limiting case. In the next section, we keep $\kappa = 0$ but relax the other assumptions. Some of the qualitative features of the present analytical model are preserved in the more sophisticated model.

First we write down the form of the basic state for the linear stability analysis, leaving some constants undetermined. When $\kappa = 0$, the radiative-diffusive equilibrium (3.10) reduces to a radiative equilibrium:

$$\bar{F}_z = F_T = \text{constant}$$

where F_T is the net outgoing thermal radiation at the top of the atmosphere, which equals the net incoming solar radiation. Inserting a constant radiative flux into the basic state radiation equation (3.11), linearized about $T = T_g = 1$, yields the basic state temperature gradient

$$\frac{d\bar{T}}{dz} = -\alpha_c F_T = -\left(T_l - T_u\right). \tag{3.21}$$

A temperature discontinuity appears at the ground because thermal diffusivity is absent. T_l denotes the air temperature adjacent the ground, and T_u denotes the temperature at the top of the domain. The basic state temperature decreases linearly with altitude.

Next we formulate radiative boundary conditions appropriate to the atmosphere. We stipulate that there is no incoming thermal radiation at the top of the domain. Then, following Goody (1995, pp. 114–115), we may show that the upper radiative boundary condition becomes

$$\frac{8}{3}F_T = \bar{T}^4\big|_{z=1} \cong 1 - 4\left(1 - T_u\right). \tag{3.22}$$

The far right-hand side has been obtained by linearization about $\bar{T} = T_g = 1$. In a similar fashion, the bottom radiative boundary condition may be derived from the assumption that the upwelling radiance near the ground is that due to a blackbody. Then we find

$$\frac{8}{3}F_T = 1 - \bar{T}^4\big|_{z=0} \cong 4\left(1 - T_l\right). \tag{3.23}$$

We may now solve for the basic state temperature gradient and radiative flux. Equations (3.21), (3.22), and (3.23) yield

$$\frac{d\bar{T}}{dz} = -\frac{\frac{3}{8}\alpha_c}{2 + \frac{3}{2}\alpha_c} \qquad F_T = \frac{3/8}{2 + \frac{3}{2}\alpha_c}. \tag{3.24}$$

If we substitute a reasonable value of the optical depth, $\alpha_c = 4$, into (3.24), the resulting value of $-d\bar{T}/dz$ is less than the average value in a more realistic radiative equilibrium calculation. The discrepancy is largely due to the various linearizations we have made.

With the basic state in hand, we may proceed to write down the linear stability eigenmodes and solve for the eigenvalues. The eigenvalue equation is (3.19), with the basic state temperature gradient given by (3.24) and s set equal to zero because of exchange of stabilities. By inspection, we see that the eigenfunctions are sinusoidal, as in Rayleigh-Bénard convection:

$$W(z) = \sin \pi z. \tag{3.25}$$

Then, from (3.16), we find

$$\Theta'(z) = \frac{(\pi^2 + a^2)^2}{a^2\,\gamma} \sin \pi z. \tag{3.26}$$

The eigenmodes fill the depth of the troposphere. They are plotted, along with the basic state temperature profile, in Figure 3-1.

We may now find the critical wavenumber and linear stability threshold as in Chapter 2. The critical wavenumber again turns out to be $a = \pi$. The critical threshold for linear stability can again be expressed in terms of a radiative Rayleigh number

$$Ra_r = -\left(\frac{d\bar{T}}{dz} + \Gamma\right)\frac{\gamma}{r}$$

with critical value $Ra_{rC} = 4\pi^2$. If we define a radiative diffusivity $\kappa_{R*} \equiv h_*^2/t_{R*}$ and a lapse rate difference from adiabatic

$$\beta_* \equiv -\frac{d\bar{T}_*}{dz_*} - \Gamma_* = \frac{3}{8}\frac{(F_{T*}/2\sigma_*)^{1/4}}{h_*}\left(\frac{\alpha_c^{4/3}}{2+\frac{3}{2}\alpha_c}\right)^{3/4} - \Gamma_*$$

then, using (3.24) and (3.5), we find

$$Ra_r = \frac{g_*\alpha_{T*}\beta_* h_*^4}{\nu_*\kappa_{R*}} = \frac{g_*\alpha_{T*}\left(\frac{3}{8}\frac{(F_{T*}/2\sigma_*)^{1/4}}{h_*}\left(\frac{\alpha_c^{4/3}}{2+\frac{3}{2}\alpha_c}\right)^{3/4} - \Gamma_*\right)h_*^4}{\nu_*\left(h_*^2/t_{R*}\right)}. \tag{3.27}$$

Because of the simplifications we have introduced, the critical condition depends on only one parameter, as in Rayleigh-Bénard convection. This parameter, Ra_r, resembles the classical Rayleigh number, except that κ_{R*} is a radiative diffusivity, not the thermal diffusivity; also, β_* does not include the temperature jump at the ground. Spiegel (1960) and Chapter 2 discuss similar radiative Rayleigh numbers for a system which is like Rayleigh-Bénard convection but includes radiative transfer.

One can gain qualitative insight into how various parameters affect the stability of a radiative-convective atmosphere by inspection of (3.27). In particular, if the radiative damping time scale t_{R*} is kept fixed, then either an increase in optical depth α_c or an increase in the net incoming solar radiation F_{T*} leads to an increase in Ra_r and hence greater instability. (However, t_{R*} depends on the emission temperature of the atmosphere and hence might be expected to change if F_{T*} changes.) The increase in Ra_r occurs through an increase in the basic state lapse rate, not a decrease in the damping of modes.

Ra_r differs from the radiative Rayleigh number Ra_R discussed in Chapter 2. First, the basic state lapse rates in Ra_r and Ra_R have different dependencies. Second, the radiative diffusivity in Ra_r is independent of α_{c*}, whereas the radiative diffusivity in Ra_R is proportional to α_{c*}.

Instead of introducing the radiative damping parameter r and using the Newtonian approximation, one may perform the linear stability calculation with a full grey equation for radiative perturbations. When the optical depth α_c is small, the solution remains unchanged except that r is replaced by $3\alpha_c$. When α_c is large, a^2 approaches $\pi^2/2$ and the stability threshold is approximated by $-\gamma\alpha_c(d\bar{T}/dz + \Gamma) = 27\pi^4/4$. This is very similar to what Goody (1956) obtains for the optically thick limit of a similar system. The full grey solutions are not too different from the solutions we have found using the Newtonian approximation.

3.5 A Linear Stability Problem with an Exponential Radiative Absorption Coefficient

To produce a more realistic basic state temperature profile, this section relaxes some of the assumptions made in the analytical linear stability problem. The stability calculations are then performed numerically. Some of the features of the linear stability threshold and eigenmodes, however, remain qualitatively unchanged from the analytic solution. The new assumptions are as follows. First, the profile of radiative absorption is no longer constant, but falls off exponentially with increasing altitude: $\alpha = b\exp(-Sz)$, where S is an inverse scale height of absorption. This profile is intended to reflect the climatological profile of water vapor, the main radiative absorber. Second, the thermal source function in the radiative transfer equation (3.11) is no longer linearized. Third, the upper lid

is lifted to the lower stratosphere, so that the eigenmodes may freely penetrate the stable portion of the temperature profile. Also, in this section we choose the temperature scale to be $\mathcal{T}_* = \Gamma_* h_*$.

The climatological water vapor profile is maintained in large part by convective transports. If convection were shut off, as in a radiative equilibrium state, the optical depth of the atmosphere would decrease greatly. Despite this, we feel that it is fruitful to study the stability of a radiative equilibrium basic state which has the same radiative absorption coefficient as the current climate. Deducing a direct connection between absorption coefficient and water vapor mixing ratio is difficult for a grey gas. Reasonable assumptions, however, lead to the conclusion that our radiative equilibrium profile corresponds to supersaturation in the mid-troposphere. The thermodynamic and radiative effects of the resulting clouds are ignored in this chapter.

The basic state is a slight modification of that obtained by Goody (1995, pp. 126–127). The basic state radiative flux is still constant, as may be seen from (3.10) with $\kappa = 0$. Then, to obtain the temperature profile, it is sufficient to solve (3.11) subject to the boundary condition (3.22), where we no longer use linearized approximation on the far right-hand side. A temperature discontinuity appears at the ground. Above this discontinuity, the temperature profile is

$$\bar{T} = \left(\frac{8}{3}F_T\right)^{1/4}\left(1 + \frac{3}{2}\frac{1}{S}\left(\alpha - be^{-S}\right)\right)^{1/4}, \tag{3.28}$$

and, taking the derivative,

$$\frac{d\bar{T}}{dz} = -\frac{3}{8}\alpha\left(\frac{8}{3}F_T\right)^{1/4}\left(1 + \frac{3}{2}\frac{1}{S}\left(\alpha - be^{-S}\right)\right)^{-3/4}. \tag{3.29}$$

The linear stability problem is again governed by (3.19) with $s = 0$ and $d\bar{T}/dz$ given by (3.29). We solve this eigenvalue equation with a pseudospectral Chebyshev numerical method, following Boyd (1989). Using linear combinations of Chebyshev polynomials, we construct a set of basis functions, each of which satisfies the free-slip boundary conditions (3.18). We expand W in terms of these basis functions, and, given a choice of a^2, solve the eigenvalue problem for the coefficients. We compute all eigenvalues and select the smallest one. To find the critical value of γ, γ_C, we minimize the eigenvalue numerically with respect to a^2. To perform this minimization, we use the golden section search, as described in Press et al. (1992). Details of the numerical method are described in Chapter 2.

We now compute the linear modes for a control run with $F_T = 2.75$, $b = 40$, and $S = 10$. If we assume the domain height is $h_* = 20$ km and the 'adiabatic' lapse rate is $\Gamma_* = 6.5$ K/km, these values of the input parameters correspond roughly to the current globally-averaged climate: net incoming solar radiation 240 W/m^2, optical depth 4, and absorber scale height 2 km. Figure 3-2 depicts the basic state temperature profile (3.28) along with the vertical velocity (W) and temperature (Θ') linear modes, as computed from (3.19) with $s = 0$ and $d\bar{T}/dz$ given by (3.29). Superposed on the temperature profile is the nongrey radiative equilibrium profile displayed in Figure 4 of Manabe and Strickler (1964). Their calculation of the basic state employs absorber profiles derived from atmospheric data at the latitude 35N. Also, their calculation includes solar radiation, using the annual mean hemispheric values of the solar constant and zenith angle. The two basic states agree qualitatively except for the fact that Manabe and Strickler's temperature profile increases with height in the stratosphere. This is because they have included absorption of solar radiation by ozone, whereas we have not. The W mode exhibits a single, broad maximum, similar in shape to the sinusoidal W mode (3.25) found in the analytic stability model. A notable feature of the W mode is that it penetrates far into the stably stratified portion of the basic state. The top of the unstably stratified portion of the basic state $z_n = z_{n*}/h_*$ has been denoted by an x-mark in Figure 3-2. z_{n*} is the altitude at which $-d\bar{T}_*/dz_* = \Gamma_*$. Although z_n in Figure 3-2 corresponds to an altitude of about 6 km, W becomes small only at about 12 km and completely vanishes only at about 15 km. The W profile extends to or above the climatological tropopause, despite the fact that a linear mode is infinitesimal in amplitude and therefore has no inertia. Overshooting of the linear modes into a stably stratified region was also found for nonradiative cases by Whitehead and Chen (1970) and Sun (1976). The Θ' mode is not sinusoidal, as in the analytical stability model, but

Varied Parameter	$Ra_{\mathcal{R}C}$	$a_C z_n$
Control run	30.50	2.24
$F_T = 0.6875$	30.11	2.27
$F_T = 11$	31.05	2.21
$b = 10$	30.56	2.30
$b = 80$	30.31	2.21
$S = 7$	30.03	2.26
$S = 40$	33.77	2.24

Table 3.1: Critical values for linear stability of a radiative Rayleigh number $Ra_{\mathcal{R}C}$ defined by (3.30) for various values of F_T, b, and S. The critical wavenumber a_C times the depth of the unstable layer z_n is also listed.

instead has a large region of negative Θ' which arises because the mode penetrates into the stably stratified region.

We now seek the dependencies of the critical value of γ/r, γ_C/r, on the governing parameters F_T, b, S. One could study how γ_C/r varies as the other parameters are varied individually, as depicted later in Figure 3-5. The study of a three-dimensional parameter space, however, is unwieldy. Instead, prompted by the analytic stability problem, we characterize the stability properties in terms of a single parameter, another radiative Rayleigh number $Ra_{\mathcal{R}C}$. Both Whitehead and Chen (1970), and Sun (1976) used modified Rayleigh numbers to characterize the stability of curved temperature profiles. However, they were not concerned with radiative damping. Also, their basic state temperature profiles were not calculated from radiative equilibrium equations. To construct a useful Rayleigh number, we need to choose appropriate length, temperature gradient, and heat diffusivity scales. In the present radiative-convective problem, convection does not fill the whole depth of the domain, and so h_* is not an appropriate length scale. Instead we use z_{n*}, the depth of the unstable portion of the basic state. As a temperature gradient scale β_*, we choose the average potential temperature gradient across the unstable portion of the basic state, excluding the discontinuity at the ground. Finally, as a diffusivity scale, we choose the radiative diffusivity $\kappa_{R*} = z_{n*}^2/t_{R*}$. Our radiative Rayleigh number is then defined as

$$Ra_{\mathcal{R}} \equiv \frac{g_* \alpha_{T*} \beta_* z_{n*}^4}{\nu_* \left(z_{n*}^2/t_{R*}\right)} = \frac{\gamma}{r}\left(\frac{\Delta T}{z_n} - 1\right) z_n^2 \tag{3.30}$$

where

$$\beta_* = \frac{\Delta T_*}{z_{n*}} - \Gamma_*.$$

We have chosen $\mathcal{T}_* = \Gamma_* h_*$. ΔT is the (nondimensionalized) temperature drop across the unstable portion of the sounding, excluding the temperature discontinuity at the ground. Note that $Ra_{\mathcal{R}}$ is independent of the height of the domain h_*. $Ra_{\mathcal{R}}$, like Ra_r or Ra, may be interpreted as measure of the relative strength of various dynamical terms (Tritton 1988, pp. 173–174). In particular, $Ra_{\mathcal{R}}$ may be regarded as the product of two ratios: the ratio of the buoyancy force over the viscous force, times the ratio of the advection of basic state potential temperature over the radiative damping term. It is unreasonable to expect to encapsulate the stability properties of a curved basic state temperature profile exactly with a single number, and indeed, $Ra_{\mathcal{R}C}$ serves only as an approximate threshold for linear stability. $Ra_{\mathcal{R}}$ is inexact in large part because it contains no information about the temperature profile above z_{n*}.

We now explore the accuracy with which $Ra_{\mathcal{R}}$ serves as an indicator of linear stability. Starting with the control run values, $F_T = 2.75$, $b = 40$, and $S = 10$, we vary each of these parameters individually over wide ranges and calculate $Ra_{\mathcal{R}C}$ and the scaled critical wavenumber $a_C z_n$. The results are summarized in Table 3.1. Table 3.1 shows that as F_T, b, and S are varied over wide ranges,

$Ra_{\mathcal{R}C}$ departs little from the control run value of 30.50. The greatest spread of tabulated values of $Ra_{\mathcal{R}C}$ is about 12 per cent. The greatest deviations occur when S is varied. This is not surprising, since varying S greatly alters the shape of the profile, of which $Ra_{\mathcal{R}C}$ contains little information. Indeed, $Ra_{\mathcal{R}C}$ contains no information about the shape of the profile above z_n. In summary, it appears that $Ra_{\mathcal{R}C}$ serves as a useful, if approximate, measure of the stability of this radiative-convective system. Values of the scaled critical wavenumber $a_C z_n$ also vary little. Therefore the preferred wavelength for linear instability remains approximately proportional to the depth of the unstable layer z_n as F_T, b, and S are varied.

It is of interest to check whether or not $Ra_{\mathcal{R}}$ is still useful for a more realistic radiative equilibrium state. Therefore we again solve the linear stability problem given by (3.19), but now we substitute for $d\bar{T}/dz$ the more realistic radiative equilibrium temperature profile displayed in Figure 4 of Manabe and Strickler (1964). Their basic state temperature profile and the corresponding linear modes are shown in Figure 3-3. For this profile, $Ra_{\mathcal{R}C} = 42.1$, about 35 per cent higher than the control run value $Ra_{\mathcal{R}C} = 30.50$. The difference arises largely because absorption of solar radiation by stratospheric ozone leads to a strongly stratified region beginning just above z_n. This feature is absent from the family of temperature profiles given by (3.28). $Ra_{\mathcal{R}}$ cannot incorporate this feature because it contains no information about the basic state above z_n. However, the value of $Ra_{\mathcal{R}}$ computed from Manabe and Strickler's profile is roughly similar to the prior values, which suggests that $Ra_{\mathcal{R}}$ still has conceptual value, even if it is not quantitatively accurate.

The advantage of writing the stability threshold approximately in terms of $Ra_{\mathcal{R}}$ is that one needs merely to inspect $Ra_{\mathcal{R}}$ in order to ascertain the approximate effects of the governing parameters on the stability threshold. For instance, inspection of $Ra_{\mathcal{R}}$ shows that increasing the radiative damping timescale t_{R*} destabilizes the radiative equilibrium state, with an approximately linear dependence. In a similar manner, we see that increasing the coefficient of viscosity ν_* stabilizes the fluid. The parameters which influence the basic state — F_T, b, and S — enter $Ra_{\mathcal{R}}$ only through the factor $(\Delta T/z_n - 1)z_n^2$. This factor's dependence on F_T, b, and S is plotted in Figure 3-4. Increasing the net incoming solar radiation F_T destabilizes the radiative equilibrium basic state. Similarly, increasing b, which corresponding to increasing the optical depth of the atmosphere while the shape of the absorber profile fixed, destabilizes the basic state. In both cases, the destabilizations occur, it turns out, both because the depth of the unstable layer z_n increases and because the average lapse rate across z_n increases. Increasing S, which corresponds to decreasing the absorber scale height, stabilizes the fluid by decreasing z_n.

The present radiative Rayleigh number $Ra_{\mathcal{R}}$ resembles the radiative Rayleigh number Ra_r for the constant absorption coefficient case $\alpha = \alpha_c$. The length scale employed in both radiative Rayleigh numbers is the depth of the unstable layer; in Ra_r, this turns out to be just the depth of the layer h_*. The damping parameters ν_* and t_{R*} enter into both radiative Rayleigh numbers in the same way. According to both radiative Rayleigh numbers, the basic state is destabilized by increasing the net incoming solar radiation and by increasing the optical depth with the shape of the absorber profile held fixed. This indicates that the analytic solution for constant radiative absorption coefficient has qualitative relevance to the case when the absorption coefficient decreases with altitude.

3.6 Energy Stability Theory

The energy method may be used to find a threshold γ_{EC} below which all perturbations, regardless of magnitude, decay to zero. The analysis proceeds as in Chapter 2. For the analytic linear stability problem of Section 3.4 with α constant, subcritical instabilities may be ruled out because the basic state temperature profile is linear. For the stability problem of Section 3.5 in which α decreases exponentially with height, the energy method does not rule out the possibility of subcritical instabilities. The equation for γ_E turns out to be

$$\left(D^2 - a^2\right)^2 W(z) = \frac{\gamma_E}{r}\left(\frac{a^2}{4\eta}\right)\left(1 - \eta\frac{d\bar{T}}{dz} - \eta\Gamma\right)^2 W(z). \tag{3.31}$$

We have reverted to the temperature scale $\mathcal{T}_* = \Gamma_* h_*$ so that $\Gamma = 1$. We solve this eigenvalue equation for γ_E/r numerically. The numerical method is described in more detail in Chapter 2.

Figure 3-5 shows plots of the threshold γ_{EC}/r versus a^2 (circles) for monotonic stability superimposed on plots of the critical threshold γ_C/r (asterisks) for linear stability problem. On these plots, the areas of parameter space below the monotonic stability curves (circles) are stable to arbitrarily large perturbations. The areas above the linear stability curves (asterisks) are unstable even to infinitesimal perturbations, if they project onto the unstable mode. The linear stability curve is typically about 1.5 times the monotonic stability curve. In the areas between the monotonic and linear stability curves, there is the possibility of subcritical instability, although the analysis we have performed cannot confirm or deny this.

It is well known that in many atmospheric soundings, there are parcels of air that remain negatively buoyant until they are lifted to their level of free convection. Therefore, in some cases, moist convection arises as a subcritical instability (Emanuel, 1994, pp. 168–169). What our analysis points out is that even in a dry radiative-convective atmosphere, subcritical instability may still occur because the basic state temperature profile is curved.

3.7 Conclusions

This chapter has investigated the linear and nonlinear stability properties of an idealized, dry radiative-convective model. The model has been simplified enough that simple, sometimes analytic, results may be obtained. These results indicate how the stability properties of the atmosphere change as various radiative and non-radiative governing parameters are varied.

When the radiative-convective model has no thermal diffusion and free-slip boundaries, we prove that exchange of stabilities is obeyed. That is, the onset of convection occurs as steadily turning cells and not an oscillatory instability. Exchange of stabilities also holds for Rayleigh-Bénard convection (Pellew and Southwell, 1940) and for the radiative-convective system of Chapter 2.

We first examined a highly idealized radiative-convective model in which the radiative absorption coefficient α is constant with altitude. A simple analytic solution is possible because, except for a discontinuity at the ground, the basic state temperature profile is linear. The linear stability threshold can be characterized by a single parameter, a radiative Rayleigh number Ra_r. Inspection of Ra_r shows how various parameters influence stability. In our model, an increase in the (dimensional) net incoming solar radiation F_{T*}, with all other parameters held fixed, is a destabilizing influence. In the earth's atmosphere, an increase in F_{T*} would occur if, for instance, the solar constant increased. An increase in the optical depth α_c, as would occur if the concentration of greenhouse gases increased, also destabilizes our system. Increasing the viscosity or radiative damping stabilizes the system. The linear modes have sinusoidal vertical velocity and temperature perturbation profiles. We can prove rigorously that no subcritical instabilities exist.

Some of these features carry over to a somewhat more realistic model in which $\alpha = b\exp(-Sz)$ decreases exponentially with altitude. In this model, the dimensionless parameters are: the net incoming solar radiation F_T; the radiative absorption parameters b and S; and the ratio γ/r, which is similar to a Rayleigh number. Three of these parameters (F_T, b, S) enter into the calculation of the basic state. The other parameter (γ/r) does not affect the basic state but incorporates the damping effects of viscosity and radiative damping. As in the analytic model, an increase in b (which increases the optical depth) or F_T destabilizes the system, and an increase in viscosity or radiative damping stabilizes the system. The linear stability threshold is given approximately by a single combination of these parameters, a radiative Rayleigh number $Ra_{\mathcal{R}}$, which is similar to Ra_r. The vertical velocity profile of the linear mode is still approximately sinusoidal, but the temperature perturbation profile is not; instead it contains a negative overshoot region. The energy method establishes a threshold below which all perturbations, whether infinitesimal or finite-amplitude, decay. Subcritical instabilities, however, cannot be ruled out as in the constant α case.

The stability results are in some ways similar to the weakly nonlinear results presented in Chapter 4. The parameters F_T, b, and S have strong effects in both cases. Specifically, increasing F_T, increasing b, or decreasing S destabilizes our radiative-convective system and also increases the

convective heat flux in the weakly nonlinear convecting case. In contrast, the dimensional damping parameters, e.g. ν_* and t_{R*}, have strong effects in the stability analyses but turn out to have only weak effects in the weakly nonlinear convecting case. Also, both the linear modes and the weakly convecting vertical velocity profile are similar in shape and vertical extent. These issues are discussed in more detail in Chapter 4.

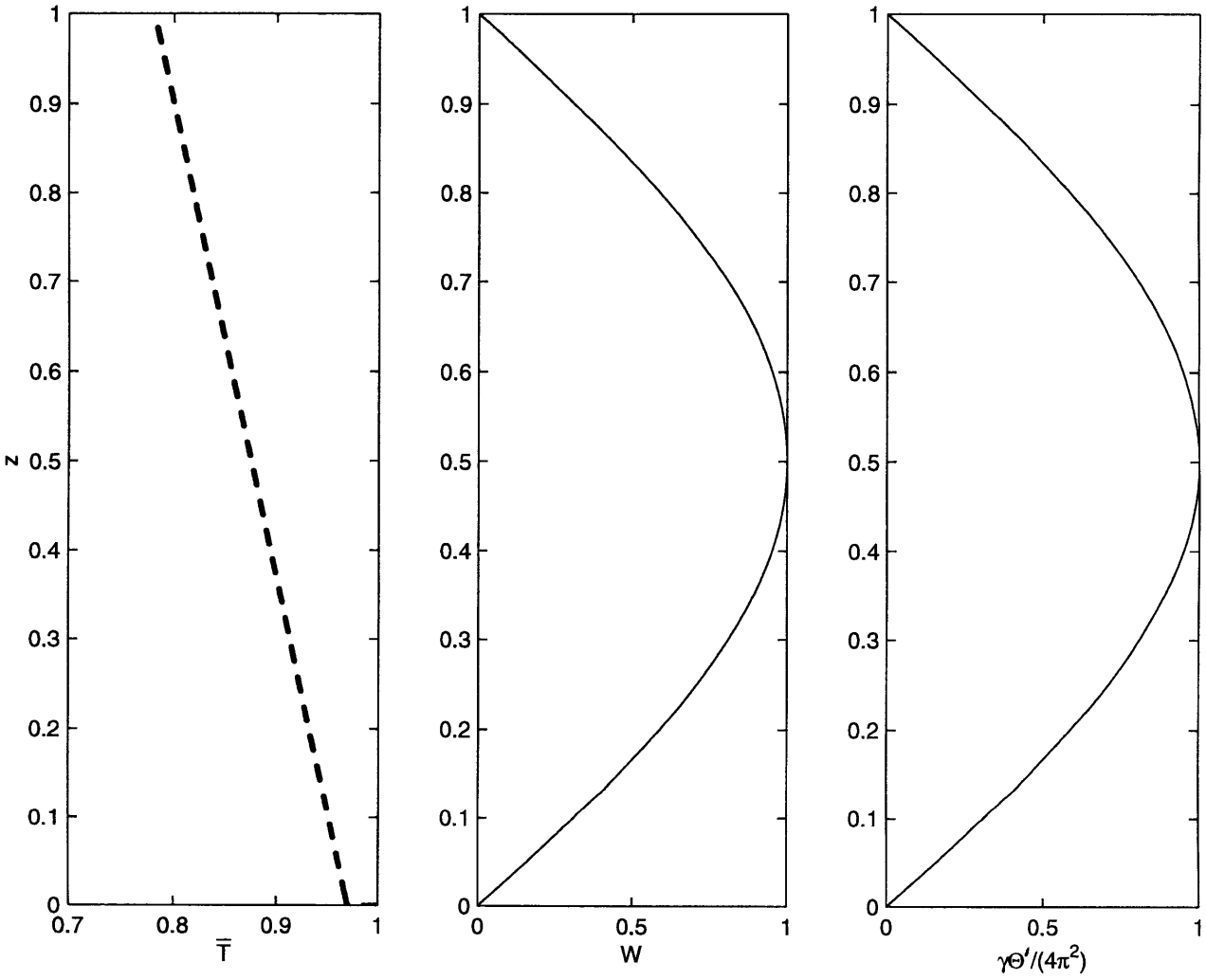

Figure 3-1: The basic state and eigenmodes plotted versus altitude for the analytic stability problem discussed in Section 3.4. The left-hand panel displays the basic state temperature profile $\bar{T}$, as computed from (3.24). There is a discontinuity at the ground. The middle panel displays the vertical velocity eigenmode (3.25), and the right-hand panel displays the temperature perturbation eigenmode (3.26) multiplied by a normalizing factor. The eigenmodes are simple sinusoids, as in Rayleigh-Bénard convection, because $\bar{T}$ is linear in the interior.

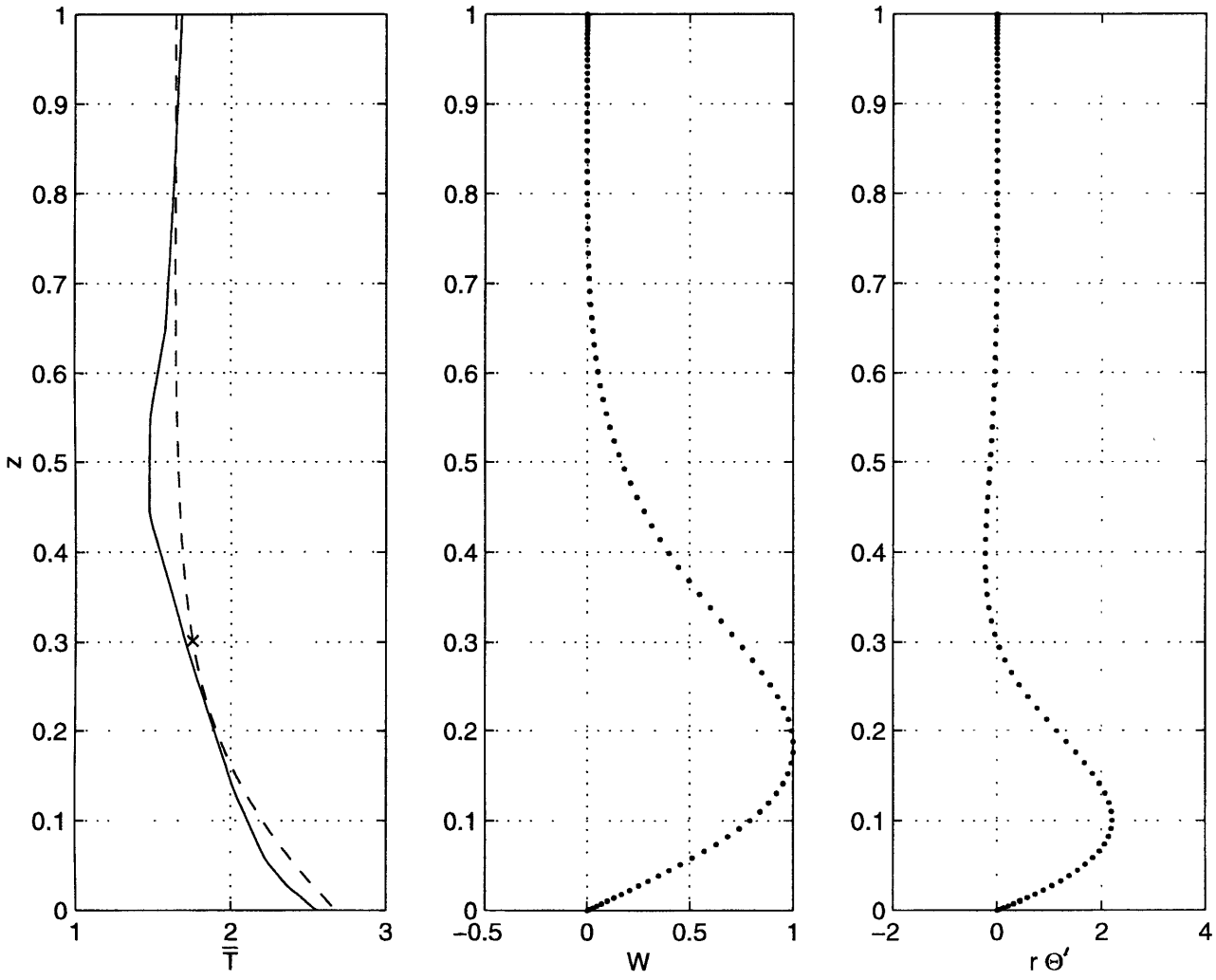

Figure 3-2: The basic state and critical linear eigenmodes of the radiative equilibrium state discussed in Section 3.5, for a control run with $F_T = 2.75$, $b = 40$, $S = 10$. The left-hand panel displays the basic state temperature profile (3.28) (dashed line) and, for comparison, the profile from Figure 4 of Manabe and Strickler (1964) (solid line), divided by the temperature scale $\Gamma_* h_* = 130$ K. The x-mark locates z_n, the top of the unstable portion of the dashed temperature profile. The middle panel shows the vertical velocity eigenmode, and the right-hand panel shows the temperature perturbation eigenmode multiplied by the radiative damping parameter r.

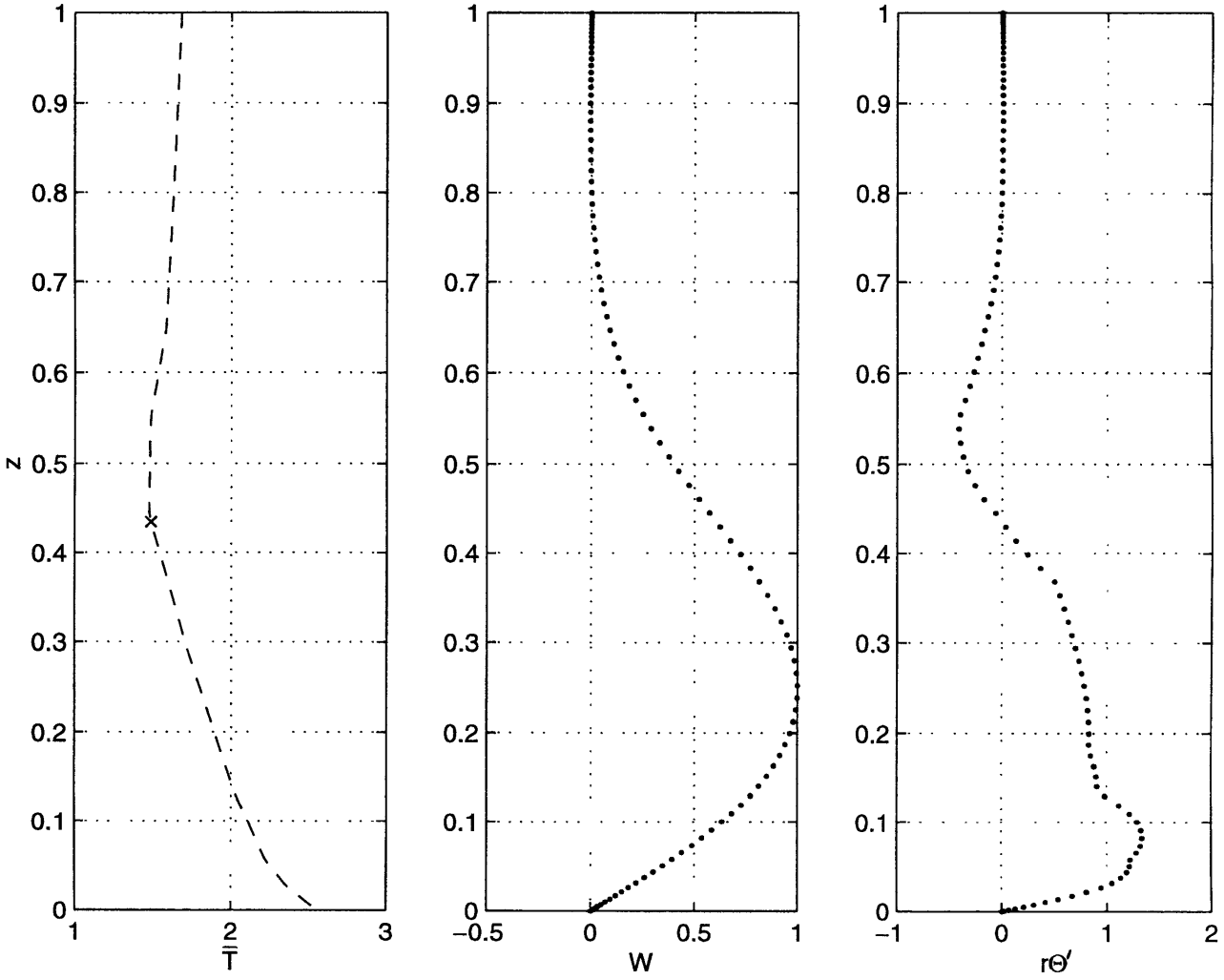

Figure 3-3: The left-hand panel displays the basic state temperature profile $\bar{T}$ from Figure 4 of Manabe and Strickler (1964), divided by $\Gamma_* h_* = 130$ K. The x-mark denotes z_n, the top of the unstable layer. The middle panel displays the vertical velocity linear eigenmode at the critical wavenumber for linear stability, $a = 5.75$. The right panel displays the corresponding temperature perturbation eigenmode, multiplied by the radiative damping parameter r. The vertical velocity eigenmode is similar to that for the grey radiative equilibrium profile (3.28), but the temperature perturbation eigenmode is less smooth.

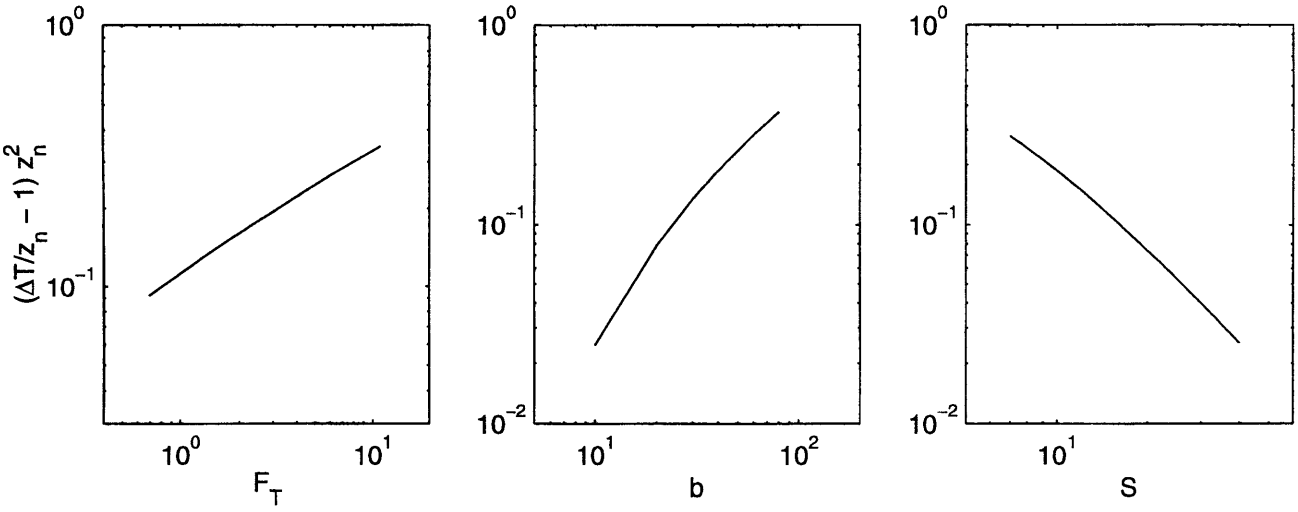

Figure 3-4: These panels illustrate the effect of F_T, b, and S on $(\Delta T/z_n - 1)z_n^2$ and hence their effect on the radiative Rayleigh number $Ra_{\mathcal{R}} = (\gamma/r)(\Delta T/z_n - 1)z_n^2$. F_T, b, and S are each varied individually while the other two parameters are held fixed at the control run values $F_T = 2.75$, $b = 40$, and $S = 10$. Increasing F_T or b destabilizes the basic state, whereas increasing S stabilizes the basic state.

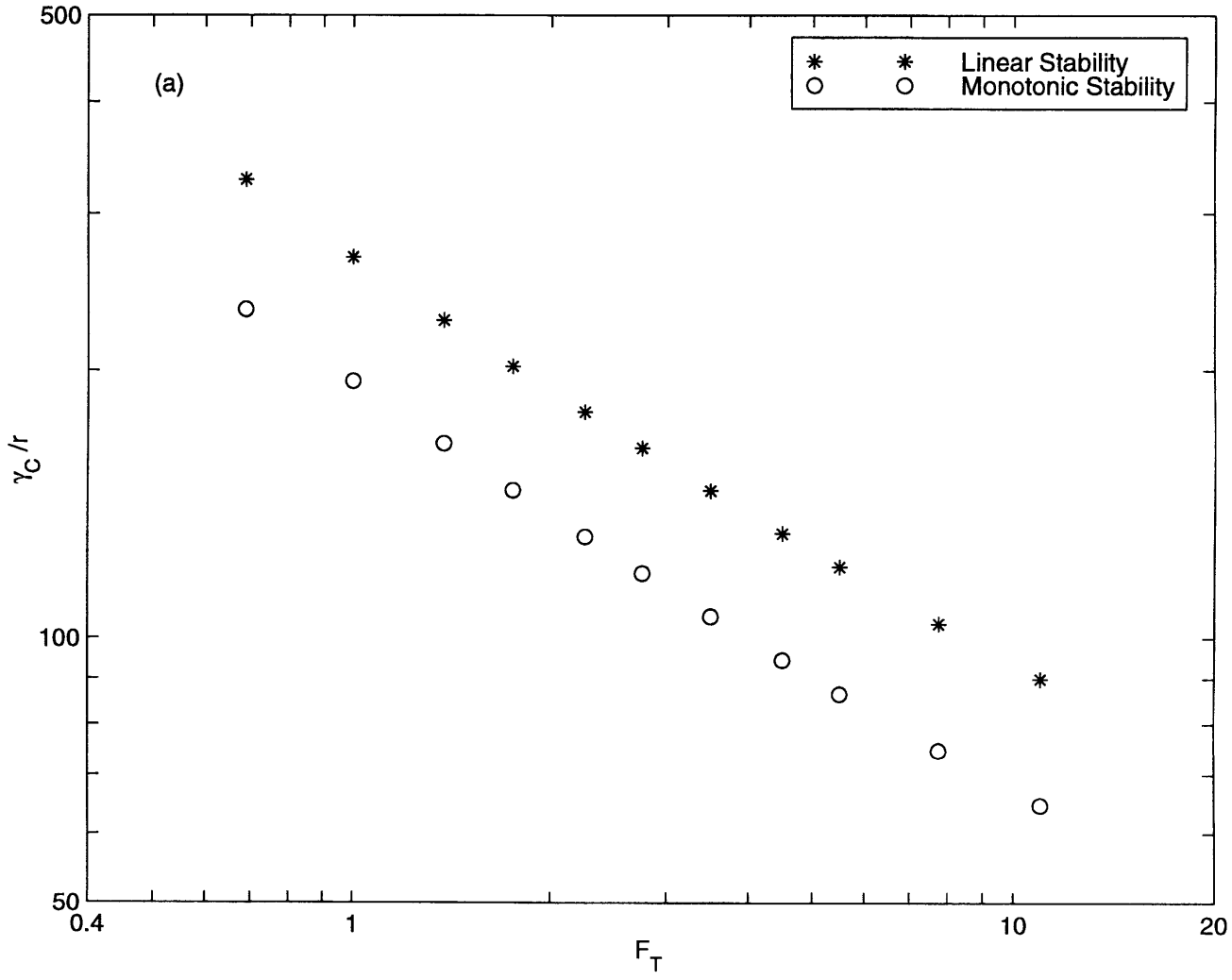

Figure 3-5: The critical threshold for linear stability γ_C/r (asterisks), as computed from (3.19), and the critical threshold for monotonic stability γ_{EC}/r (circles), as computed from (3.31). One parameter at a time is varied, while the other parameters are held fixed at the control run values, $F_T = 2.75$, $b = 40$, and $S = 10$. In (a), F_T is varied. In (b), b is varied. In (c), S is varied.

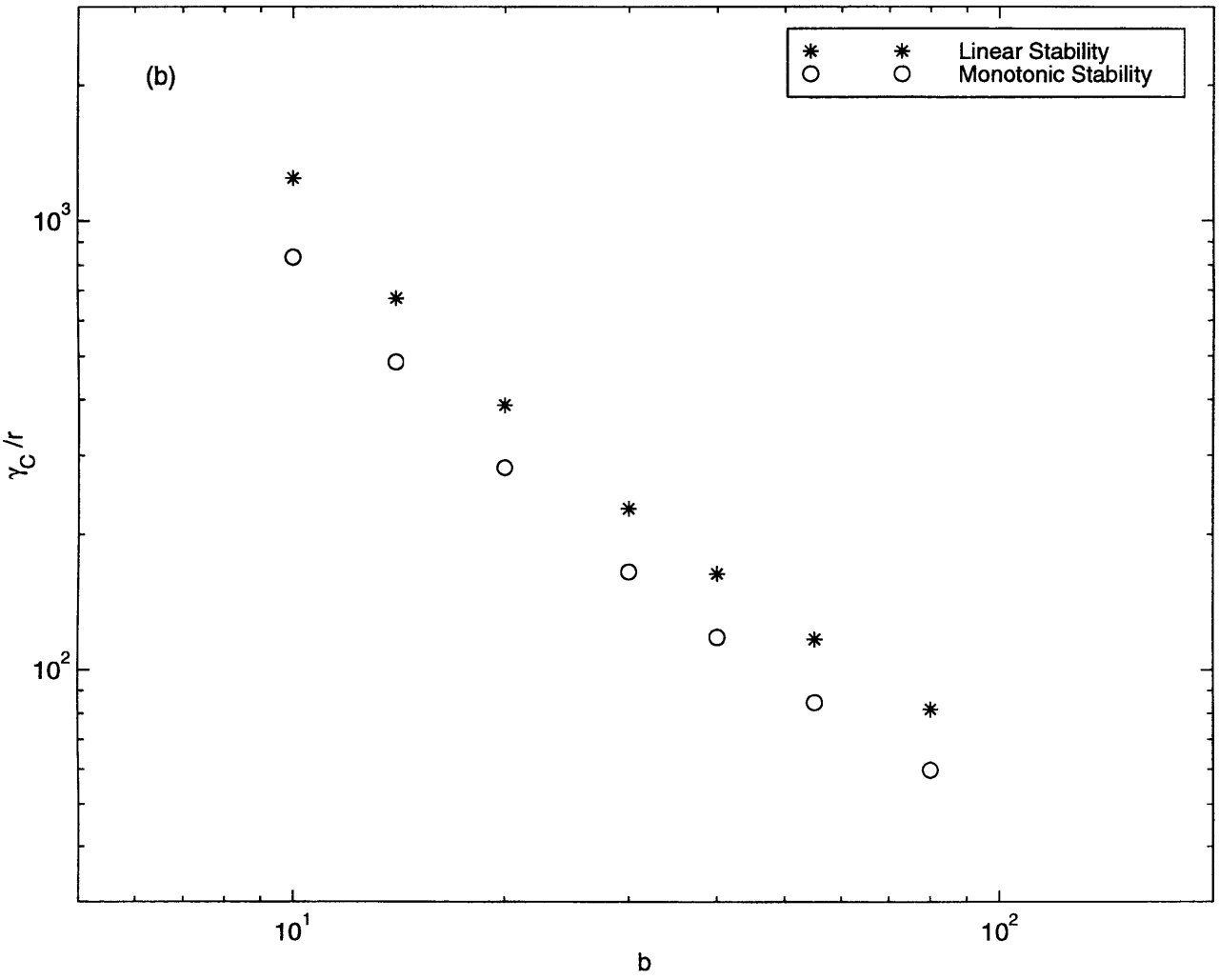
(b)
Linear Stability
Monotonic Stability
10^3
10^2
γ_C / r
10^1
10^2
b

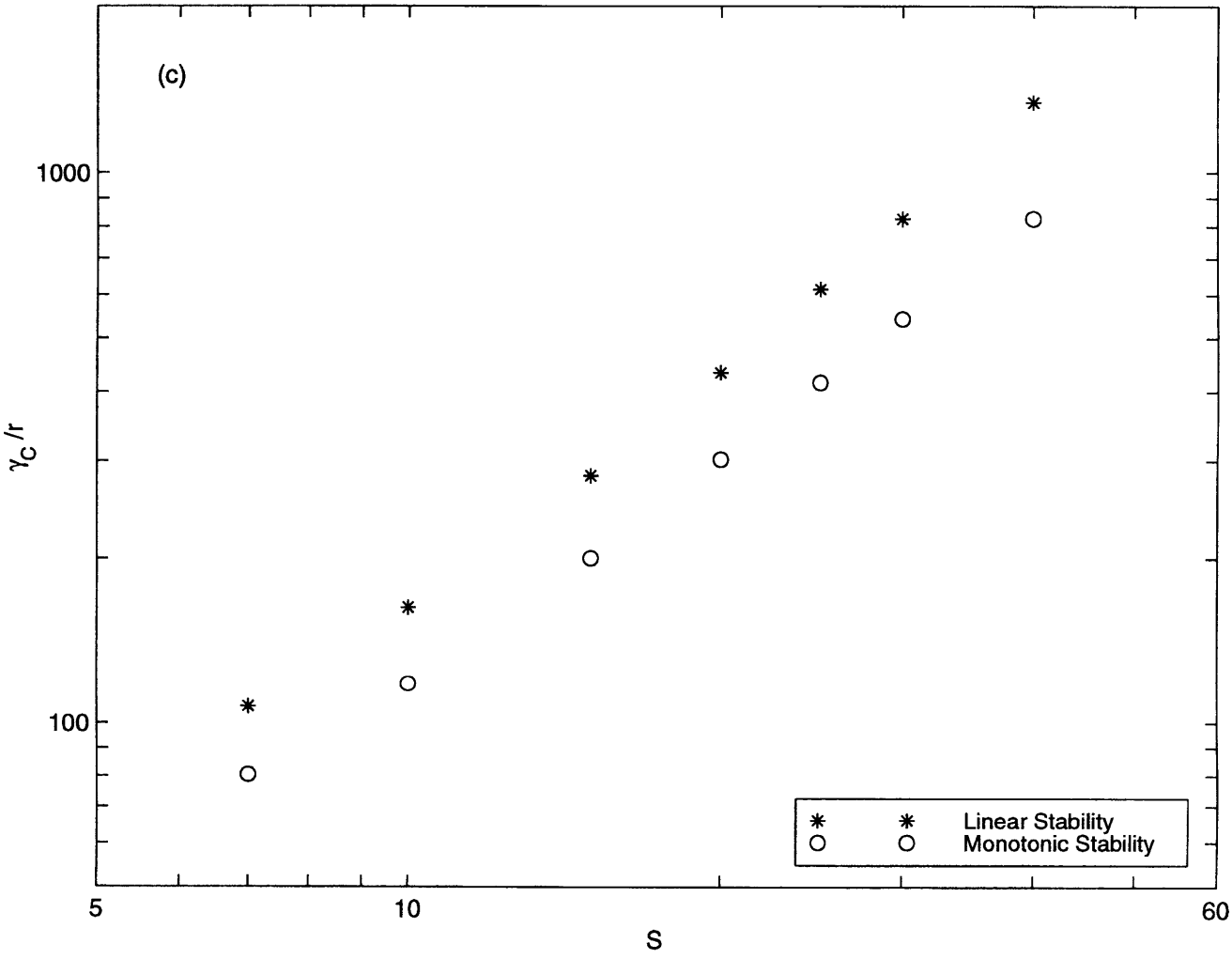
(c)
1000
100
γ_c/r
5
10
60
S
Linear Stability
Monotonic Stability

Chapter 4

Weakly Nonlinear Convection in an Idealized Atmospheric Radiative-Convective Model

4.1 Introduction

Radiative-convective models have proven to be convenient tools for addressing fundamental questions about climate (Ramanathan and Coakley 1978). Such models vary in complexity from relatively simple convective adjustment models which set the temperature to some 'adiabatic' profile when the profile becomes superadiabatic (e.g. Goody 1949; Manabe and Strickler 1964), to convective parameterizations based on a cloud model (e.g. Rennó et al. 1994a,b), to cloud resolving models which explicitly resolve much of the convection (e.g. Islam et al. 1993; Held et al. 1993). The primary question that such models have been used to address is, How does a perturbation in forcing (e.g. a doubling of carbon dioxide) alter the surface temperature? This question has received much attention because of its great practical importance.

It is also of interest to ask, How does a perturbation in forcing (e.g. a doubling of carbon dioxide) alter the convective strength? This question is important because of its implications for convective feedbacks, such as the water vapor feedback and various cloud feedbacks. Since the radiative-convective model used in this chapter contains no moist convection nor any feedbacks, we have little to say about the issue of feedbacks. Instead we restrict our attention to the first question posed in this paragraph. Specifically, we focus on the basic question of how, in a dry, weakly nonlinear radiative-convective model, perturbations in forcing affect the vertical convective heat flux, the vertical velocity, and the temperature perturbations from the mean.

Our radiative-convective model is based upon the mean field equations (Herring 1963, 1964). Although the model is restricted to dry, weakly nonlinear, high-Prandtl-number flows, it is one-dimensional and hence fast. We compare the model solutions to the stability properties of a similar radiative-convective model discussed in Chapter 3. The present calculations indicate which aspects of the stability calculations from Chapter 3 carry over to the weakly nonlinear convecting case.

In our model, the damping parameters — that is, the radiative damping parameter, the viscosity, and the thermal diffusivity — turn out to have only a weak effect on the convective heat flux. Prior authors have suggested various reasons why viscosity and thermal diffusivity should not matter in atmospheric convection (Emanuel 1994, pp. 88–91). We suggest another reason why viscosity and thermal diffusivity ought to be unimportant in an atmospheric radiative-convective equilibrium. The unimportance of viscosity and thermal diffusivity turns out to be related to the strong constraints imposed by radiation on the flow.

The Rayleigh number is sometimes used to convey the extremely high levels of turbulence associated with atmospheric convection. In our numerical results, however, a variant of the Rayleigh number is shown to have little bearing on the convective heat flux. This casts doubt on the meaning-

fulness of the Rayleigh number as a measure of turbulence in an atmosphere in radiative-convective equilibrium.

We propose two scaling laws for the convective heat flux in our dry, weakly nonlinear model. Each scale fits the output from the numerical runs we have performed fairly well. We also propose scales for the individual vertical velocity w and temperature perturbation T' fields, for weakly and strongly nonlinear convection. Prandtl (1932) suggested vertical scales for w and T', but his scale for w increases without bound as altitude increases. Our scale modifies Prandtl's scale to capture the fact that in a radiative-convective atmosphere, w reaches a maximum in the midtroposphere and then decreases with altitude.

4.2 Development of the Mean Field Equations

We wish to examine the nature of convection when the linear stability threshold has been exceeded. To do so, we choose to study an approximation to the Boussinesq equations known as the mean field approximation (Herring 1963, 1964; Elder 1969; Musman 1968; Spiegel 1971). This approximation yields a set of equations which is one-dimensional and whose solutions, therefore, may be rapidly computed. This is important because we wish to derive scaling laws, and hence we must perform many computations with the governing parameters varied over wide ranges. Unlike many convective parameterizations, the mean field equations are derived directly from the Boussinesq equations and do not rely on modeling assumptions like convective adjustment. Furthermore, the mean field equations provide profiles of the individual vertical velocity field w and the temperature perturbation field T' in addition to their correlation, the heat flux $\overline{wT'}^m$. The speed and rigor of the mean field equations, however, come at a cost: they are valid only for weakly nonlinear, high-Prandtl-number flows, whereas the atmosphere is strongly nonlinear and has a moderate Prandtl number. Furthermore, including moist processes is problematic; we do not attempt to do so here.

We now derive the mean field equations. Our notation will be the same as in Chapter 3. Asterisks shall denote dimensional quantities. An equation for w is obtained by applying $\mathbf{k} \cdot \nabla \times \nabla \times$ to the momentum equation (3.6) and using the continuity equation (3.8):

$$\chi \frac{\partial}{\partial t} \nabla^2 w = \gamma \nabla_h^2 T' + \nabla^2 \nabla^2 w + \mathbf{k} \cdot \nabla \times \nabla \times (\chi \mathbf{v} \cdot \nabla \mathbf{v}), \tag{4.1}$$

where $\nabla_h^2 \equiv (\partial^2/\partial x^2 + \partial^2/\partial y^2)$ is the horizontal Laplacian. Horizontal averages shall be denoted by $\overline{()}^m$. To find an equation for $\overline{T}^m$, we substitute $T = \overline{T}^m(z) + T'$ into the heat equation (3.7) and average over the horizontal:

$$\frac{\partial \overline{T}^m}{\partial t} = -\frac{d\overline{F}_z^m}{dz} + \kappa \frac{d^2 \overline{T}^m}{dz^2} - \frac{d\overline{wT'}^m}{dz}. \tag{4.2}$$

In this chapter, we shall choose the temperature scale $\mathcal{T}_* = \Gamma_* h_*$, where h_* is the depth of the domain, and Γ_* is the model's 'adiabatic' lapse rate. As in many convective adjustment models, however, we choose Γ_* to be 6.5 K/km, a climatological average, instead of the dry adiabatic lapse rate. With this temperature scale, the nondimensionalized adiabatic lapse rate Γ is unity. To form an equation for the temperature perturbation from the mean, we subtract the mean temperature equation (4.2) from the heat equation (3.7) and use the Newtonian approximation (3.13):

$$\frac{\partial T'}{\partial t} + w\left(\frac{d\overline{T}^m}{dz} + 1\right) = -rT' + \kappa \nabla^2 T' + \left\{-\nabla \cdot (\mathbf{v}T') + \frac{d}{dz}\overline{wT'}^m\right\}. \tag{4.3}$$

An equation for the mean radiative flux $\overline{F}_z^m$ may be derived as follows. We assume that the radiative absorption coefficient $\alpha = b \exp(-Sz)$ decreases exponentially with height, where b and S are specified parameters. To a good approximation, the nondimensionalized thermal source function in the radiative flux equation (3.9) may be linearized about the local horizontal mean:

$$T^4 \cong \overline{T}^{m4} + 4\overline{T}^{m3} T'.$$

Then, since α is a function of z alone, horizontally averaging the radiative flux equation (3.9) yields

$$\frac{d}{dz}\frac{1}{\alpha}\frac{d\overline{F}_z^m}{dz} - 3\alpha\overline{F}_z^m = 3\overline{T}^{m3}\frac{d\overline{T}^m}{dz}. \tag{4.4}$$

This is the horizontally averaged Eddington equation. Now we neglect the fluctuating self-interaction terms in (4.1) and (4.3). This yields

$$\chi\frac{\partial}{\partial t}\nabla^2 w = \gamma\nabla_h^2 T' + \nabla^2\nabla^2 w \tag{4.5}$$

and

$$\frac{\partial T'}{\partial t} + w\left(\frac{d\overline{T}^m}{dz} + 1\right) = -rT' + \kappa\nabla^2 T'. \tag{4.6}$$

The neglect of these terms restricts the validity of the system to weakly nonlinear, high-Prandtl-number flows. In particular, the system of equations cannot represent the advection of turbulent kinetic energy. Turbulent kinetic energy is generated locally by buoyancy and dissipated locally by friction. The two equations (4.5) and (4.6) for w and T' are identical to linear stability equations for the *mean* temperature field $\overline{T}^m$ (Howard 1964). However, the mean field equations do retain some nonlinearity: namely, they retain the $d(\overline{wT'}^m)/dz$ term in the mean heat flux equation (4.2) and the $wd\overline{T}^m/dz$ term in the temperature perturbation equation (4.6). Convective heating is permitted to alter $\overline{T}^m$, whose effects can then be felt through equation (4.6).

Only one horizontal mode is retained. If the horizontal planform is described by the function $f(x,y)$, then

$$w = W(z)f(x,y) \qquad\qquad T' = \Theta'(z)f(x,y), \tag{4.7}$$

where

$$\nabla_h^2 f(x,y) = -a^2 f(x,y) \qquad\qquad \overline{f^2}^m = 1.$$

We have assumed perfect horizontal correlation between w and T'. In the mean field equations, the horizontal wavenumber, a, is a free parameter. We choose the value of a used in a mean field calculation to be the critical wavenumber obtained from a linear stability calculation for the same system with the same or similar values of the governing parameters. We focus exclusively on steady-state solutions, the most relevant case for questions of average climate. Assuming a steady state and substituting the modal forms (4.7) into the equations for w (4.5) and T' (4.6) yields, respectively,

$$0 = -a^2\gamma\Theta' + \left(D^2 - a^2\right)^2 W \tag{4.8}$$

and

$$W\left(\frac{d\overline{T}^m}{dz} + 1\right) = -r\Theta' + \kappa\left(D^2 - a^2\right)\Theta'. \tag{4.9}$$

where $D \equiv d/dz$.

We impose the following boundary conditions. We assume the fluid is a horizontally infinite slab bounded by horizontal, rigid, free-slip boundaries located at the altitudes $z = 0$ and $z = 1$. This leads to the boundary conditions $W|_{z=0,1} = D^2W|_{z=0,1} = 0$. At the top of the domain, we set $dT/dz|_{z=1} = 0$ so that the temperature at the top boundary can freely vary. At the bottom boundary, we specify the temperature, $T|_{z=0} = T_g$, and then compute the outgoing radiative flux at the top of the domain, F_T. Conceptually, however, it is simpler to regard F_T as an external parameter and T_g as an internally determined one. Therefore in the experiments described herein we shall specify F_T and then perform a numerical search to find the ground temperature T_g which yields the desired radiative flux at the top. We derive the boundary conditions on radiative flux following the procedure of Goody (1956a, 1995). We find

$$\left.\frac{1}{\alpha}\frac{d\overline{F}_z^m}{dz} - 2\overline{F}_z^m\right|_{z=0} = 0, \tag{4.10}$$

which assumes a black lower surface, and

$$\left.\frac{1}{\alpha}\frac{d\overline{F}_z^m}{dz} + 2\overline{F}_z^m\right|_{z=1} = \left.\frac{3}{4}\,\overline{T}^{m4}\right|_{z=1}, \tag{4.11}$$

which states that there is no incoming thermal radiation into the top of the domain. We assume that the atmosphere ends abruptly at z=1, so that no thermal radiation can originate above z=1.

Our set of governing equations consists of the steady state versions of the following ordinary differential equations: equation (4.8) for W, (4.9) for Θ', (4.4) for $\overline{F}_z^m$, and (4.2) for $\overline{T}^m$. These equations are solved numerically, following Boyd (1989). To resolve the thin boundary layers which form in $\overline{T}^m$ and Θ', we expand all fields in Chebyshev polynomials, modified to span the interval $z = [0, 1]$. The boundary conditions are imposed with the 'boundary-bordering' method described by Boyd (1989). To compute the solutions, we choose a first-guess solution, linearize the equations about this solution, and then solve for the perturbations iteratively, using Newton's method (Press et al., 1992). Newton's method converges only if a sufficiently close first-guess solution is postulated. When γ is just supercritical, the first guess is chosen to be a marginally stable linear mode. Specifically, we use the radiative equilibrium solution as a first guess for $\overline{T}^m$ and $\overline{F}_z^m$, and the linear modes as a first guess for W and Θ'. To find highly supercritical solutions, we use the continuation method. That is, we use the mean field solution for a low value of γ as a first guess solution for a slightly higher value of γ. We continue to march in this way to higher and higher values of γ.

We illustrate the solutions of the mean field equations with the output of a control run based on the following parameter values: $F_T = 2.75$, $r = 17$, $b = 40$, $S = 10$, $a^2 = 45.2$, $\gamma = 7 \times 10^5$, and $\kappa = 1/30$. If we take the height of the domain to be $h_* = 20$ km and the 'adiabatic' lapse rate to be $\Gamma_* = 6.5$ K/km, then these parameter values correspond approximately to the following dimensional quantities, assuming reasonable values for the air density, heat capacity, and so forth: net incoming solar radiation 238 W/m^2, Newtonian cooling time scale of 10 days, optical depth of 4, and scale height of radiative absorber (i.e. water vapor) 2 km. Because the mean field equations are valid only for weakly nonlinear flows and because very fine resolution is required for highly nonlinear flows, we cannot reach the values of γ and κ appropriate to the atmosphere, if molecular values of ν_* and κ_* are assumed.

The $\overline{T}^m$, W, and Θ' fields are plotted in Figure 4-1. The $\overline{T}^m$ profile corresponds to a tropopause height of about 11.5 km and a nearly isothermal lower stratosphere with temperature 209 K. The tropospheric lapse rate is nearly the adiabatic lapse rate. The nearly neutral troposphere has not been specified *a priori*, as in convective adjustment calculations, but emerges from the calculation instead. This indicates that although the convection is weakly nonlinear, it is strong enough to lead to a nearly neutral tropospheric lapse rate. Although the aforementioned features are in reasonable agreement with the current average climate, there is a very large and unrealistic ($\sim$ 29 K) jump in $\overline{T}^m$ at the lower boundary. This jump, we believe, results primarily from the absence of evaporation in this dry model (although turbulent mixing may also reduce the size of the jump). Large temperature jumps do exist in the earth's climate over dry regions such as the Sahara desert, due to a lack of evaporative cooling at the surface (Pierrehumbert 1995). The temperature (279 K) just above the jump and the earth's average surface temperature (about 288 K) are fairly close.

The vertical extent of the mean field W profile is similar to that of the linear stability W mode (see Figure 3-2), but the linear mode actually penetrates slightly higher than the mean field W. Therefore convection does not penetrate further upwards as viscosity decreases, at least not while the convection is still weakly nonlinear. The mean field W exhibits a single, broad maximum in the mid-troposphere, as does the linear W mode. Also, the mean field W profile qualitatively resembles the atmospheric numerical and observational data of Stull (1988, p. 125). In these data, the variance of the vertical velocity in convective boundary layers has a single, broad maximum.

The shape of the mean field Θ' profile can be rationalized once $\overline{T}^m$ and W are known. For

example, the positive spike in Θ' near the ground is a consequence of upward motion in the presence of the superadiabatic region near the ground. There are also some small wiggles in Θ' near the tropopause. Figure 4-2 provides a detailed plot of the fields in this region. The negative bump in Θ' is due to rising motion in the stably stratified region near the tropopause. A very weak reverse cell in W begins just above the tropopause. The positive bump in Θ' above the tropopause arises from subsidence warming in this reverse cell.

Figure 4-3 depicts the mean field conductive, convective, and radiative vertical heat fluxes. In a steady state, these three fluxes must sum to a constant with altitude (see equation 4.13 below). The sharp increase in $\overline{wT'}^m$ near the ground is balanced by sharp decreases in the conductive and radiative fluxes. Above this boundary layer, $\overline{F_z}^m$ increases roughly linearly, $\overline{wT'}^m$ decreases roughly linearly, and the diffusive heat flux is negligible. $\overline{wT'}^m$ is mostly positive, but does contain a vertically extensive region near the tropopause of weak negative heat flux.

Following Musman (1968), we check the validity of neglecting the self-fluctuating interaction terms in equations (4.1) and (4.3). To estimate the size of the nonlinear terms, we assume that the flow consists of rolls aligned perpendicular to the x direction, and then write the neglected terms in terms of W and Θ'. For example, the neglected terms in the heat perturbation equation (4.3) become

$$-\frac{1}{\sqrt{2}}\nabla\cdot(\mathbf{v}T') + \frac{1}{\sqrt{2}}\frac{d}{dz}\overline{wT'}^m = \frac{1}{\sqrt{2}}\cos 2ax\left(\Theta'\frac{dW}{dz} - W\frac{d\Theta'}{dz}\right). \tag{4.12}$$

We may estimate the magnitude of these terms *a posteriori* by substituting the control run values of W and Θ' into the neglected terms. In the troposphere, the T' equation (4.3) is predominantly a balance between two terms: $wd\overline{T}^m/dz$ and w. The main effect of this equation is to set the tropospheric lapse rate to the adiabatic value. As seen in Figure 4-4, the nonlinear term (4.12), denoted by plusses, does not disrupt the main balance; however, a small distance above the surface it is the largest term, and it is often larger than the small dissipative terms which are retained. The nonlinear term in (4.1) may be made as small as desired by choosing a sufficiently small value of χ. If κ is held fixed, this corresponds to choosing a sufficiently large Prandtl number ν_*/κ_*. In the runs performed here $\chi = 0.05$ appears to be adequate. When $\kappa = 1/30$, as in the control run, this corresponds to $Pr = 600$. Hence the mean field approximation restricts us to the high Prandtl number limit. In contrast, the molecular Prandtl number for a typical gas is $\mathcal{O}(1)$. To summarize, in the high-Prandtl-number regime, the mean field equations appear to yield qualitatively, but not quantitatively, correct solutions for typical parameter values we consider.

4.3 Dependence of the Convective Heat Flux on the Governing Parameters

How does the convective heat flux averaged over the whole domain, $\langle wT'\rangle$, depend on the governing parameters of our radiative-convective model?

In the study of high-Rayleigh-number Rayleigh-Bénard convection, there arises an analogous question, namely, How does the nondimensionalized total heat flux (i.e. the Nusselt number Nu) depend on the governing nondimensional parameters, the Rayleigh number Ra and Prandtl number Pr? Often, a power law dependence $Nu \sim Ra^p Pr^q$, where p and q are constants, has been proposed. Several early experiments and theories (Malkus 1954; Chan 1971; see also Spiegel 1971) favored the exponent $p = 1/3$. With this scaling, the dimensional heat flux is independent of the layer depth and is determined by local processes at each boundary. Other experiments have found the exponent $p = 2/7$ (Castaing et al. 1989; see also Siggia 1994). Both these exponents imply that the dimensional heat flux depends on the values of molecular viscosity and diffusivity. However, Kraichnan (1962) proposed, on the basis of mixing length theory, that at very high Rayleigh numbers (roughly $\geq 10^{24}$), a $Nu \sim Ra^{1/2}$ scaling with logarithmic corrections would result. $p = 1/2$ is the exponent which implies no dependence on viscosity or thermal diffusivity, if Pr is held fixed. Experimental observations of this scaling have been reported by Chavanne et al. (1997). Their

experiment, however, was performed in a small aspect ratio container (1/2), rather than a large aspect ratio more relevant to geophysical applications and more amenable to simple theory.

If the atmospheric heat flux depended on the values of the molecular viscosity or thermal diffusivity, such dependencies could not be studied by explicit computation, since atmospheric models cannot resolve the smallest fluid scales. Furthermore, molecular dependencies would complicate meteorological theory, by, for instance, introducing extra parameters into dimensional analyses. Prior work has suggested various reasons why atmospheric convection might not depend on molecular quantities. For instance, the ground is invariably rough, and an externally-induced mean wind usually blows over the surface (Emanuel 1994, pp. 88–91). Both these factors might sufficiently disrupt the microlayer near the earth's surface to destroy the bottleneck in heat flux near the surface that gives rise to the dependence on molecular quantities. Also, atmospheric convection itself may generate sufficient mechanical turbulence near the ground to render at least the thermal diffusivity unimportant, as suggested by the mixing length argument of Kraichnan (1962). The system we study has neither a rough lower surface nor a mean wind nor a high degree of turbulence, and yet the convective heat flux still depends only weakly on viscosity and thermal diffusivity. Therefore, we are led to propose yet another reason why viscosity and thermal diffusivity are unimportant in atmospheres in radiative-convective equilibrium. The reason is related to the fact that in such atmospheres, the heat flux, rather than the temperature, is fixed at the top of the domain. In this regard, atmospheric convection differs fundamentally from Rayleigh-Bénard convection. The total heat flux at the top of the atmosphere is equal to the net incoming solar radiation F_T, which is independent of viscosity and thermal diffusivity in our model. (In the earth's atmosphere, F_T depends on cloud cover and ice cover, which, in turn, could conceivably depend on viscosity and thermal diffusivity.) Several more steps are needed to reach the conclusion that the *convective* portion of the total heat flux depends only weakly on viscosity and thermal diffusivity. This discussion is taken up below.

The six external parameters in our radiative-convective problem may be placed into two groups. One group consists of the three 'basic state parameters' — b, S, and F_T — which help determine the radiative equilibrium state. The other group consists of three 'damping parameters' — γ, κ, and r — which do not affect the radiative equilibrium basic state. The numerical calculations show that the basic state parameters have a strong effect on $\langle wT' \rangle$, whereas the damping parameters have only a weak influence on $\langle wT' \rangle$.

To interpret the dependence of $\langle wT' \rangle$ on the governing parameters, we draw attention to two features of our radiative-convective model. First, in the interior of the troposphere, the convective heating is almost entirely balanced by radiative cooling. Mathematically, this may be expressed by assuming a steady state and integrating the mean heat flux equation (4.2) vertically:

$$\overline{wT'}^m = F_T - \overline{F}_z^m + \kappa \frac{d\overline{T}^m}{dz}. \tag{4.13}$$

Neglecting the diffusion term and integrating over the whole domain yields

$$\langle wT' \rangle \cong F_T - \langle F_z \rangle . \tag{4.14}$$

Hence the convective heat flux is essentially determined once the radiative flux profile is known. Second, the radiative flux is determined entirely, in our model at least, by the radiative absorption coefficient α and the mean temperature profile $\overline{T}^m$, through the Eddington equation (4.4) and the boundary conditions (4.10) and (4.11). Taken together, these two features of our model show that α and $\overline{T}^m$ are the sole quantities which determine $\langle wT' \rangle$. For the most part, a greater optical depth and/or a higher tropopause tends to correspond to a greater convective heat flux.

In each of Figures 4-5, 4-6, 4-8, 4-9, and 4-10, we have varied a single parameter while fixing the others at their control run values. In Figure 4-7, we vary both S and a^2. As S is varied, the depth z_n of the unstable portion of the basic state varies markedly, and hence the wavelength of the most unstable linear mode also varies greatly. For each value of S in Figure 4-7, we choose a to be the critical wavenumber of the most unstable mode. This keeps the aspect ratio of the convective cells approximately constant. When the other external parameters are varied, z_n does not vary strongly, and so a^2 is kept at the control run value ($a^2 = 45.2$).

The integrated convective heat flux $\langle wT' \rangle$ varies strongly with the basic state parameters. Figure 4-5 shows that, to a crude approximation, $\langle wT' \rangle \sim F_T$, as might have been anticipated on dimensional grounds. Figure 4-6 shows that $\langle wT' \rangle$ increases with increasing b. As b increases, with S held constant, the optical depth of the layer and the tropopause height increases. Both effects tend to increase radiative cooling and convective heat flux. Figure 4-7 shows that $\langle wT' \rangle$ decreases with increasing S. An increase in S at constant b leads to a decrease in optical depth and tropopause height, which in turn lead to smaller $\langle wT' \rangle$. The aforementioned figures also display the maximum convective heat flux in the layer and F_T, which is the maximum possible convective heat flux if the temperature everywhere decreases with altitude. When b or S is varied and the convection is strong, the maximum convective heat flux is close to F_T and does not vary as much as $\langle wT' \rangle$.

The damping parameters have little effect on $\langle wT' \rangle$, for sufficiently weak damping. This is illustrated for the radiative damping parameter r in Figure 4-8. (It is only the radiative damping of temperature perturbations which has little importance; the radiative cooling due to the mean temperature profile strongly constrains the convective heat flux.) Radiative damping enters the equations only through the temperature perturbation equation (4.6). This equation serves mainly to keep the temperature profile nearly adiabatic in the troposphere. As long as r is not so strong that it prevents the formation of an adiabatic troposphere, changes in r cannot alter $\overline{T}^m$ much and hence cannot greatly affect $\langle wT' \rangle$. (Another reason for the weak effect is that in these weakly nonlinear calculations, if r decreases sufficiently, thermal diffusion dominates radiative damping.) Figure 4-9 shows that κ also has a weak effect on $\langle wT' \rangle$, for small thermal diffusivity. If the three points in Figure 4-9 with the highest values of $\langle wT' \rangle$ are fitted to a power law, the exponent is about -0.018. For comparison, the corresponding exponent for Figure 4-6, in which b is varied, is about 0.54. Similarly, Figure 4-10 shows that γ, which goes as $1/\nu_*$, has little effect on $\langle wT' \rangle$. This is again due to the fact that $\overline{T}^m$ follows an approximately adiabatic profile in the troposphere, regardless of the particular value of κ or ν_*, as long as they are small enough. κ and γ do affect the magnitude of the sharp jump in $\overline{T}^m$ near the ground, but the mean temperature near the surface is only loosely coupled to the temperatures aloft because the atmosphere is optically thick. (Since real atmospheric gases are nongrey, the ground temperature can be communicated to higher altitudes through relatively transparent regions in the spectrum. However, over most of the earth's surface, there is strong evaporation, which tends to eliminate any temperature jump at the surface. Hence for the real atmosphere we would again expect κ and γ to have little importance.) Spiegel (1971) has invoked similar reasoning to suggest that convection in stars does not depend on the viscosity or thermal diffusivity.

The unimportance of the damping parameters is due in part to the fact that effectively a constant heat flux boundary condition has been imposed at the top boundary. Hence there may be analogies between our radiative-convective system and Rayleigh-Bénard convection with fixed heat flux boundary conditions. Such flows have been the subject of numerous stability analyses. The chief result of these studies is that convection sets in at a much longer wavelength than for fixed temperature boundaries. However, the author is not aware of any work which discusses the effects of viscosity and thermal diffusivity on a convecting flow with fixed flux boundaries.

The weak dependence of $\langle wT' \rangle$ on the damping parameters could have been surmised from a convective adjustment model (Goody 1949; Manabe and Strickler 1964; Goody 1995). Convective adjustment provides a reasonably accurate prediction of $\overline{T}^m$ for an atmosphere in radiative-convective equilibrium, without requiring the values of the damping parameters. From the temperature profile, $\overline{F}^m_z$ can be calculated. Then $\overline{wT'}^m$ can be backed out from the heat flux equation (4.13). Hence convective adjustment is capable of predicting reasonable values for the convective heat flux without consideration of the values of the damping parameters. Unlike convective adjustment, the mean field equations explicitly compute the damping terms and hence can be used to confirm that the effects of the damping parameters are small.

As κ is decreased, or γ is increased, $\langle wT' \rangle$ increases slowly and does not convincingly asymptote to a constant in our computations. Hence one might doubt that the effects of κ and γ can be ignored. It is rather implausible, however, that the trend in $\langle wT' \rangle$ continues without bound. Inspection of the heat flux equation (4.13) reveals that if the net incoming solar radiation F_T were kept fixed while $\overline{wT'}^m$ increased without bound, then $\overline{F}^m_z - \kappa \frac{d\overline{T}^m}{dz}$ would eventually become negative and then

become increasingly more negative without bound! Such a downward radiative and/or diffusive heat flux is associated with temperature increasing with altitude somewhere in the domain. If a region of increasing temperatures with height were to occur in the troposphere, it would tend to shut off convection and thereby reduce $\overline{wT'}^m$. In fact, one can rigorously prove that for our idealized, steady-state system,

Theorem 1: If $\frac{d\overline{T}^m}{dz} < 0$ everywhere, then $\overline{wT'}^m < F_T$ everywhere.

Figure 4-3 shows that throughout a sizable portion of the troposphere, $\overline{wT'}^m$ exceeds $\overline{F}_z^m$. At first sight, this may appear somewhat surprising, since it is the radiative forcing which gives rise to the convection in the first place. However, in Figure 4-3, we see that have $\overline{wT'}^m < F_T$ everywhere. If this condition were violated, but $\kappa d\overline{T}^m/dz < 0$ everywhere, then equation (4.13) would show that $\overline{F}_z^m < 0$. This is physically rather implausible, and as shown below, mathematically prohibited when $\kappa d\overline{T}^m/dz < 0$ everywhere. Hence as κ is decreased or γ is increased, $\langle wT' \rangle$ cannot increase indefinitely.

The proof is by construction: we find a solution $\overline{F}_z^m$ for the Eddington equation (4.4) in terms of the temperature profile; inspection of this solution reveals that $\overline{F}_z^m > 0$. Then the theorem follows easily. The proof is deferred to the appendix to Chapter 4. We may extend the theorem to write (loose, but rigorous) upper and lower bounds on $\langle wT' \rangle$ for our radiative-convective model. Upon integrating $\overline{wT'}^m$ vertically, the theorem leads, if $\kappa d\overline{T}^m/dz < 0$, to an upper bound on $\langle wT' \rangle$, $\langle wT' \rangle < F_T$. Also, regardless of the profile of $\overline{T}^m$, we may obtain the well-known result $\langle wT' \rangle = \langle |\nabla \mathbf{v}| \rangle / \gamma \geq 0$, by taking the dot product of the velocity with the momentum equation (3.6), averaging over all space, using the continuity equation, assuming a steady state, and assuming that all fields are periodic in the horizontal. Therefore, in our steady-state radiative-convective model, the integrated convective heat flux must fall within the range

$$0 \leq \langle wT' \rangle < F_T, \qquad \text{if } \frac{d\overline{T}^m}{dz} < 0 \text{ everywhere.}$$

Because of the constraints imposed by radiation, deriving an upper bound on heat flux is straightforward, given that the temperature everywhere decreases with altitude. Establishing an upper bound on heat flux in Rayleigh-Bénard convection is much more difficult (Malkus 1954; Howard 1963).

4.4 Scaling Laws

Although Figures 4-5 to 4-10 illustrate how each of the governing parameters individually affects $\langle wT' \rangle$, it is useful to have a formula which collapses all the weakly damped points in Figures 4-5 to 4-10 onto one curve. In high-Rayleigh-number Rayleigh-Bénard convection, $\langle wT' \rangle$ can be collapsed in terms of the Rayleigh number (Siggia 1994). Therefore the Rayleigh number serves as a measure of the magnitude of $\langle wT' \rangle$ in convecting flows, as well as a threshold for linear stability. Chapter 3 showed that a radiative Rayleigh number $Ra_{\mathcal{R}}$ serves as an approximate linear stability threshold for a $\kappa = 0$ version of our radiative-convective model. One might hope, therefore, that $Ra_{\mathcal{R}}$ serves as a suitable measure of the magnitude of $\langle wT' \rangle$ for our radiative-convective model. Figure 4-11 shows that it does not. This figure plots those points of output from Figures 4-5 to 4-10 which have moderate to small damping, that is, $\gamma \geq 7 \times 10^5$, $\kappa \leq 1/30$, and $r \leq 17$. The legend indicates which variable has been varied from the control run values. For instance, squares denote numerical runs for which F_T has been varied, with all other parameters held fixed; i.e. squares denote the points from Figure 4-5. $Ra_{\mathcal{R}}$ fails as a scaling parameter in large part because $\langle wT' \rangle$ depends only weakly on the damping parameters γ and r, for sufficiently weak damping. Therefore when γ, for instance, is varied, $Ra_{\mathcal{R}}$ varies greatly, but $\langle wT' \rangle$ varies little. On the other hand, when b, for instance, is varied, $Ra_{\mathcal{R}}$ varies greatly, but so does $\langle wT' \rangle$. Therefore, varying both b and γ independently does not produce a compact curve on the $\langle wT' \rangle$-$Ra_{\mathcal{R}}$ plane, but instead fills a two-dimensional region.

Sometimes the Rayleigh number Ra is used as a measure of the strength of turbulence in atmospheric convection, usually to note the extremely strong turbulence associated with atmospheric

convection (see e.g. Emanuel 1994, p. 82; Kraichnan 1962, p. 1384). However, the present numerical calculations suggest that no Rayleigh-number-like quantity which goes as $1/\nu_*$ is likely to be a meaningful measure of heat flux (or turbulence level) in an atmosphere in radiative-convective equilibrium. Instead, the present calculations, at least, exhibit the curious phenomenon that a decrease in viscosity, with all other dimensional parameters (including κ_*) held fixed, leads to only a marginal increase in convective heat flux. To compare the turbulence intensity in Rayleigh-Bénard convection and radiative-convective equilibrium atmospheres, we suggest comparing Reynolds numbers based on plume velocity and size.

We now derive two scalings, a simple one and a more sophisticated one, which do accurately collapse the $\langle wT' \rangle$ points. We begin by noting that Figure 4-3 shows that in the middle and upper troposphere, thermal diffusion is negligible, and $\overline{wT'}^m$ decreases roughly linearly with altitude. Then dimensional reasoning and mixing length theory applied to the mean heat flux equation (4.2) both suggest the following expression for the convective heat flux:

$$\begin{aligned} \overline{wT'}^m &\sim \frac{d\overline{F}_z^m}{dz}(z_n - z) && 0 < z < z_n \\ &\cong 0 && z \geq z_n. \end{aligned} \tag{4.15}$$

The depth of the radiative equilibrium unstable layer, z_n, may be regarded as an external parameter, since an approximation to z_n for small κ can be expressed in terms of the external parameters b, S, and F_T via equation (3.29). (Although in our model b and S are external parameters, in the earth's atmosphere they are not.) However, we still need to express $d\overline{F}_z^m/dz$ in terms of external parameters. Our numerical calculations show that for low to moderate S, the last two terms in the Eddington equation (4.4) are the largest. Neglecting the first term in (4.4) and rearranging yields the crude approximation

$$\overline{F}_z^m \cong \frac{1}{\alpha}\left(-\overline{T}^{m3}\frac{d\overline{T}^m}{dz}\right). \tag{4.16}$$

The radiative absorption coefficient $\alpha = b\exp(-Sz)$ varies more rapidly with altitude than $\overline{T}^{m3}d\overline{T}^m/dz$. Therefore, differentiating both sides of (4.16) with respect to z yields approximately

$$\frac{d\overline{F}_z^m}{dz} \cong S\frac{1}{\alpha}\left(-\overline{T}^{m3}\frac{d\overline{T}^m}{dz}\right) \cong S\overline{F}_z^m \sim SF_T. \tag{4.17}$$

We have estimated the derivative of $\overline{F}_z^m$ as a radiative scale F_T divided by a length scale $1/S$. Substituting this scale for $d\overline{F}_z^m/dz$ into (4.15) yields a scaling for $\overline{wT'}^m$:

$$\begin{aligned} \overline{wT'}^m &= c_1 F_T S(z_n - z) && 0 < z < z_n \\ &\cong 0 && z \geq z_n, \end{aligned} \tag{4.18}$$

where c_1 is a constant. Integrating (4.18) over the domain, we find

$$\langle wT' \rangle = \frac{1}{2}c_1 F_T S z_n^2. \tag{4.19}$$

The most important features of this scale are that it has an explicit linear dependence on F_T and no dependence on the damping parameters. Hence the scale is quite different from the radiative Rayleigh number $Ra_{\mathcal{R}}$. In Figure 4-12, this scaling is tested against the same set of points displayed in Figure 4-11. Considering its simplicity, the scaling collapses the output fairly well. A least-squares fit yields $c_1 = 0.296 \pm 0.0025$, which has a fairly low standard deviation. But inspection of Figure 4-12 reveals, for instance, that the points for which S has been varied (denoted by diamonds) have a greater slope than the points for which b has been varied (asterisks), which in turn have a greater

slope than the points for which F_T has been varied (squares). The agreement is worst for low values of b or high values of S, both of which correspond to small $\langle wT' \rangle$. Therefore we seek a new scaling which more nearly collapses the data.

We return to (4.16), but we retain the term in the Eddington equation that we had previously neglected:

$$\overline{F_z}^m = \frac{1}{\alpha}\left(-\overline{T}^{m3}\frac{d\overline{T}^m}{dz}\right) + \frac{1}{3}\frac{1}{\alpha}\frac{d}{dz}\frac{1}{\alpha}\frac{d\overline{F_z}^m}{dz}.$$

We apply d/dz to both sides. Then we approximate the first term on the right-hand side as in (4.17) and approximate the second term on the right-hand side using the standard mixing length procedure of replacing derivatives by length scales. We find

$$\frac{d\overline{F_z}^m}{dz} \cong \frac{d}{dz}\left(\frac{1}{\alpha}\left(-\overline{T}^{m3}\frac{d\overline{T}^m}{dz}\right)\right) + \frac{1}{3}\frac{d}{dz}\left(\frac{1}{\alpha}\frac{d}{dz}\frac{1}{\alpha}\frac{d\overline{F_z}^m}{dz}\right) \cong SF_T - \frac{S}{z_n}\frac{1}{3}\frac{1}{\alpha^2}\frac{d\overline{F_z}^m}{dz}.$$

In this problem, mixing length theory has two length scales at its disposal: $1/S$ and z_n. We have used both length scales because this yields a better fit. The minus sign arises because of the curvature in $\overline{F_z}^m$. We need to choose an altitude at which to evaluate α. This altitude is effectively a fitting coefficient, which we choose to be $z = z_n/2$. Then, solving for $d\overline{F_z}^m/dz$, we find

$$\frac{d\overline{F_z}^m}{dz} \sim \frac{F_T S}{1 + \frac{1}{3}\frac{S}{z_n}\frac{1}{b^2}e^{Sz_n}}.$$

This radiative cooling scale may be interpreted as a radiative flux scale F_T divided by a length scale $1/S$, modified by the correction factor in the denominator. Substituting this radiative cooling scale into (4.15) yields the new scaling:

$$\begin{aligned} \overline{wT'}^m &= c_2 \frac{F_T S}{1 + \frac{1}{3}\frac{S}{z_n}\frac{1}{b^2}e^{Sz_n}}(z_n - z) && 0 < z < z_n \\ &\cong 0 && z \geq z_n, \end{aligned} \tag{4.20}$$

where c_2 is a constant. Integrating over the domain,

$$\langle wT' \rangle = \frac{1}{2} c_2 \frac{F_T S}{1 + \frac{1}{3}\frac{S}{z_n}\frac{1}{b^2}e^{Sz_n}} z_n^2. \tag{4.21}$$

In Figure 4-13, we test the new scaling (4.21) using the same output points as in Figure 4-12. The new scaling shows less scatter than the scaling (4.19). A least-squares fit of the coefficient c_2 in (4.21) yields $c_2 = 0.333 \pm 0.001$. The fit for c_2 has less than half the standard deviation of c_1, indicating a better fit for the new scaling. However, an improved fit is expected, because the scaling (4.21) has effectively two fitting coefficients — c_2, and the altitude at which α is evaluated — whereas the scaling (4.19) has only one fitting coefficient. Although some points in Figure 4-13 associated with b are still slightly in error, the slope of the points for which S is varied (diamonds) coincides with the slope of the points for which F_T is varied (squares).

We have obtained scales for the correlation of w and T' (i.e. $\overline{wT'}^m$), but it is also of interest to develop individual scales for w and T'. To do so, we use mixing length theory (see e.g. Kraichnan 1962). We find a relationship between w and T' from the vertical component of the momentum equation (3.6). In the steady-state mean field equations, the inertia terms vanish, leaving only the pressure perturbation force, the buoyancy force, and the viscous force. Ignoring the pressure perturbation force in the manner typical of mixing length theory, we balance the viscous and buoyancy forces to obtain

$$\frac{w}{z^2} = c_3 \gamma T', \tag{4.22}$$

where c_3 is a constant. Although this balance is appropriate for weakly nonlinear flows, in more turbulent flows, we would expect the inertia term to contribute. Multiplying both sides of (4.22) by w, averaging over the horizontal, and taking the square root of both sides, we find a vertical velocity scale:

$$\left(\overline{w^2}^m\right)^{1/2} = \left(c_3\gamma\overline{wT'}^m\right)^{1/2} z \qquad \text{for} \qquad \overline{wT'}^m \geq 0. \tag{4.23}$$

Similarly, to find a temperature perturbation scale, we multiply both sides of (4.22) by T', average horizontally, and take the square root of both sides:

$$\left(\overline{T'^2}^m\right)^{1/2} = \left(\overline{wT'}^m/(\gamma c_3)\right)^{1/2} \frac{1}{z} \qquad \text{for} \qquad \overline{wT'}^m \geq 0. \tag{4.24}$$

The scales (4.23) and (4.24) are only valid when $\overline{wT'}^m \geq 0$. We find a least-squares best fit for the coefficient c_3 by evaluating (4.22) at $z = 0.2$ for all the runs shown in Figure (4-12) except the runs for which $S = 15, 20$, because in these runs $\overline{wT'}^m < 0$ at $z = 0.2$. The result is $c_3 = 0.217 \pm 0.002$. The small standard deviation associated with the coefficient indicates that the scaling fits the numerical output well at $z = 0.2$ as the governing parameters are varied.

Figure 4-14 depicts the scales (4.23) and (4.24), superimposed upon the control run numerical output. The w scale exhibits a single, broad maximum in the mid-troposphere, as does the linear stability analysis, the mean field numerical calculations, and some atmospheric observations. The magnitude and shape of the w scale agrees well with the numerical output except in the upper troposphere, where the w scale falls off too rapidly. This is associated with the fact that in the upper troposphere, $\overline{wT'}^m$ approaches zero and then becomes negative. The scale for T' agrees fairly well with the numerical output except near the surface. In the numerical runs, T' vanishes at the lower surface because of the boundary condition on temperature. No such constraint exists on the scale for T'. Perhaps the poorest fit occurs for low S, as shown in Figure 4-15. The maximum for the w scale occurs about 1–2 km higher than in the numerical output.

Although the scales (4.23) and (4.24) seem to work well, they express w and T' in terms of $\overline{wT'}^m$, and hence are not closed. To obtain closed scales, we may substitute the expression (4.18) for $\overline{wT'}^m$ into (4.23) and (4.24), yielding, respectively:

$$\left(\overline{w^2}^m\right)^{1/2} = (\gamma c_3 c_1 F_T S)^{1/2} (z_n - z)^{1/2} z \qquad 0 < z < z_n \tag{4.25}$$

and

$$\left(\overline{T'^2}^m\right)^{1/2} = \left(\frac{c_1 F_T S}{c_3 \gamma}\right)^{1/2} \frac{(z_n - z)^{1/2}}{z} \qquad 0 < z < z_n. \tag{4.26}$$

These scales and the numerical output from the control run are displayed in Figure 4-16, along with the scale (4.18) for $\overline{wT'}^m$. The scale for $\overline{wT'}^m$ agrees reasonably well with the output, except for the fact that near the ground, the boundary conditions force the numerical $\overline{wT'}^m$ to go to zero, and the fact that the scale for $\overline{wT'}^m$ approaches zero more rapidly with increasing height than the numerical $\overline{wT'}^m$. The scale for w agrees reasonably well with the numerical output except that w again tapers off too rapidly with increasing height above its maximum. This is because the scale for $\overline{wT'}^m$ rapidly approaches zero in the midtroposphere. The fit is poorest at low S; then the maximum for w scale lies above the maximum for the data, as for the scale (4.23). The scale for T' is also reasonable, except near the ground, where the scale for T' diverges but the numerically computed T' vanishes at the ground.

Although the scales (4.25) and (4.26) adequately approximate the weakly nonlinear mean field profiles for w and T' respectively, they would not be expected to describe the highly nonlinear convection characteristic of the atmosphere. As one indication of this, we note that substituting typical atmospheric numbers into the scaling relations (4.25) and (4.26) yields a velocity scale $\mathcal{O}(10^4)$ m/s and a temperature perturbation scale of $\mathcal{O}(10^{-6})$ K! We also note that although the scalings (4.18) or (4.20) for $\overline{wT'}^m$ are independent of viscosity, the scales (4.25) and (4.26) for w and T'

are not. The difficulty is that the inertia terms, which are important in atmospheric convection, are neglected in the mean field equations. In the atmospheric momentum equation, we expect a balance between the buoyancy and inertia terms. Mixing length theory then leads to the following relationship, written in dimensional quantities:

$$\frac{w_*^2}{z_*} \sim g_* \alpha_{T*} T'_*. \tag{4.27}$$

Assuming that w and T' are well correlated, we may obtain scales for w_* and T'_* in terms of $\overline{w_* T'_*}^m$:

$$w_* \sim \left(g_* \alpha_{T*} \overline{w_* T'_*}^m z_* \right)^{1/3} \qquad \text{for} \qquad \overline{w_* T'_*}^m \geq 0, \tag{4.28}$$

$$T'_* \sim \frac{\left(\overline{w_* T'_*}^m \right)^{2/3}}{\left(g_* \alpha_{T*} z_* \right)^{1/3}} \qquad \text{for} \qquad \overline{w_* T'_*}^m \geq 0. \tag{4.29}$$

These scales are similar to those obtained by Prandtl (1932), Priestley (1959), and Deardorff (1970), except that here $\overline{w_* T'_*}^m$ is not a constant kinematic heat flux scale, but a function of z_* determined largely by $\overline{F_z}^m$. Leaving $\overline{w_* T'_*}^m$ as a function of z_* leads to a more realistic prediction for w_* in the upper troposphere. When $\overline{w_* T'_*}^m$ is taken to be a constant, the w_* scale increases monotonically with increasing altitude. In a radiative-convective atmosphere, however, $\overline{w_* T'_*}^m$ is expected to become small near the tropopause and remain small in the stratosphere. Hence the expression (4.28) for w_* would be expected to reach a maximum in the midtroposphere and decrease from there upwards. Note also that the scales (4.28) and (4.29) for w_* and T'_* are independent of viscosity, as one might expect for strongly nonlinear atmospheric convection.

Although the scales (4.25) and (4.26) for the individual fields w and T' fail for strongly nonlinear flows, it is reasonable to suppose that the scale (4.19) for $\overline{wT'}^m$ is adequate for dry, strongly nonlinear, radiative-convective flows. We first note that the scales (4.25) and (4.26) for w and T' depend on viscosity, whereas the scales for $\langle wT' \rangle$ do not. Second, in the mid to upper troposphere, convective heating is almost entirely balanced by radiative cooling. In a dry system, $\overline{wT'}^m$ is determined once $\overline{F_z}^m$ is known, regardless of whether the system is weakly nonlinear or strongly nonlinear. But $\overline{F_z}^m$ depends only on α and $\overline{T}^m$. Therefore, if our model predicts $\overline{T}^m$ correctly, it may also be expected to predict $\overline{wT'}^m$ correctly. Even the weakly nonlinear flows that we have modeled here are capable of producing a nearly adiabatic troposphere and a stratosphere which is in approximate radiative equilibrium. This temperature profile is not likely to change in a strongly nonlinear flow. Therefore we may expect that the $\overline{wT'}^m$ profile remains the similar in weakly nonlinear and strongly nonlinear systems, even if the scalings of w and T' differ in the two systems.

If the above reasoning is correct, we may write scales for w_* and T'_* in terms of F_T and S. Rewriting the expression (4.18) for $\overline{wT'}^m$ in terms of dimensional parameters and substituting it into (4.28) and (4.29) yields, respectively,

$$w_* \sim \left(g_* \alpha_{T*} \frac{F_{T*}}{\rho_* c_{p*}} S_* (z_{n*} - z_*) z_* \right)^{1/3} \qquad 0 < z < z_n \tag{4.30}$$

and

$$T'_* \sim \left(\frac{F_{T*}}{\rho_* c_{p*}} S_* \right)^{2/3} \frac{1}{(g_* \alpha_{T*})^{1/3}} \frac{(z_{n*} - z_*)^{2/3}}{z_*^{1/3}} \qquad 0 < z < z_n. \tag{4.31}$$

The scale (4.30) predicts that w_* has a single, broad maximum in the mid-troposphere. Substituting reasonable numbers into (4.30) and (4.31) yields $w_* \sim 3$ m/s and $T'_* \sim 0.1$ K at $z_* = 3$ km. Nearer to the ground, w_* is smaller and T'_* is larger. These values are much closer to atmospheric values than those obtained from the scales (4.25) and (4.26).

4.5 Conclusions

This chapter has examined a dry, weakly nonlinear, high-Prandtl-number radiative-convective model. The behavior of the convecting flow is in some ways different and in some ways similar to the linear modes studied in Chapter 3. The vertical velocity profiles of the linear modes and the weakly nonlinear convection are similar in shape and vertical extent. As viscosity decreases, the convective layer does not penetrate further upwards, but actually becomes slightly shallower. The temperature perturbation profiles are different in the two cases. There are six governing dimensionless parameters in the weakly nonlinear convecting case. The three basic state parameters (F_T, b, S) have similar effects in the linear stability and convecting cases. For instance, an increase in the net incoming solar radiation F_T increases the instability of the basic state and also increases the convective heat flux in the convecting case. On the other hand, the three damping parameters, γ, r, and κ, produce quite different effects in the two cases. For instance, increasing the radiative damping r strongly stabilizes the basic state but has little effect on the convective heat flux in the convecting system.

In fact, all the damping parameters in our model have only weak effects upon the convective heat flux. The reason for this may be summarized as follows. In radiative-convective equilibrium, the total vertical heat flux is constant with altitude and equals the net incoming solar radiation F_T, a quantity which in our model is independent of the damping parameters. In the mid-troposphere, the total vertical heat flux consists primarily of two contributions, a convective contribution $\overline{wT'}^m$ and a radiative contribution $\overline{F}_z^m$. Therefore, if F_T and $\overline{F}_z^m$ are independent of the damping parameters, then so is the residual $\overline{wT'}^m$. But $\overline{F}_z^m$ depends only on the radiative absorption coefficient α and the mean temperature $\overline{T}^m$. In our model α is fixed. Also, unless damping is very strong, $\overline{T}^m$ adopts an adiabatic profile in the troposphere and a radiative equilibrium profile in the stratosphere; $\overline{T}^m$ is influenced by the damping parameters only near the ground. Therefore, in the mid-troposphere, the convective heat flux must also be insensitive to the values of the damping parameters.

Although the individual effects of the six governing parameters on the convective heat flux may be readily explored, it is of interest to seek a single scaling law which incorporates the effects of all the governing parameters. The radiative Rayleigh number $Ra_{\mathcal{R}}$, used in Chapter 3 to approximate the linear stability threshold, fails as a scaling parameter for the convective heat flux. We have constructed alternative, approximate scaling laws. These laws do not depend on the damping parameters. We have also found approximate scaling laws for the individual vertical velocity w and temperature perturbation T' fields. These scales extend the validity of the Prandtl scales to higher altitudes in the troposphere. In particular, our vertical velocity scale does not increase indefinitely with altitude.

The tropospheric convective heat flux in our model routinely exceeds the tropospheric radiative heat flux. We have proven for our model equations, however, that the convective heat flux can nowhere reach F_T, in the special case that $d\overline{T}^m/dz < 0$ everywhere.

Do our dry, weakly nonlinear results have relevance to a moist, strongly nonlinear atmosphere in radiative-convective equilibrium? Some of our results, such as the dry, weakly nonlinear scalings for w (4.25) and T' (4.26), would not apply to such an atmosphere. However, such an atmosphere might plausibly have the property that the vertical convective heat flux depends little on the values of the damping parameters. This result followed largely from the fact that a constant heat flux boundary condition is imposed at the top of the domain and the fact that a radiative-convective atmosphere seeks an adiabatic tropospheric lapse rate. We would not expect strongly nonlinear convection to depart from an adiabatic temperature profile. (However, in our model α is specified and cloud cover is absent. If values of the damping parameters were to influence α or cloud cover, then the vertical convective heat flux would also be influenced.) A related result from our model which may apply to a realistic atmosphere in radiative-convective equilibrium is the result that the Rayleigh number Ra and radiative Rayleigh number $Ra_{\mathcal{R}}$ bear little relation to the vertical convective heat flux. In this case they are unlikely to be good measures of the strength of turbulence.

4.6 Appendix: A Bound on Convective Heat Flux

This appendix proves Theorem 1 for our grey, two-stream, steady-state radiative-convective model. Namely, we prove that if the temperature profile decreases monotonically with increasing altitude, then the vertical convective heat flux cannot reach or exceed the net incoming solar radiation:

If $\frac{d\overline{T}^m}{dz} < 0$ everywhere, then $\overline{wT'}^m < F_T$ everywhere.

The proof is by construction. From the heat flux equation (4.13), the theorem follows if $\overline{F}_z^m - \kappa d\overline{T}^m/dz > 0$. By assumption, $-\kappa d\overline{T}^m/dz > 0$ everywhere. So we only need to show that $\overline{F}_z^m > 0$ everywhere. To do so, we solve for $\overline{F}_z^m$ in terms of the Green's function for the Eddington equation. As we shall see, inspection of this solution shows that $\overline{F}_z^m > 0$ everywhere, if $d\overline{T}^m/dz < 0$ everywhere.

We allow the radiative absorption coefficient to have any profile with altitude, and define an optical depth τ as follows:

$$\tau = \int_z^1 dz' \alpha(z').$$

Rewriting the radiative equation (4.4) in terms of τ, we find

$$\frac{d^2\overline{F}_z^m}{d\tau^2} - 3\overline{F}_z^m = -3\overline{T}^{m3}\frac{d\overline{T}^m}{d\tau}. \tag{4.32}$$

The boundary conditions (4.10) and (4.11) become

$$\left.\frac{d\overline{F}_z^m}{d\tau} + 2\overline{F}_z^m\right|_{\tau=\tau_g} = 0 \qquad \left.-\frac{d\overline{F}_z^m}{d\tau} + 2\overline{F}_z^m\right|_{\tau=0} = \left.\frac{3}{4}\overline{T}^{m4}\right|_{\tau=0},$$

where τ_g is the optical depth at the ground.

We regard $\overline{T}^m$ as a given source function; then the equation for $\overline{F}_z^m$ is linear. Therefore we may express $\overline{F}_z^m$ as a linear superposition of two functions,

$$\overline{F}_z^m = F_h + F_G,$$

where F_h satisfies the full boundary conditions and the homogeneous form of equation (4.32), and F_G satisfies the homogeneous form of the boundary conditions and the full equation (4.32). We shall show that both $F_h > 0$ and $F_G > 0$ if $d\overline{T}^m/dz < 0$ everywhere.

It is straightforward to show that the homogeneous solution F_h is

$$F_h = \left(\frac{\left.\frac{3}{4}\overline{T}^{m4}\right|_{\tau=0}}{2+\sqrt{3}}\right)\frac{1}{1-C^2e^{-2\sqrt{3}\tau_g}}e^{-\sqrt{3}\tau}\left(1-Ce^{-2\sqrt{3}(\tau_g-\tau)}\right) \cong \left(\frac{\left.\frac{3}{4}\overline{T}^{m4}\right|_{\tau=0}}{2+\sqrt{3}}\right)e^{-\sqrt{3}\tau},$$

where $C \equiv \frac{2-\sqrt{3}}{2+\sqrt{3}} \cong 0.0718$. The approximation on the far right-hand side is valid because C is small. The approximation shows that F_h is large near the top of the domain, and decreases approximately exponentially in τ as one moves down. Since $C < 1$ and $\tau < \tau_g$, we have $F_h > 0$.

We now show that $F_G > 0$, by writing F_G in terms of the Green's function $G(\tau;\tau')$ for equation (4.32). G satisfies the equation

$$\frac{d^2G}{d\tau^2} - 3G = -\delta(\tau-\tau'),$$

and homogeneous boundary conditions, where δ denotes the Dirac delta function. The solution for G is

$$G(\tau;\tau') = \frac{1}{2\sqrt{3}} \frac{1 - Ce^{-2\sqrt{3}\tau_<}}{1 - C^2 e^{-2\sqrt{3}\tau_g}} e^{-\sqrt{3}(\tau_> - \tau_<)} \left(1 - Ce^{-2\sqrt{3}(\tau_g - \tau_>)}\right) \cong \frac{1}{2\sqrt{3}} e^{-\sqrt{3}|\tau - \tau'|}, \qquad (4.33)$$

where $\tau_> \equiv \max(\tau, \tau')$ and $\tau_< \equiv \min(\tau, \tau')$. The value of F_G at a field point τ is little affected by a source point τ' very far in optical depth from τ. Likewise, F_G receives little contribution from those regions with small $d\overline{T}^m/d\tau'$. By inspection, we see that $G > 0$. F_G is constructed from G by the integral,

$$F_G(\tau) = \int_0^{\tau_g} d\tau' G(\tau;\tau') 3\overline{T(\tau')}^m \frac{d\overline{T}^m}{d\tau'}. \qquad (4.34)$$

If $d\overline{T}^m/dz < 0$ everywhere, then $d\overline{T}^m/d\tau > 0$. Since we also have $G > 0$, we conclude that $F_G > 0$.

We have shown that F_h and F_G are both positive everywhere; therefore the radiative flux $\overline{F}_z^m$ is upward everywhere, if $d\overline{T}^m/dz < 0$ everywhere. That is, when the temperature gradient is single-signed, radiation transports heat downgradient. Note that the proof leaves the radiative absorption coefficient $\alpha(z)$ arbitrary. The proof relies only on the steady-state heat flux equation (4.13), the radiative transfer equation (4.4), and the radiative boundary conditions (4.10,4.11).

How strong must a temperature inversion in the sounding be in order to provide a significant negative contribution to the radiative flux? Suppose we wish to know how an inversion at τ' contributes to the radiative flux at τ. Equations (4.34) and (4.33) show that the effect of the inversion on the radiative flux is strong if the temperature jump across the inversion is strong and if the inversion is located near the level of interest, τ. Weak or remote inversions give only weak negative contributions to the radiative flux.

It is actually easier to prove that $\overline{F}_z^m > 0$ when we relax the two-stream approximation and the assumption of greyness. Then, using the formal solution to the Schwarzschild equation of transfer, we may write the radiative flux in terms of various integrals (Liou 1980, p. 94). After performing an integration by parts, inspection of the formal solution shows that if $d\overline{T}^m/dz < 0$, then $\overline{F}_z^m > 0$. One may also write an analogue to the dry heat flux equation (4.13) for a statistically steady, hydrostatic, moist atmosphere (Cotton and Anthes 1989, p. 203). For such an atmosphere, Theorem 1 becomes

$$-\frac{1}{g_*}\overline{\omega_*' h_*'}^m < F_{T*} + \frac{c_{pd*}}{g_*} \int_{p_{t*}}^{p_*} dp(Q_{1*} - Q_{2*}).$$

Here ω_*' is the perturbation pressure velocity (from the horizontal mean), h_*' the perturbation moist static energy, Q_{1*} the apparent heat source, Q_{2*} the apparent moisture sink, p_* the pressure coordinate, p_{t*} the pressure at the top of the convecting layer, g_* the acceleration due to gravity, and c_{pd*} the specific heat at constant pressure for dry air.

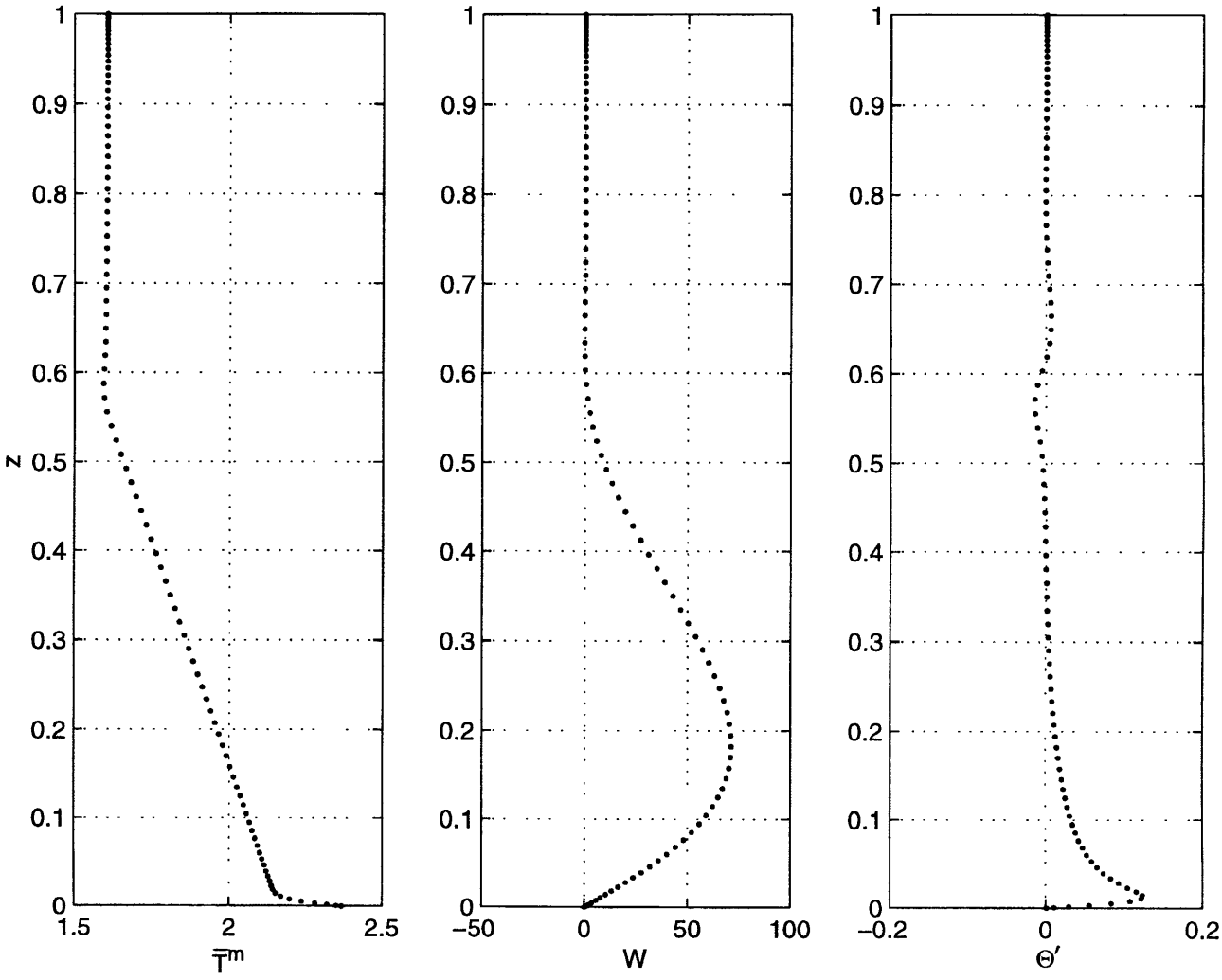

Figure 4-1: The mean temperature $\overline{T}^m$, vertical velocity W, and temperature perturbation Θ' obtained from the mean field equations. W and Θ' are periodic in the horizontal; the ascending branch is displayed here. This is a control run with parameter values $F_T = 2.75$, $b = 40$, $S = 10$, $r = 17$, $\kappa = 1/30$, $\gamma = 7 \times 10^5$, and $a^2 = 45.2$. The mean lapse rate is nearly adiabatic in the troposphere, and W has a single, broad maximum, as in the linear stability calculations from Chapter 3.

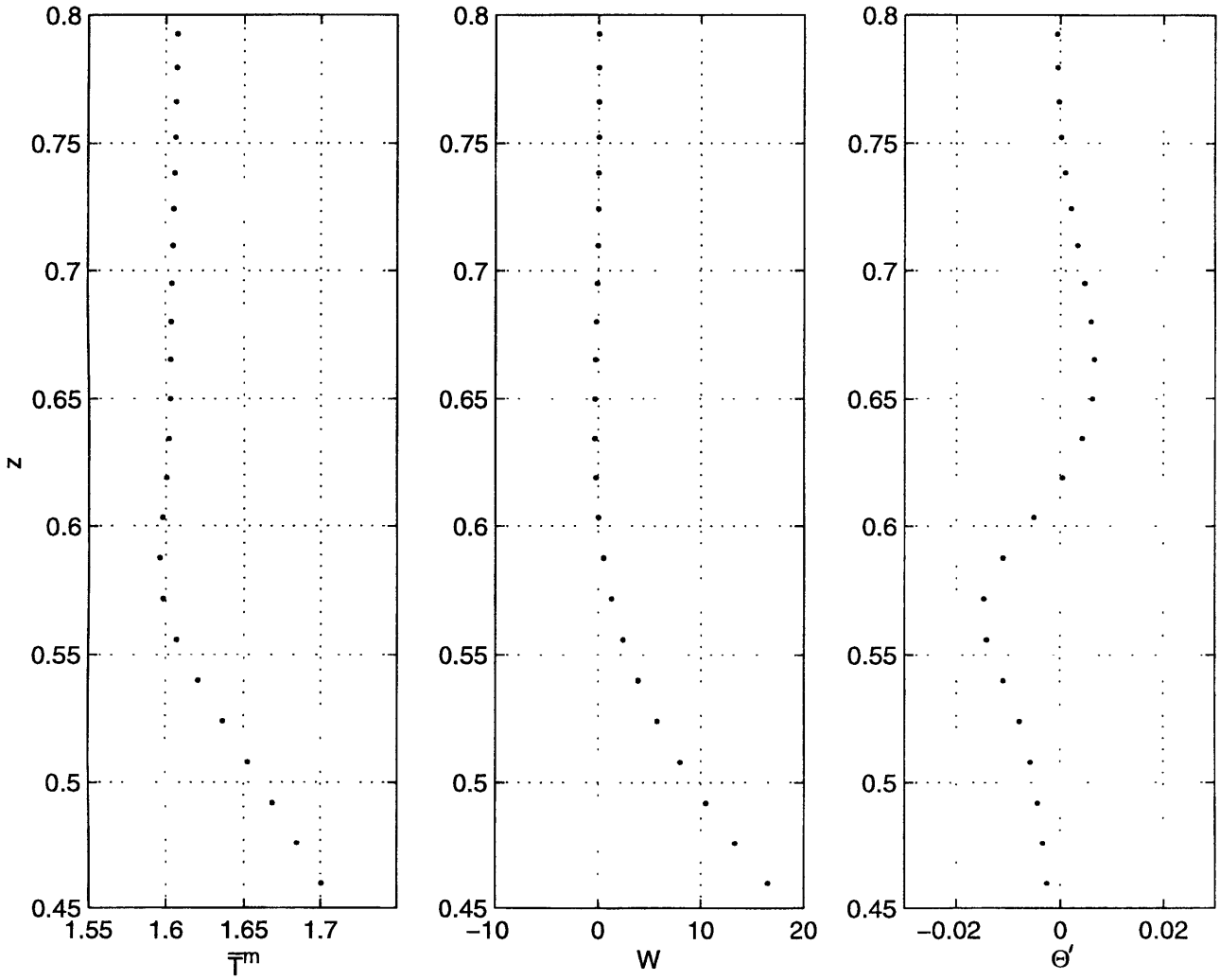

Figure 4-2: A detailed view of the $\overline{T}^m$, W, and Θ' fields near the tropopause, for the control run plotted in Figure 4-1. The structure of Θ' can be rationalized given W and the stratification of $\overline{T}^m$.

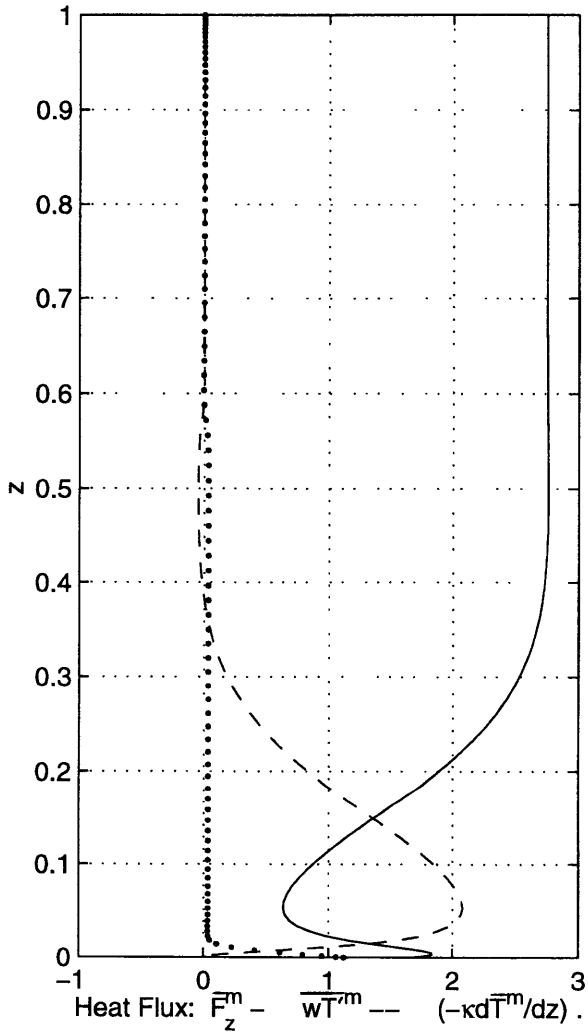

Figure 4-3: The radiative flux $\overline{F}_z^m$ (solid), convective heat flux $\overline{wT'}^m$ (dashed), and diffusive heat flux $-\kappa d\overline{T}^m/dz$ (dotted) for the control run. In the mid-troposphere, the radiative and convective fluxes nearly balance, and the convective heat flux decreases roughly linearly with altitude.

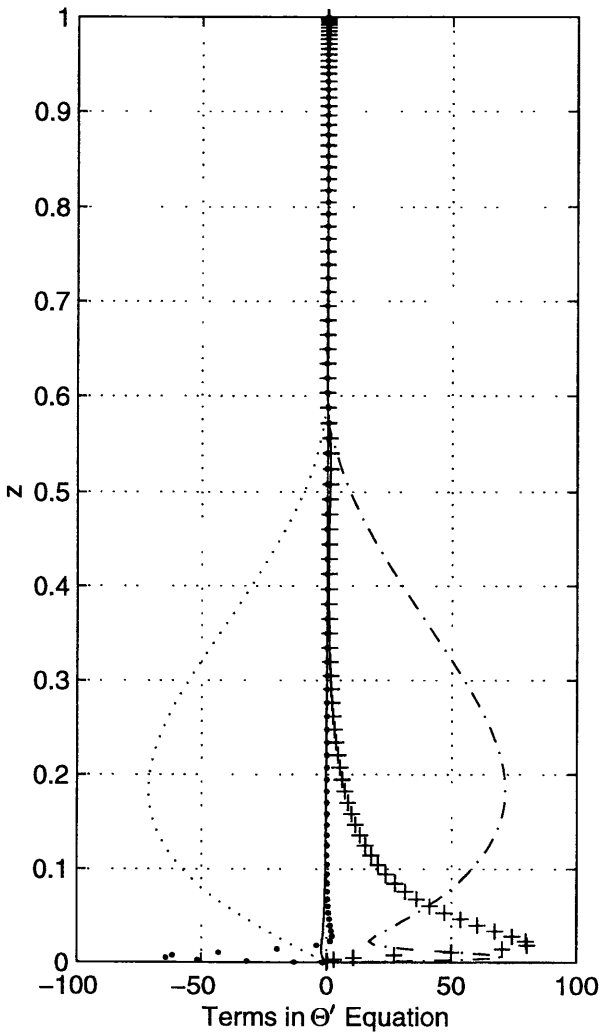

Figure 4-4: The terms from the heat perturbation equation Θ' (4.9) for the control run along with an estimate of the nonlinear term (4.12) with x set to zero in that term (plusses). The heat perturbation terms are $-W d\overline{T}^m/dz$ (dash-dot), $-W$ (dashes), $-r\Theta'$ (solid), thermal diffusion (dotted).

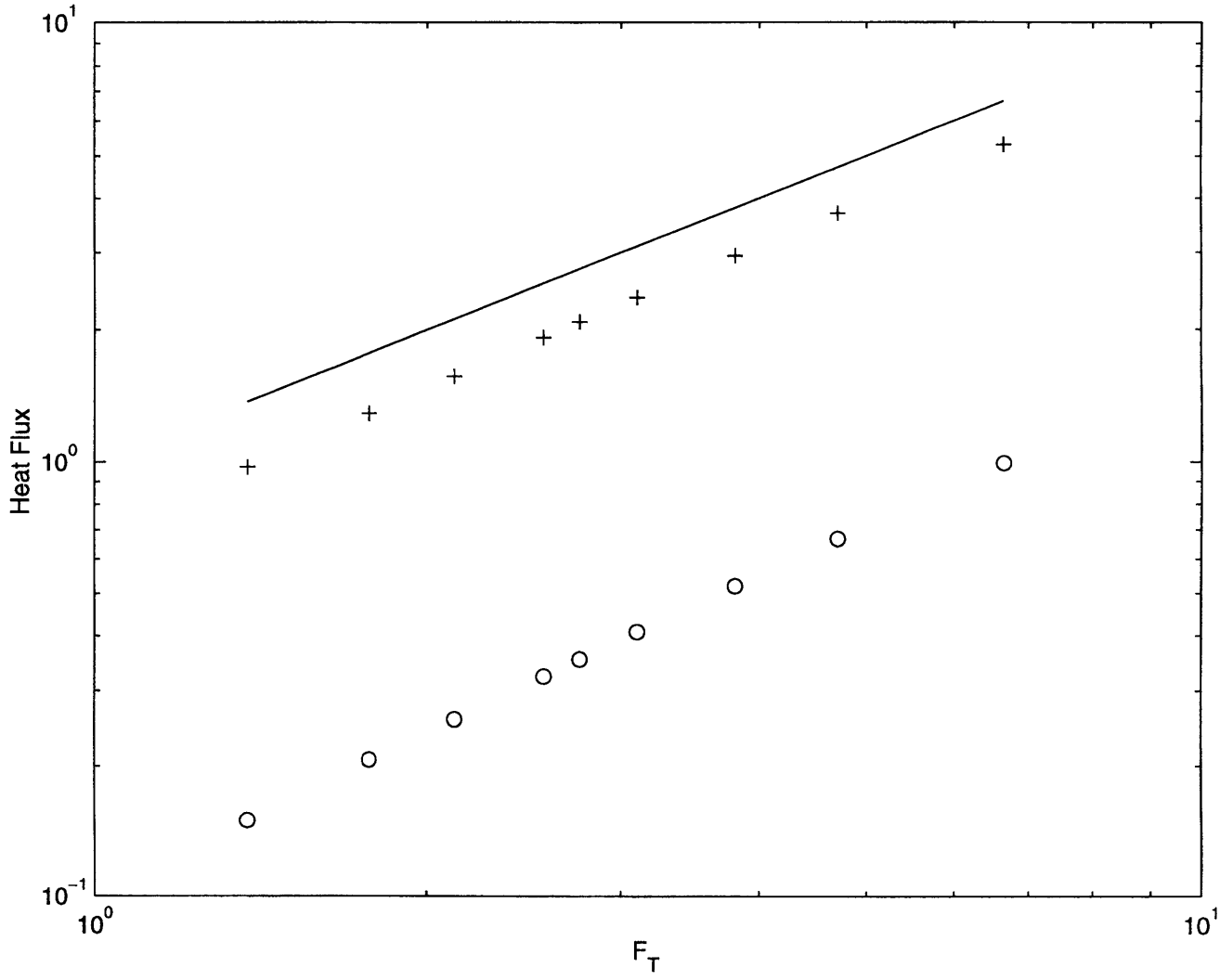

Figure 4-5: The domain averaged convective heat flux $\langle wT' \rangle$ (circles), maximum convective heat flux (plusses), and F_T, plotted versus the net incoming solar radiation F_T. The other governing parameters are fixed at the control run values.

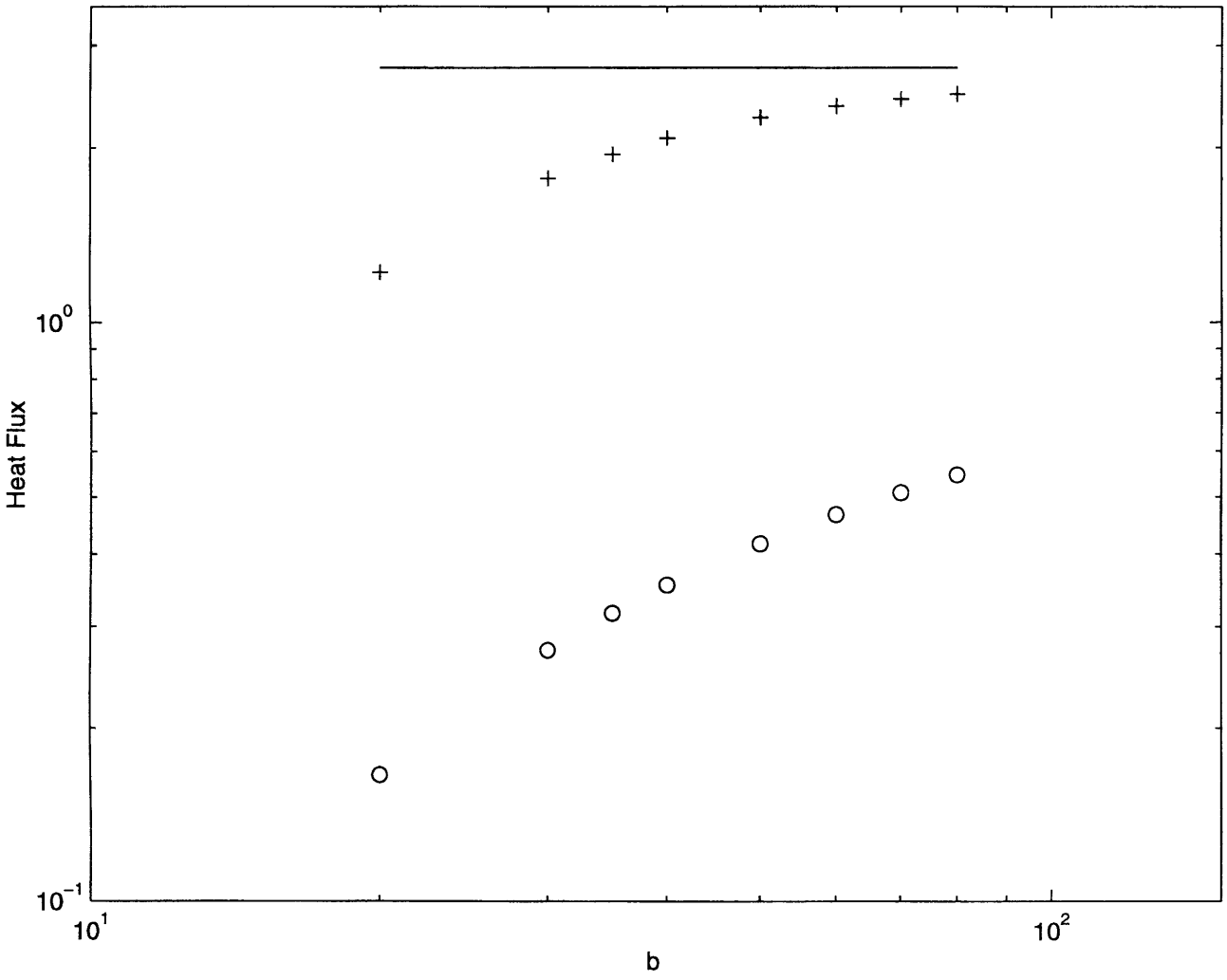

Figure 4-6: As in Figure 4-5, but the varied parameter is b.

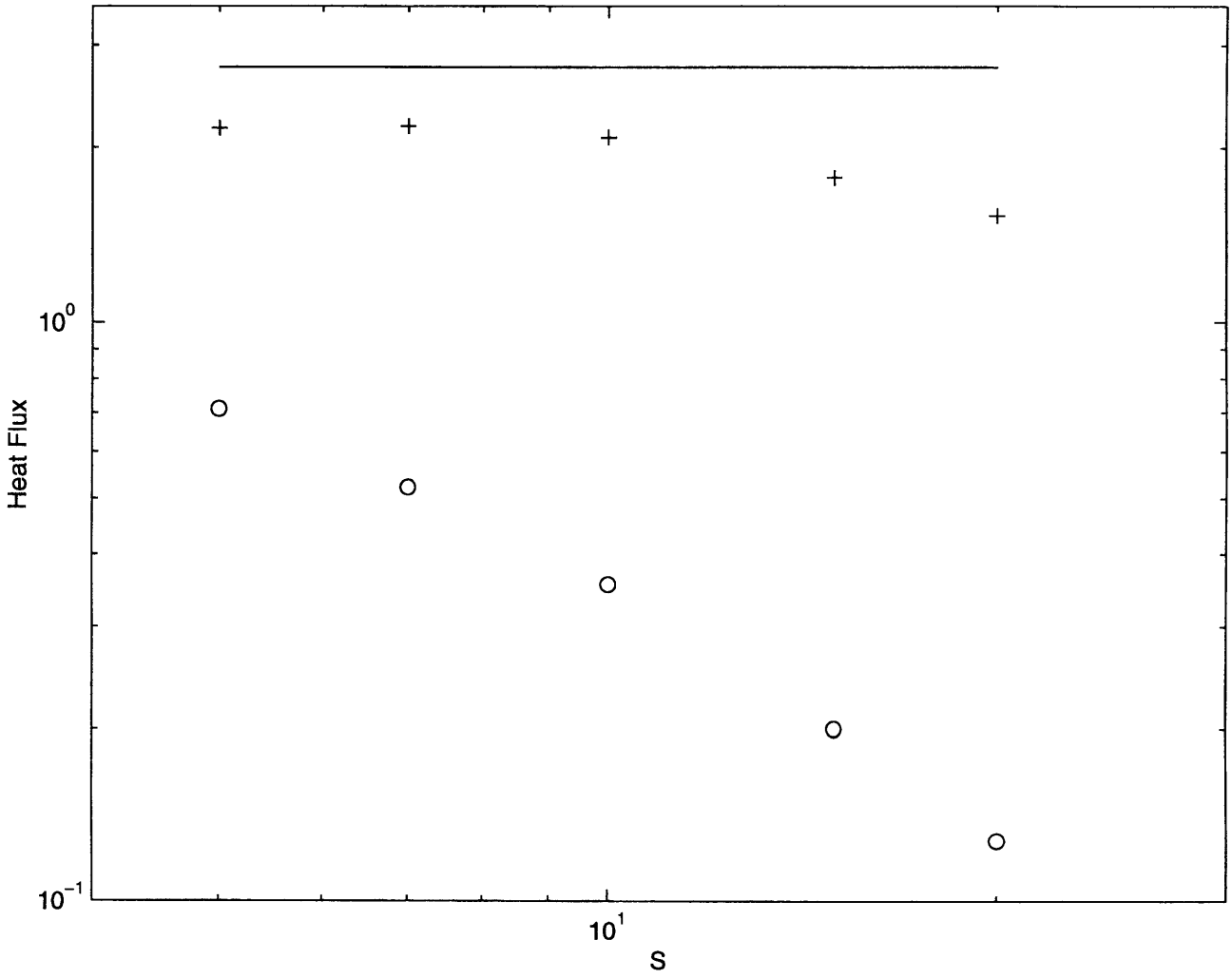

Figure 4-7: As in Figure 4-5, but the varied parameters are S and a^2, as described in the text. Also, when $S = 20$, we set $\gamma = 1.4 \times 10^6$ to prevent the flow from being excessively damped compared to the other runs.

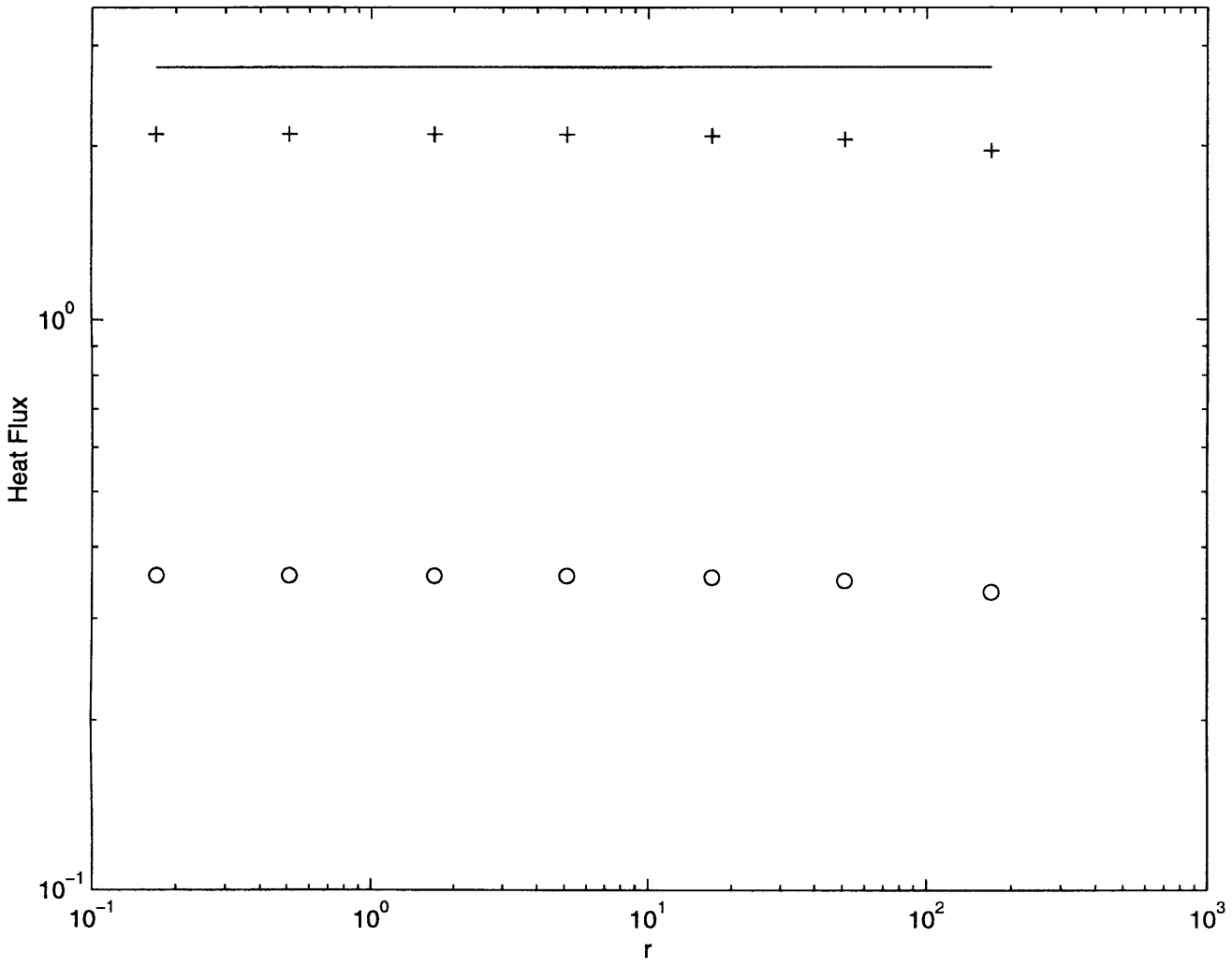

Figure 4-8: As in Figure 4-5, but the varied parameter is r.

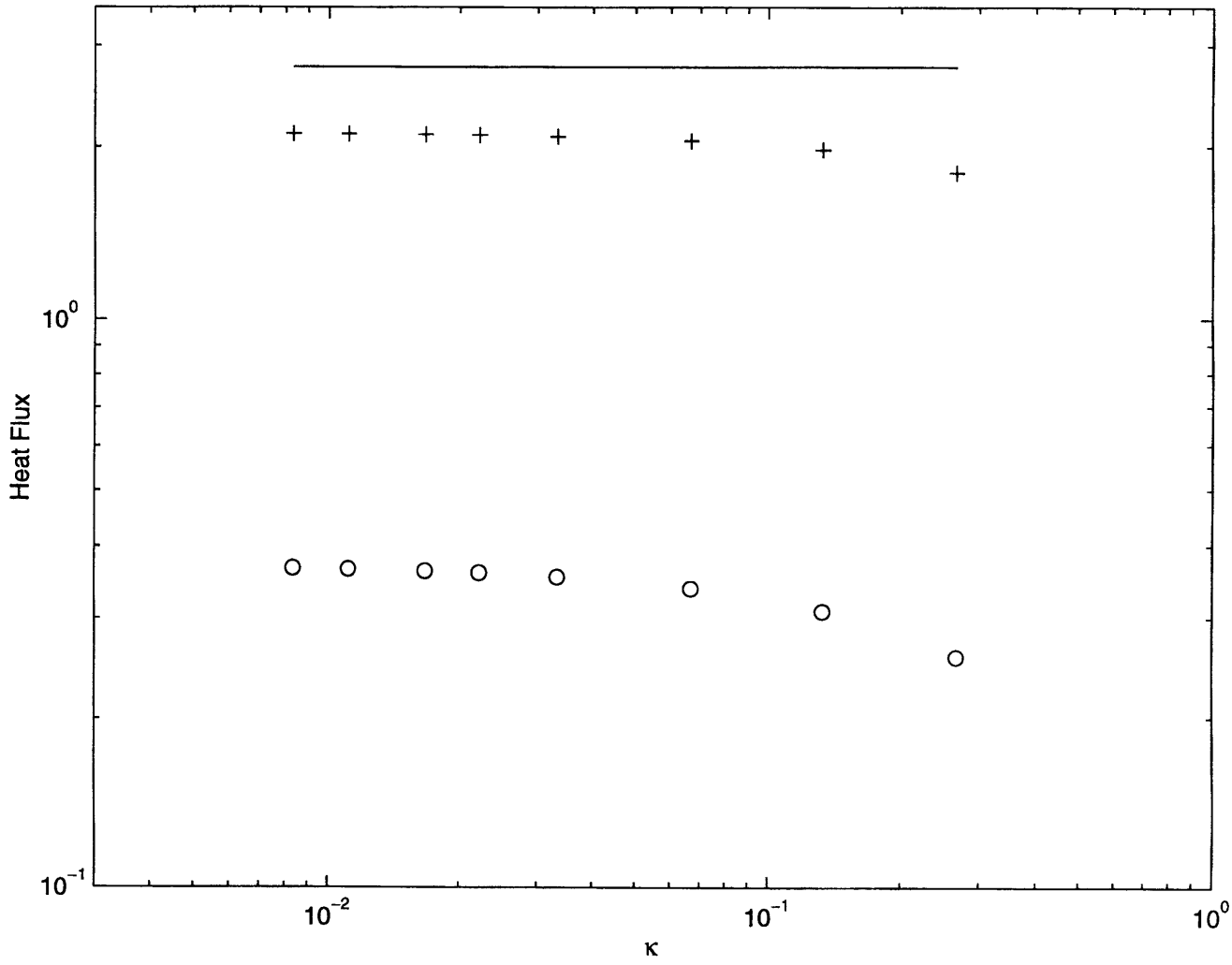

Figure 4-9: As in Figure 4-5, but the varied parameter is κ.

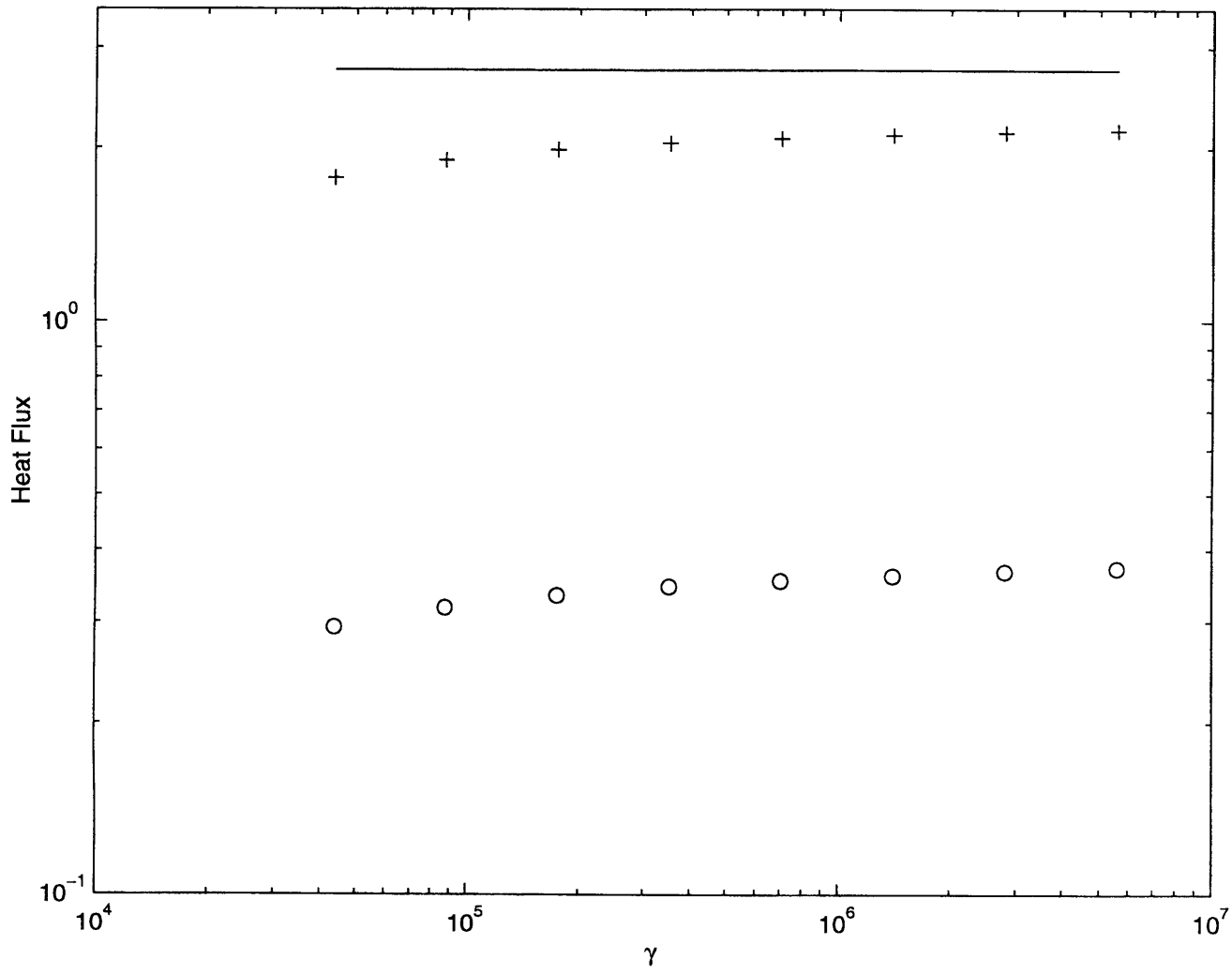

Figure 4-10: As in Figure 4-5, but the varied parameter is γ.

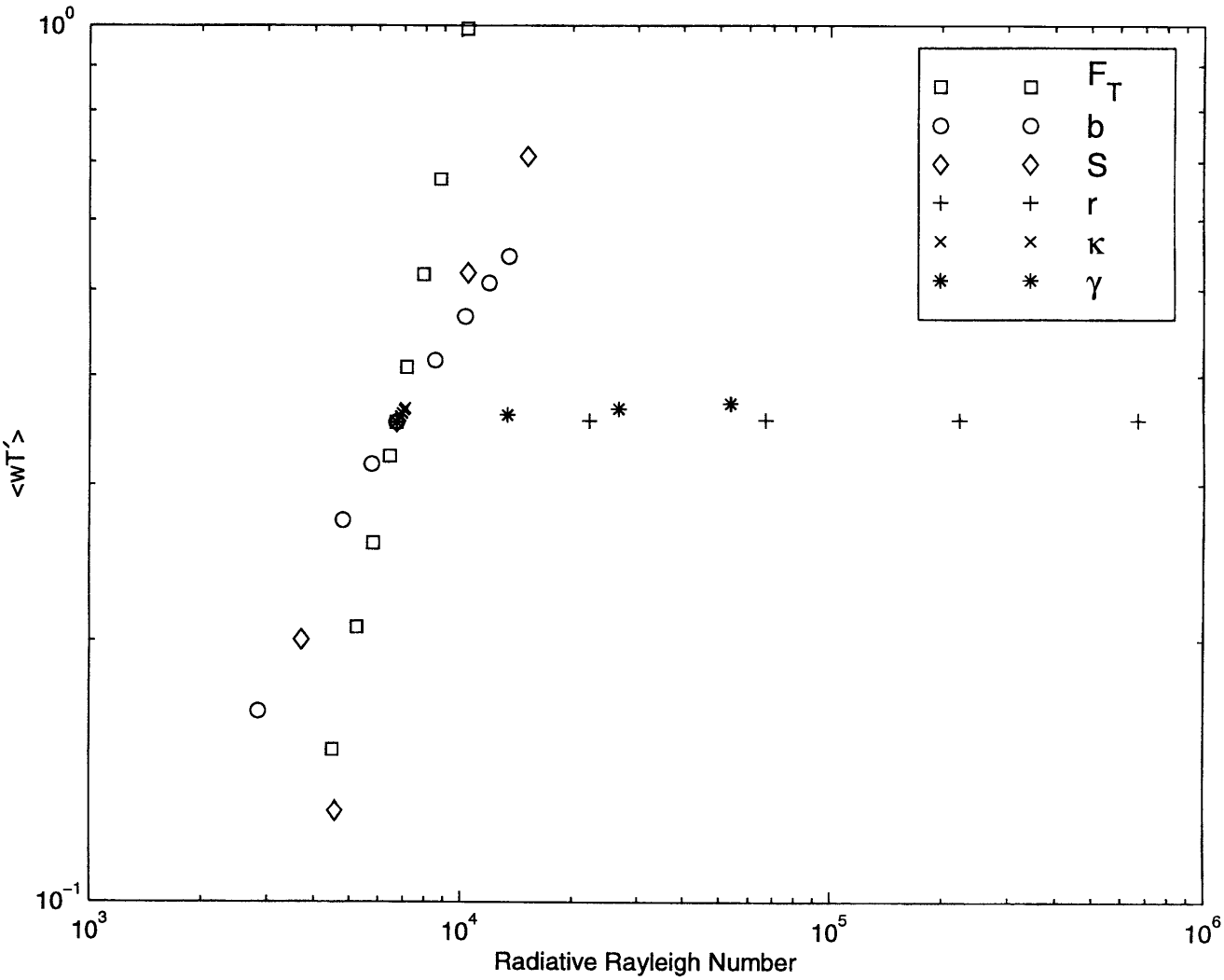

Figure 4-11: The domain averaged convective heat flux versus the radiative Rayleigh number $Ra_{\mathcal{R}}$ (3.30) for moderate to small values of radiative, viscous, and diffusive damping. Each marker style corresponds to a parameter which is varied, as indicated in the legend. All other parameters are held at the control run values. An exception is when S is varied; then a^2 is varied as described in the text, but all other parameters are fixed at the control run values. $Ra_{\mathcal{R}}$ does not collapse $\langle wT' \rangle$ onto one curve.

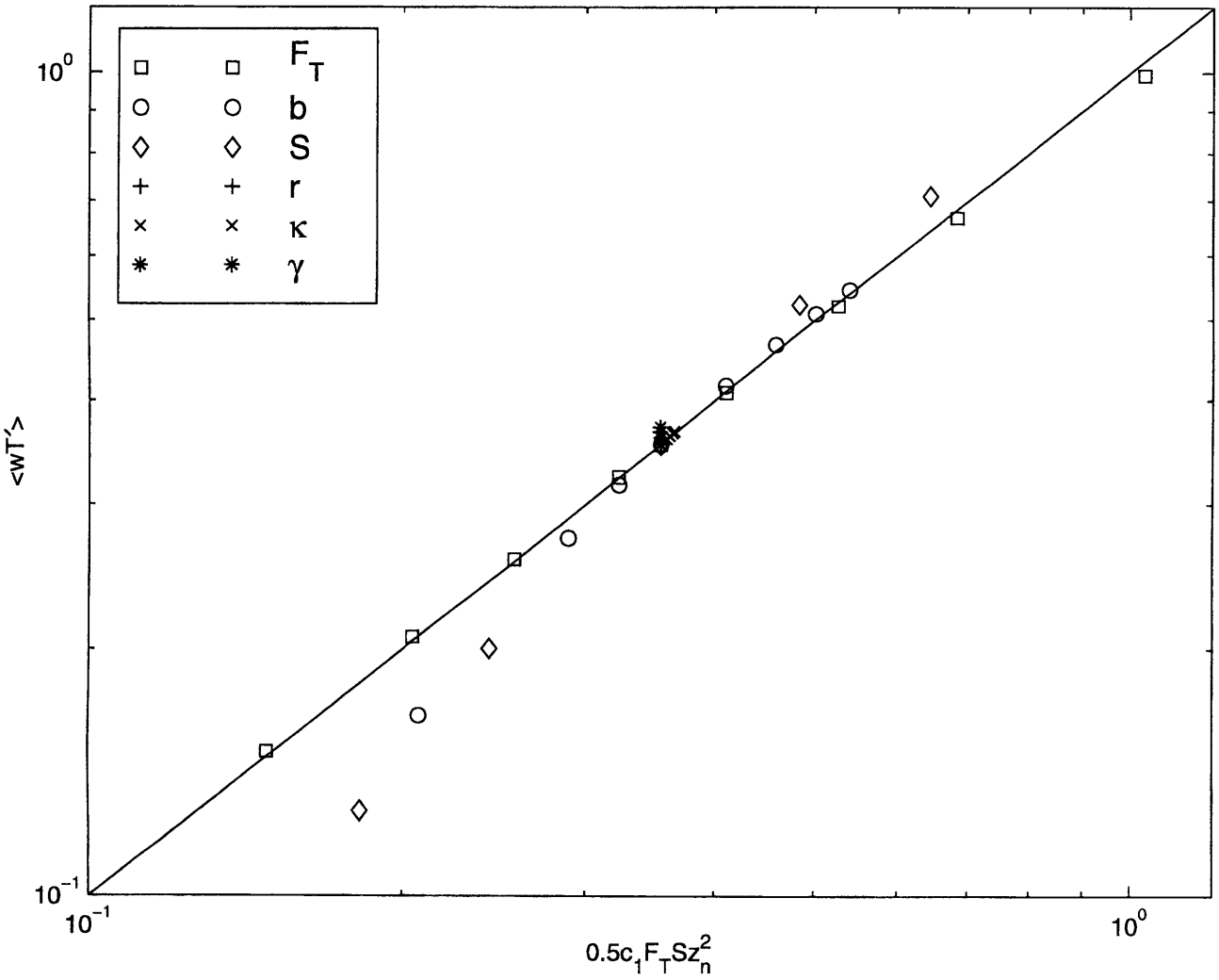

Figure 4-12: As in Figure 4-11, except that the domain averaged convective heat flux is plotted versus the scale (4.19), with $c_1 = 0.296$. If the scaling were perfect, all points would lie along the solid line.

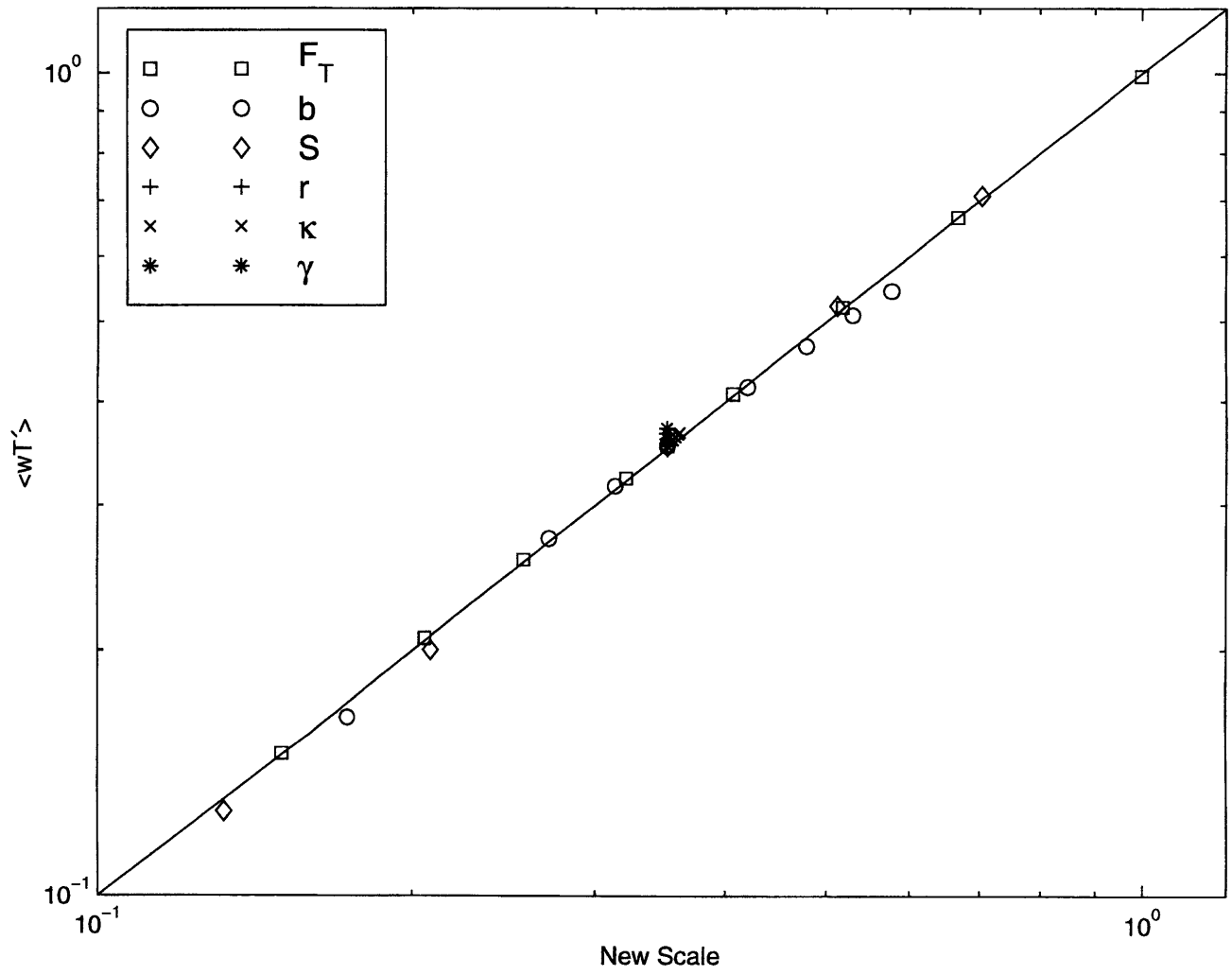

Figure 4-13: As in Figure 4-12, except that the domain averaged convective heat flux is plotted versus the new scale (4.21), with $c_2 = 0.333$. The new scale fits the mean field output better than the scale (4.19), particularly at those values of S and b for which $\langle wT' \rangle$ is small.

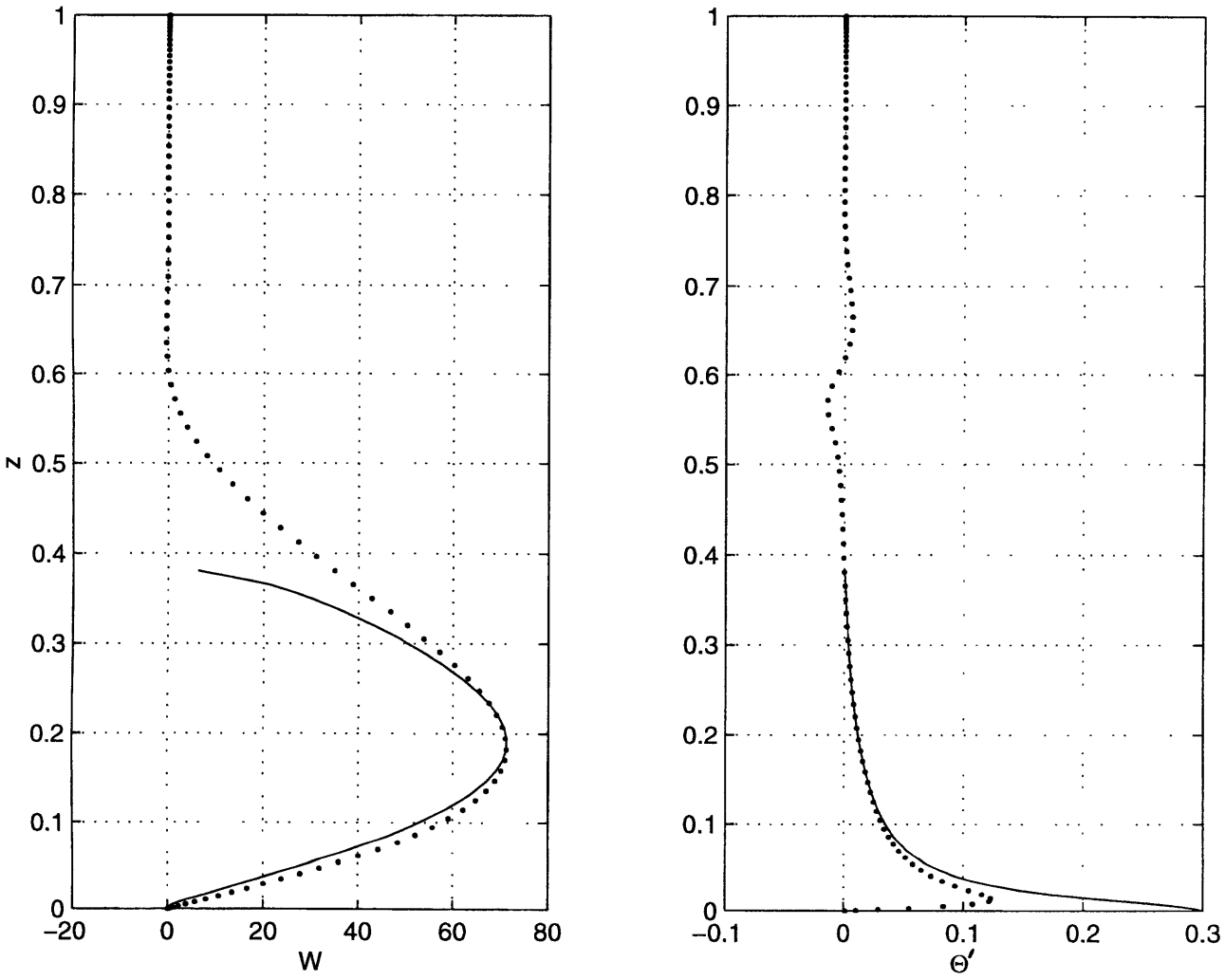

Figure 4-14: The control run output from the mean field equations (dots), plus the scalings (4.23) and (4.24) for $\left(\overline{w^2}^m\right)^{1/2}$ and $\left(\overline{T'^2}^m\right)^{1/2}$ (solid). Here, $c_3 = 0.217$.

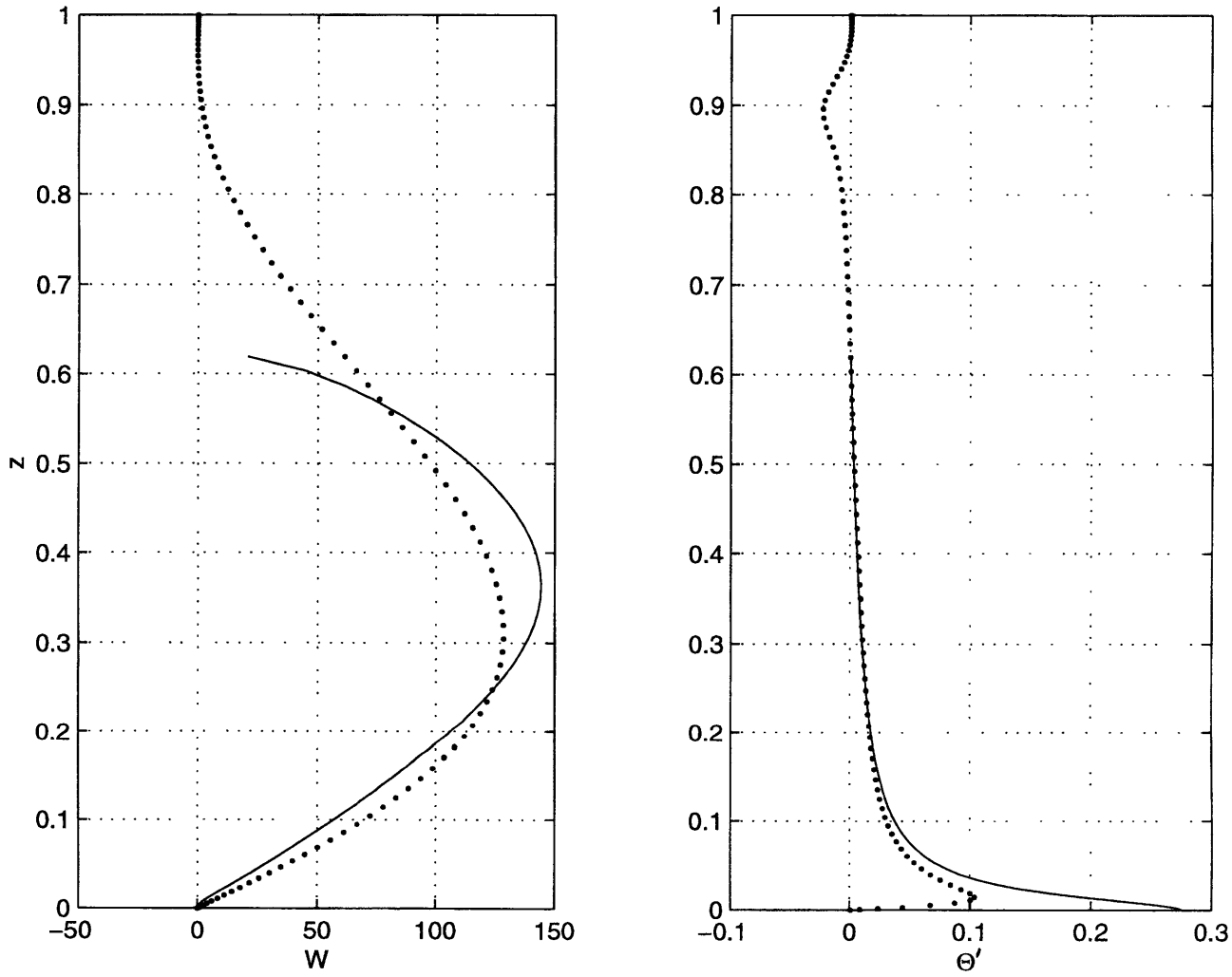

Figure 4-15: As in Figure 4-14, except that we now set $S = 5$ and $a^2 = 14.56$. The scaling produces a maximum in W which is roughly 1.5 km too high.

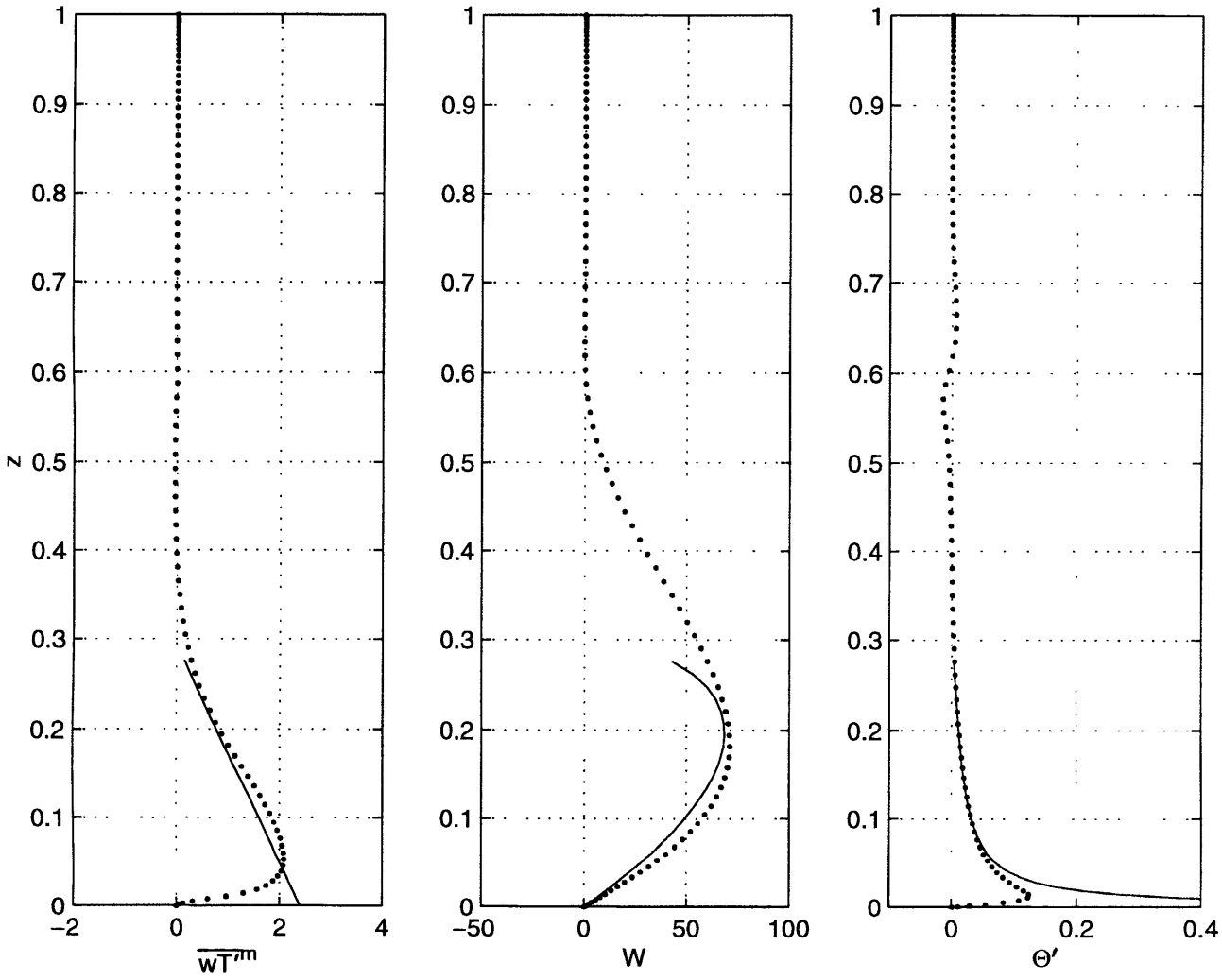

Figure 4-16: The control run output from the mean field equations (dots), plus the scalings (4.18), (4.25), and (4.26) for $\overline{wT'}^m$, $\left(\overline{w^2}^m\right)^{1/2}$, and $\left(\overline{T'^2}^m\right)^{1/2}$ (solid). In these equations, $c_1 = 0.296$ and $c_3 = 0.217$.

Chapter 5

Conclusions and Discussion

The results of this thesis may be summarized as follows.

(1) Over a fairly broad range of conditions, we can prove exchange of stabilities. However, for the atmospheric radiative-convective model of Chapter 4, which includes thermal diffusivity, our method of proving exchange of stabilities fails.

(2) We perform a linear stability analysis for several radiative equilibrium states. The primary result is that in most cases the critical threshold for linear stability can be approximately or exactly described by some form of radiative Rayleigh number. The radiative Rayleigh numbers we propose are similar to the standard Rayleigh number, except that the thermal diffusivity is replaced by a radiative diffusivity, and the lapse rate is modified appropriately.

(3) We used the energy method to determine a threshold below which all perturbations, regardless of amplitude, decay. When the basic state temperature profile is linear, the energy stability threshold coincides with the linear stability threshold. In this case, subcritical instabilities are not possible. When the basic state temperature profile is nonlinear, the energy stability threshold lies somewhat below the linear stability threshold.

(4) For an atmospheric radiative-convective model, we investigate the weakly convecting state using the mean field approximation. We find that the vertical convective heat flux is little affected by the values of the damping parameters — i.e. the nondimensionalized viscosity, thermal diffusivity, and radiative damping parameters. In contrast, the vertical convective heat flux is strongly affected by the net incoming solar radiation and the parameters specifying the radiative absorption coefficient. We construct scaling laws for heat flux, temperature perturbation, and velocity.

How are the dry radiative-convective models in this thesis related to a moist atmosphere? Some of the major differences are mentioned now.

A moist atmosphere contains latent heating, whereas a dry atmosphere does not. In a dry atmosphere with no water vapor, the enthalpy and buoyancy are represented by the same thermodynamic quantity, the potential temperature. Therefore the quantity which is transported via the heat equation is the same quantity which influences the momentum balance through the buoyancy term. In moist atmospheres, this connection is lost. For this reason, using our simple mixing length approach to find moist velocity and buoyancy scales is not straightforward.

In the (moist) tropical atmosphere, only a small fraction of the horizontal area is occupied by convection, i.e. strong updrafts and downdrafts. The convecting regions are surrounded by vast regions of slow subsidence. Hence the turbulence is highly intermittent. The scales, of say vertical velocity, in the convective and non-convective regions are quite different. It is not obvious how to relate the single velocity scale produced by a dry radiative-convective model to the two velocity scales inherent in a moist radiative-convective model.

A moist atmosphere may contain clouds, whereas a dry atmosphere does not. Clouds directly influence the radiative fluxes by reflecting sunlight and trapping longwave radiation. In our dry calculations, the albedo has been fixed. In a moist atmosphere, however, the albedo is determined partly by cloud cover, which is an internal model parameter. Also, in some of our dry calculations, we have assumed that the (thermal) radiative absorption coefficient falls off exponentially with altitude.

This is a reasonable assumption for a clear-sky atmosphere with water vapor decreasing with altitude. If, however, the atmosphere contains a cirrus anvil, the (thermal) absorption coefficient becomes very large within the cloud anvil. Hence the absorption coefficient is no longer well approximated by a function which decreases with altitude.

Despite the large differences between moist and dry atmospheres, it is plausible to suppose that some of our results have relevance to a moist atmosphere. In particular, it seems plausible that the damping factors (viscosity, thermal diffusivity, and radiative damping) are unimportant in moist radiative-convective atmospheres, if the absorption coefficient is regarded as fixed. For a dry atmosphere this conclusion was based on only a small number of assumptions which probably also hold for a moist atmosphere. It is also plausible to suppose that an increase in net incoming solar radiation or (longwave) optical depth is associated with an increase in vertical convective heat flux for moist as well as dry atmospheres. However, this conclusion is considerably complicated by the cloud effects discussed in the previous paragraph.

References

Arpaci, V. S. and D. Gőzűm, 1973: Thermal stability of radiating fluids: The Bénard problem. *Phys. Fluids*, **16**, 581–588.

Bdéoui, F., and A. Soufiani, 1997: The onset of Rayleigh-Bénard instability in molecular radiating gases. *Phys. Fluids A*, **9**, 3858–3872.

Boyd, J. P., 1989: *Chebyshev and Fourier Spectral Methods.* Springer-Verlag, 798 pp.

Castaing, B., G. Gunaratne, F. Heslot, L. Kadanoff, A. Libchaber, S. Thomae, X.-Z. Wu, S. Zaleski, G. Zanetti, 1989: Scaling of hard thermal turbulence in Rayleigh-Bénard convection. *J. Fluid Mech.*, **204**, 1–30.

Cess, R. D., and coauthors, 1990: Intercomparison and interpretation of climate feedback processes in 19 atmospheric general circulation models. *J. Geophys. Res.*, **95**, 16601–16615.

Chan, S.-K., 1971: Infinite Prandtl Number Turbulent Convection. *Stud. Appl. Math.*, **50**, 13–49.

Chavanne, X., F. Chillà, B. Castaing, B. Hébral, B. Chabaud, and J. Chaussy, 1997: Observation of the ultimate regime in Rayleigh-Bénard convection. *Phys. Rev. Lett.*, **79**, 3648–3651.

Christophorides, C. and S. H. Davis, 1970: Thermal instability with radiative transfer. *Phys. Fluids*, **13**, 222–226.

Cotton, W. R., and R. A. Anthes, 1989: *Storm and cloud dynamics.* Academic Press, 883 pp.

Davis, S. H., 1969: On the principle of exchange of stabilities. *Proc. R. Soc. London A*, **310**, 341–358.

Deardorff, J. W., 1970: Convective velocity and temperature scales for the unstable planetary boundary layer and for Rayleigh convection. *J. Atmos. Sci.*, **27**, 1211–1213.

Del Genio, A. D., M.-S. Yao, W. Kovari, and K.-W. Lo, 1996: A prognostic cloud water parameterization for global climate models. *J. Climate*, **9**, 270–304.

Drazin, P. G. and W. H. Reid, 1981: *Hydrodynamic Stability.* Cambridge University Press, 527 pp.

Eady, E. T., 1949: Long waves and cyclone waves. *Tellus*, **1**(3), 33–52.

Elder, J. W., 1969: The temporal development of a model of high Rayleigh number convection. *J. Fluid Mech.*, **35**, 417–437.

Emanuel, K. A., 1994: *Atmospheric Convection.* Oxford University Press, 580 pp.

Emanuel, K. A. and M. Bister, 1996: Moist convective velocity and buoyancy scales. *J. Atmos. Sci.*, **53**, 3276–3285.

Emanuel, K. A., J. D. Neelin, and C. S. Bretherton, 1994: On large-scale circulations in convecting atmospheres. *Q. J. R. Meteorol. Soc.*, **120**, 1111–1143.

Getling, A. V., 1980: On the scales of convection flows in a horizontal layer with radiative energy transfer. *Atmos. Oceanic Phys.*, **16**, 363–365.

Gille, J. and R. M. Goody, 1964: Convection in a radiating gas. *J. Fluid Mech.*, **20**, 47–79.

Goody, R. M., 1949: The thermal equilibrium at the tropopause and the temperature of the lower stratosphere. *Proc. Roy. Soc. London Ser. A*, **197**, 487–505.

Goody, R. M., 1956a: The influence of radiative transfer on cellular convection. *J. Fluid Mech.*, **1**, 424–435.

Goody, R. M., 1956b: Corrigendum. *J. Fluid Mech.*, **1**, 670.

Goody, R. M., 1964: *Atmospheric radiation I. Theoretical basis*, Oxford University Press, 436 pp.

Goody, R. M., 1995: *Principles of Atmospheric Physics and Chemistry.* Oxford University Press, 324 pp.

Goody, R. M. and Y. L. Yung, 1989: *Atmospheric radiation: theoretical basis*, 2nd ed. Oxford University Press, 519 pp.

Held, I. M., R. S. Hemler, and V. Ramaswamy, 1993: Radiative-convective equilibrium with explicit two-dimensional moist convection. *J. Atmos. Sci.*, **50**, 3909–3927.

Herring, J. R., 1963: Investigation of problems in thermal convection. *J. Atmos. Sci.*, **20**, 325–338.

Herring, J. R., 1964: Investigation of problems in thermal convection: Rigid boundaries. *J. Atmos. Sci.*, **21**, 277–290.

Howard, L. N., 1963: Heat transport by turbulent convection. *J. Fluid Mech.*, **17**, 405–432.

Howard, L. N., 1964: Convection at high Rayleigh number. *Proc. Eleventh Int. Congress Applied Mechanics, Munich* (ed. H. Görtler), pp. 1109–1115.

Ingersoll, A. P., 1964: Convective instabilities in plane Couette flow. *Phys. Fluids*, **9**, 682–689.

Islam, S., R. L. Bras, and K. A. Emanuel, 1993: Predictability of mesoscale rainfall in the tropics. *J. Appl. Meteorol.*, **32**, 297–310.

Joseph, D. D. 1965: Nonlinear stability of the Boussinesq equations by the method of energy. *Arch. Ration. Mech. Anal.*, **22**, 163–184.

Kraichnan, R. H., 1962: Turbulent thermal convection at arbitrary Prandtl number. *Phys. Fluids*, **5**, 1374–1389.

Lindzen, R. S., 1994: Climate dynamics and global change. *Annu. Rev. Fluid Mech.*, **26**, 353–378.

Liou, K. N., 1980: *An introduction to atmospheric radiation.* Academic Press, 392 pp.

Malkus, W. V. R., 1954: The heat transport and spectrum of thermal turbulence. *Proc. Roy. Soc. London A*, **225**, 196–212.

Manabe, S. and R. F. Strickler, 1964: Thermal equilibrium of the atmosphere with a convective adjustment. *J. Atmos. Sci.*, **21**, 361–385.

Murgai, M. P. and P. K. Khosla, 1962: A study of the combined effect of thermal radiative transfer and a magnetic field on the gravitational convection of an ionized fluid. *J. Fluid Mech.*, **14**,

433–451.

Musman, S., 1968: Penetrative convection. *J. Fluid Mech.*, **31**, 343–360

Pellew, A., and R. V. Southwell, 1940: On maintained convective motion in a fluid heated from below. *Proc. Roy. Soc. A*, **176**, 312–343.

Pierrehumbert, R. T., 1995: Thermostats, radiator fins, and the local runaway greenhouse. *J. Atmos. Sci.*, **52**, 1784–1806.

Prandtl, L., 1932: Meteorologische Anwendung der Strömungslehre, *Beitr. Phys. freien Atmosphäre*, **19**, 188-202.

Press, W. H., S. A. Teukolsky, W. T. Vetterling, and B. P. Flannery, 1992: *Numerical recipes in C: The art of scientific computing*, 2nd ed. Cambridge University Press, 994 pp.

Priestley, C. H. B., 1959: *Turbulent transfer in the lower atmosphere.* The University of Chicago Press, 130 pp.

Ramanathan, V., and J. A. Coakley, Jr. 1978: Climate modeling through radiative-convective models. *Rev. Geophys. Space Phys.*, **16**, 465–489.

Rayleigh, Lord, 1916: On convection currents in a horizontal layer of fluid, when the higher termpature is on the under side. *Phil. Mag.*, (6) **32**, 529–546.

Rennó, N. O., K. A. Emanuel, and P. H. Stone, 1994a: Radiative-convective model with an explicit hydrologic cycle 1. Formulation and sensitivity to model parameters. *J. Geophys. Res.*, **99**, 14429–14441.

Rennó, N. O., P. H. Stone, and K. A. Emanuel, 1994b: Radiative-convective model with an explicit hydrologic cycle 2. Sensitivity to large changes in solar forcing. *J. Geophys. Res.*, **99**, 17001–17020.

Siggia, E. D., 1994: High Rayleigh number convection. *Annu. Rev. Fluid Mech.*, **26**, 137–168.

Spiegel, E. A., 1960: The convective instability of a radiating fluid layer. *Astrophys. J.*, **132**, 716–728.

Spiegel, E. A., 1962: On the Malkus theory of turbulence. *Mécanique de la Turbulence*, Paris, Centre National de la Recherche Scientifique, 181–201.

Spiegel, E. A., 1971: Convection in stars I. Basic Boussinesq convection *Annu. Rev. Astron. Astrophys.*, **9**, 323–352.

Spiegel, E. A. and G. Veronis, 1960: On the Boussinesq approximation for a compressible fluid. *Astrophys. J.*, **131**, 442–447.

Stull, R. B., 1988: *An introduction to boundary layer meteorology.* Kluwer Academic Publishers. 666 pp.

Straughan, B., 1992: *The energy method, stability and nonlinear convection.* Springer-Verlag, 242 pp.

Sun, W.-Y., 1976: Linear stability of penetrative convection. *J. Atmos. Sci.*, **33**, 1911–1920.

Tritton, D. J., 1988: *Physical fluid dynamics*, 2nd ed. Oxford University Press, 519 pp.

Veronis, G., 1963: Penetrative convection. *Astrophys. J.*, **137**, 641–663.

Vincenti, W. G., and S. C. Traugott, 1971: The coupling of radiative transfer and gas motion. *Annu. Rev. Fluid Mech.*, **3**, 89–116.

Whitehead, J. A., and M. M. Chen, 1970: Thermal instability and convection of a thin fluid layer bounded by a stably stratified region. *J. Fluid Mech.*, **40**, 549–576.